Investigation of Core High-Z Impurity Transport in Tokamaks: Physics, Tools and Techniques

M.L. Reinke

UNIVERSITY of York

w/ thanks from A. Loarte (ITER), J.E. Rice (MIT)

F. Casson (CCFE), C. Angioni & T. Pütterich (IPP)

and contributions from

The Alcator C-Mod Team

JET Contributors

Alcator C-Mod

Background

"In summary, the observed tungsten concentration in PLT discharges is often sufficient to strongly affect the discharge characteristics, both directly by radiative energy losses, and indirectly by changing radial temperature and current density distributions."

"The critical parameter that determines the tungsten concentration appears to be the peripheral temperature…"

"The complexity of tungsten spectra, the number of ionization states simultaneously present, and the scarcity of basic data on tungsten ions pose formidable problems in development of plasma diagnostics based on tungsten."

E. Hinnov *et al* 1978 *Nucl. Fusion* **18** 1305

Background

"In summary, the observed tungsten concentration in PLT discharges is often sufficient to strongly affect the discharge characteristics, both directly by radiative energy losses, and indirectly by changing radial temperature and current density distributions."

"The critical parameter that determines the tungsten concentration appears to be the peripheral temperature…"

"The complexity of tungsten spectra, the number of ionization states simultaneously present, and the scarcity of basic data on tungsten ions pose formidable problems in development of plasma diagnostics based on tungsten."

E. Hinnov *et al* 1978 *Nucl. Fusion* **18** 1305

The patient says, "Doctor, it hurts when I do this." "Then don't do that!"

Henny Youngman

- interim decades saw the use of carbon walls, but nuclear compatibility and long-pulse are moving the community back to high-Z walls
- we're finding much of the same to be true > 30 years later, but now with the added complexity of H-modes, ELMs, high-$\beta_{N,}$ low aspect ratio…
- but we also have better tools to understand and mitigate high-Z effects

Overview

- **describe our present understanding of high-Z impurity transport**
  - parallel impurity transport leading to poloidal n_Z variation
  - neoclassical & turbulent radial transport and role of asymmetries
- **discuss diagnosing high-Z impurities & interpreting measurements**
  - estimating concentrations from 0-D spectroscopy
  - imaging x-ray spectroscopy for kinetic profiles & high-Z transport
  - questions/concerns of atomic physics data for high-Z impurities
- **present experimental results from recent studies of Mo and W transport on JET and Alcator C-Mod**

High-Z Impurity Transport Physics (PARALLEL & RADIAL)

Neoclassical Parallel Force Balance Relevant for Core High-Z Impurities

$$\underbrace{\frac{m_z n_z \omega^2}{2}\nabla_{||}R^2}_{\text{inertia (centrifugal)}} + \underbrace{Z n_z e \nabla_{||}\Phi}_{\text{electrostatic}} + \underbrace{T_z \nabla_{||} n_z}_{\text{pressure}} = \underbrace{R_{z,||}}_{\text{friction}}$$

inertia: widely observed, understood for strong flows, possible issues $(\mathbf{v}\cdot\nabla)\mathbf{v}$ for $v_\theta/v_\phi \sim 1$

electrostatic: non-thermal particle densities lead to $\Phi(\theta)$ with $Ze\Phi(\theta)/T_e \sim 1$, demonstrated for ICRH, need to validate for ECH/NBI

friction: disagreements seen, critical for setting $v_{\theta,z}$ and core up/down asymmetries

other: sources/sinks, C-X closer to boundary

Centrifugal and Poloidal Electric Field Driven Impurity Density Asymmetries

- for a tor. rotating plasma, centrifugal force leads to ions to the low-field side
  - effect scales as $m_z\omega^2R^2/T_z$ (w/ T_z ~ T_i) scales with $\mathbf{M_i^2(m_z/m_i)}$

OUTBOARD LOCALIZATION

centrifugal force from toroidal rotation moves impurities to LFS

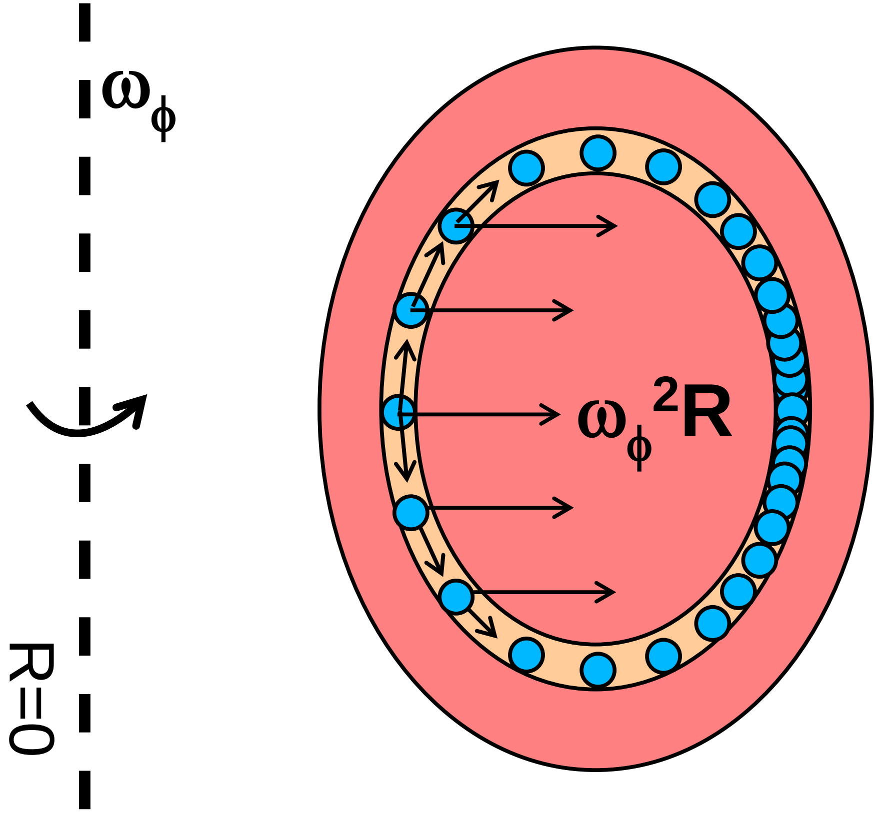

Centrifugal and Poloidal Electric Field Driven Impurity Density Asymmetries

- for a tor. rotating plasma, centrifugal force leads to ions to the low-field side
  - effect scales as $m_z\omega^2R^2/T_z$ (w/ $T_z \sim T_i$) scales with $\mathbf{M_i^2(m_z/m_i)}$
- the high charge of impurities causes sensitivity to poloidal variation of electrostatic potential

$$\mathbf{n_z/\langle n_z\rangle = \exp[-Ze\Phi(\theta)/T_z]}$$

  - ICRH minority heating leads to ion on the high-field side

INBOARD LOCALIZATION

electric field from rf-heated minority ions moves impurities to HFS

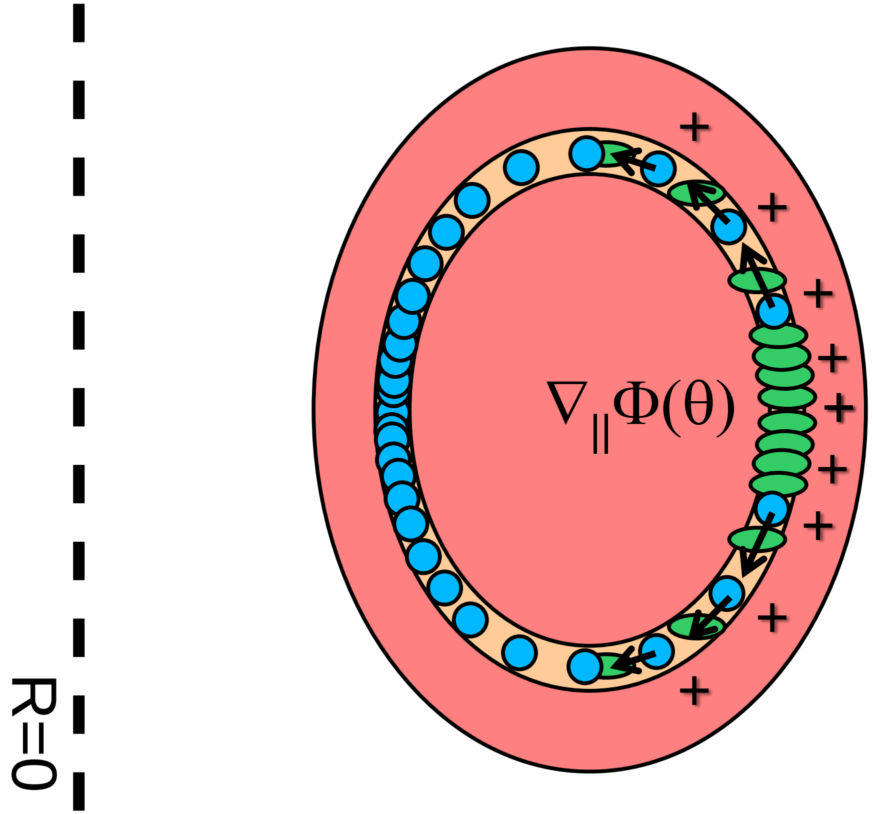

Dedicated AXUV Diode Diagnostic Developed to Study Poloidal Impurity Variation in C-Mod

- dominant asymmetry ‘in/out’, favors multiple tangentially viewing arrays over standard ‘polodial tomography system’
- methodology: M.L. Reinke, *et al*. PoP **20** 056109 (2013)

LFS Resonance Layer @ r/a ~ 0.3

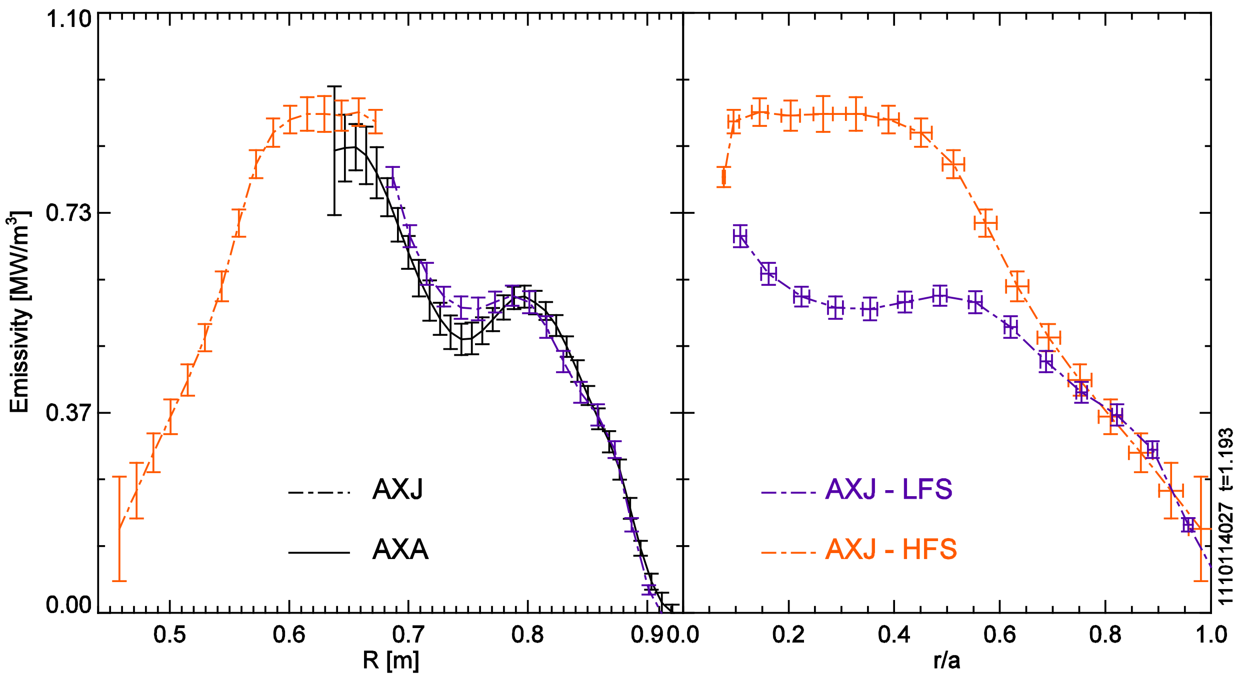

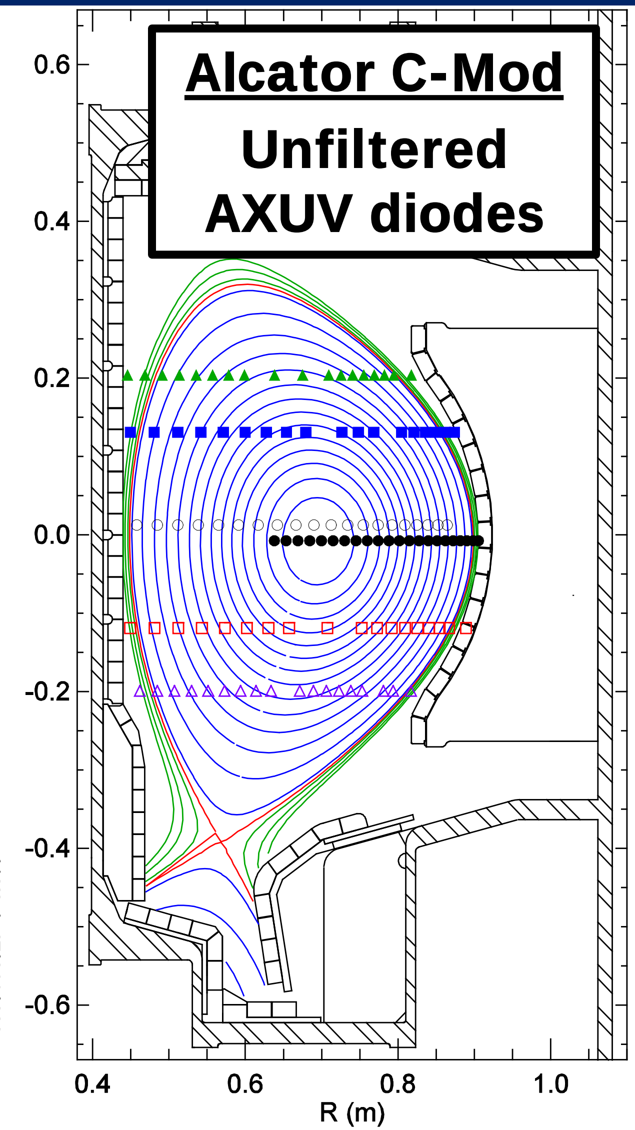

Dedicated AXUV Diode Diagnostic Developed to Study Poloidal Impurity Variation in C-Mod

- dominant asymmetry ‘in/out’, favors multiple tangentially viewing arrays over standard ‘polodial tomography system’
- methodology: M.L. Reinke, *et al*. PoP **20** 056109 (2013)
- used to determine m=1,2 cosine & sine terms

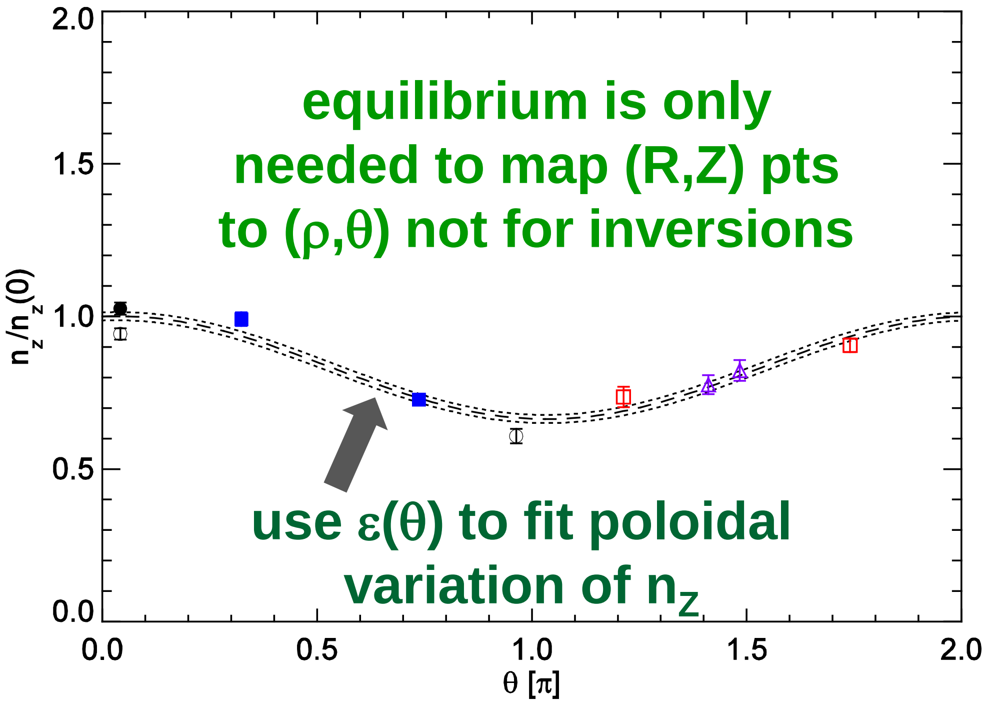

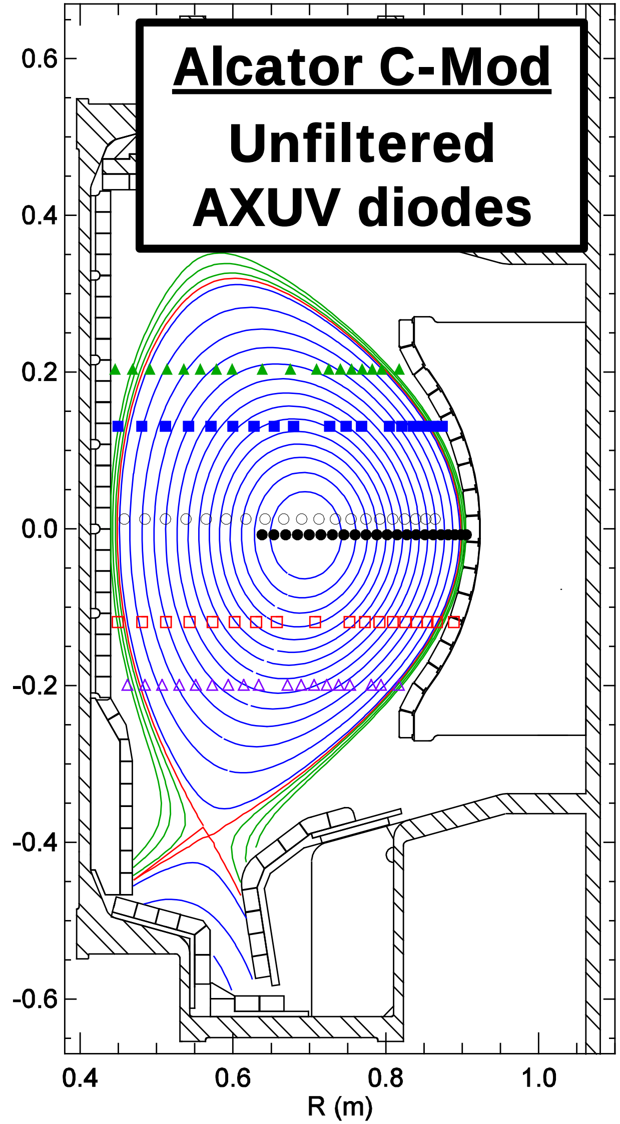

Predictive Capability Demonstrated for Dominant Mechanisms of Core 'In/Out' Asymmetries

$$\frac{n_{z,cos}}{\langle n_z \rangle} = 2\frac{r}{R_o}\left[\boxed{\frac{m_z \omega^2 R_o^2}{2T_i}\left(1 - \frac{Z m_i}{m_z}\frac{Z_{eff} T_e}{Z_{eff} T_e + T_i}\right)} \boxed{- Z f_m \frac{T_e}{Z_{eff} T_e + T_i}\left(\frac{T_\perp}{T_\parallel} - 1\right)}\right]$$

LFS localization due to centrifugal force

HFS accumulation due to minority anisotropy

M.L. Reinke, *et al,* PPCF **54** 045004 (2012)

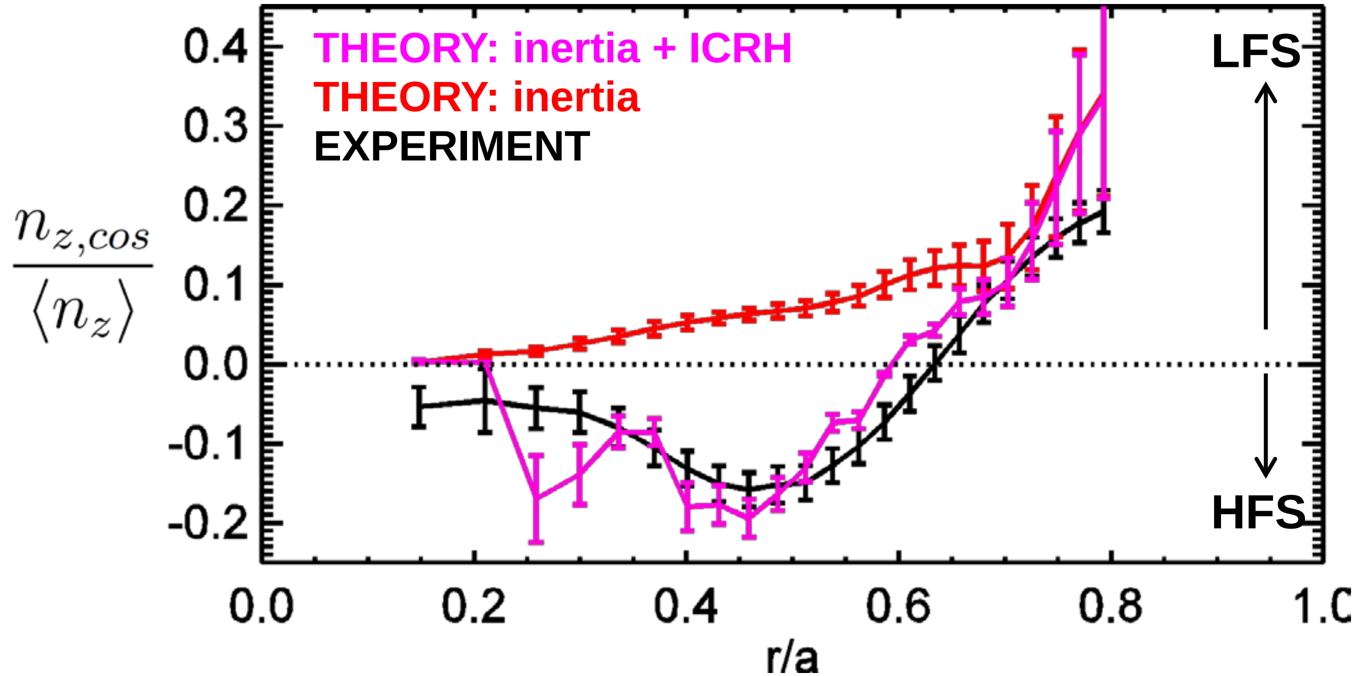

centrifugal force cannot explain **measurements** near the resonance layer

adding **ICRH minority effects** brings theory in good agreement with experiments

Standard High-Z Neoclassical Impurity Transport

- impurities are generally Pfirsch-Schlüter, main-ions will be collisionless
  - calculate from the FSA of parallel friction*: $\langle \boldsymbol{\Gamma_z} \cdot \boldsymbol{\nabla\psi} \rangle = -\left\langle \frac{\boldsymbol{IR_{z,\parallel}}}{\boldsymbol{ZeB}} \right\rangle$

$$\boldsymbol{R_{z,\parallel}} = -\frac{\boldsymbol{p_i I}}{\boldsymbol{\Omega_i \tau_{iz}}}\left(\frac{\boldsymbol{1}}{\boldsymbol{n_i}}\frac{\boldsymbol{dn_i}}{\boldsymbol{d\psi}} - \boldsymbol{0.5}\frac{\boldsymbol{1}}{\boldsymbol{T_i}}\frac{\boldsymbol{dT_i}}{\boldsymbol{d\psi}}\right) + \frac{\boldsymbol{m_i n_i}}{\boldsymbol{\tau_{iz}}}\left(\boldsymbol{u} - \frac{\boldsymbol{K_z}}{\boldsymbol{n_z}}\right)\boldsymbol{B} \quad \text{w/ } \boldsymbol{\tau_{iz}} = \frac{\boldsymbol{n_i}}{\boldsymbol{Z^2 n_z}}\boldsymbol{\tau_{ii}}$$

  - assume n_i, T_i, n_z and K_z are flux functions, K_z from $\left\langle \frac{\boldsymbol{BR_{z,\parallel}}}{\boldsymbol{n_z}} \right\rangle = \boldsymbol{0}$

$$\langle \boldsymbol{\Gamma_z} \cdot \boldsymbol{\nabla\psi} \rangle = \frac{\boldsymbol{p_i m_i I^2}}{\boldsymbol{Z\tau_{iz} e^2}}\left(\frac{\boldsymbol{1}}{\boldsymbol{n_i}}\frac{\boldsymbol{dn_i}}{\boldsymbol{d\psi}} - \boldsymbol{0.5}\frac{\boldsymbol{1}}{\boldsymbol{T_i}}\frac{\boldsymbol{dT_i}}{\boldsymbol{d\psi}}\right)\left(\left\langle \frac{\boldsymbol{1}}{\boldsymbol{B^2}} \right\rangle - \frac{\boldsymbol{1}}{\langle \boldsymbol{B^2} \rangle}\right)$$

  - **inward flux for peaked density**, **outward flux for peaked temperature**

Important constraint for reactor design – negative impact of density peaking which is favoured for bootstrap current

- want to consider sum of classical, PS and banana-plateau at arbitrary, shape, number/amount of impurities - codes: NCLASS, NEOART, etc.

*simplified formalism from Helander and Sigmar

Impurity Density Asymmetries Modify Radial Neoclassical Impurity Transport

- poloidal n_z variation interacts with poloidal variation in magnetic field[1]
  - can **change the magnitude** of the standard neoclassical flux (P_A)
  - an **additional term** originating from the difference in poloidal flow (P_B)

$$\langle \boldsymbol{\Gamma_z \cdot \nabla\psi} \rangle = \frac{\boldsymbol{Z p_i m_i I^2}}{\boldsymbol{\tau_{ii} e^2}} \left[\left(\frac{\mathbf{1}}{\boldsymbol{n_i}} \frac{\boldsymbol{dn_i}}{\boldsymbol{d\psi}} - \mathbf{0.5} \frac{\mathbf{1}}{\boldsymbol{T_i}} \frac{\boldsymbol{dT_i}}{\boldsymbol{d\psi}} \right) \left(\left\langle \frac{\boldsymbol{n_z}}{\boldsymbol{B^2}} \right\rangle - \left\langle \frac{\boldsymbol{B^2}}{\boldsymbol{n_z}} \right\rangle^{-\mathbf{1}} \right) + \mathbf{0.33} \boldsymbol{f_c} \frac{\mathbf{1}}{\boldsymbol{T_i}} \frac{\boldsymbol{dT_i}}{\boldsymbol{d\psi}} \left(\frac{\langle \boldsymbol{n_z} \rangle}{\langle \boldsymbol{B^2} \rangle} - \left\langle \frac{\boldsymbol{B^2}}{\boldsymbol{n_z}} \right\rangle^{-\mathbf{1}} \right) \right]$$

- assume[1] $\varepsilon \ll 1,\ n_z/\langle n_z \rangle = 1 + \delta \cos\theta$

$$\langle \boldsymbol{\Gamma_z \cdot \nabla\psi} \rangle \sim \left[\left(\frac{\mathbf{1}}{\boldsymbol{n_i}} \frac{\boldsymbol{dn_i}}{\boldsymbol{d\psi}} - \mathbf{0.5} \frac{\mathbf{1}}{\boldsymbol{T_i}} \frac{\boldsymbol{dT_i}}{\boldsymbol{d\psi}} \right) \left(\mathbf{1} + \frac{\boldsymbol{\delta}}{\boldsymbol{\varepsilon}} + \frac{\boldsymbol{\delta^2}}{\mathbf{4}\boldsymbol{\varepsilon^2}} \right) + \mathbf{0.33} \boldsymbol{f_c} \frac{\mathbf{1}}{\boldsymbol{T_i}} \frac{\boldsymbol{dT_i}}{\boldsymbol{d\psi}} \left(\frac{\boldsymbol{\delta}}{\mathbf{2}\boldsymbol{\varepsilon}} + \frac{\boldsymbol{\delta^2}}{\mathbf{4}\boldsymbol{\varepsilon^2}} \right) \right]$$

- $-1 < \delta < 1$ depending on driving asymmetry[2] $T_Z = T_e = T_i\ , Z_{eff} = 1$

$$\frac{\delta}{\varepsilon} = 2 \left[\frac{m_z \omega^2 R_o^2}{2T_i} \left(1 - \frac{Z m_i}{2 m_z} \right) - \frac{Z f_m}{2} \left(\frac{T_\perp}{T_\parallel} - 1 \right) \right]$$

- for large asymmetries, the neoclassical flux is enhanced by $\sim 1/\varepsilon^2$
- codes like NEO solve parallel + radial force balance self-consistently for the centrifugal force should be valid at high main-ion Mach numbers, arbitrary ε

[1]C. Angioni & P. Helander PPCF **56** 124001 (2014) [2]M.L. Reinke PhD Thesis (2011)

Impurity Density Asymmetries Can Weaken or Enhance Effect of Temperature Screening

- poloidal n_z variation interacts with poloidal variation in magnetic field[1]
  - have **change the magnitude (P_A)** and **additional term (P_B)** and add back in the **diffusive term**[2] ordered out as 1/Z

$$\langle \Gamma_z \cdot \nabla\psi \rangle \sim \left[\left(\frac{1}{n_i}\frac{dn_i}{d\psi} - 0.5\frac{1}{T_i}\frac{dT_i}{d\psi} - \frac{1}{Z}\frac{1}{n_z}\frac{dn_z}{d\psi} \right) P_A + 0.33 f_c \frac{1}{T_i}\frac{dT_i}{d\psi} P_B \right]$$

  - Compute the zero-flux impurity density scale length: a/L_{nZ}

$$\frac{a}{L_{n,Z}} = Z\left(\frac{a}{L_{n,i}} - 0.5\frac{a}{L_{T,i}}\right) + 0.33\frac{Z f_c P_B}{P_A}\frac{a}{L_{T,i}}$$

$\delta/\varepsilon = 0, P_A = 1 \;\&\; P_B = 0$

$|\delta|/\varepsilon \sim 1$ modifies effect of temperature screening, RF effects enhance it

CF effects weaken it

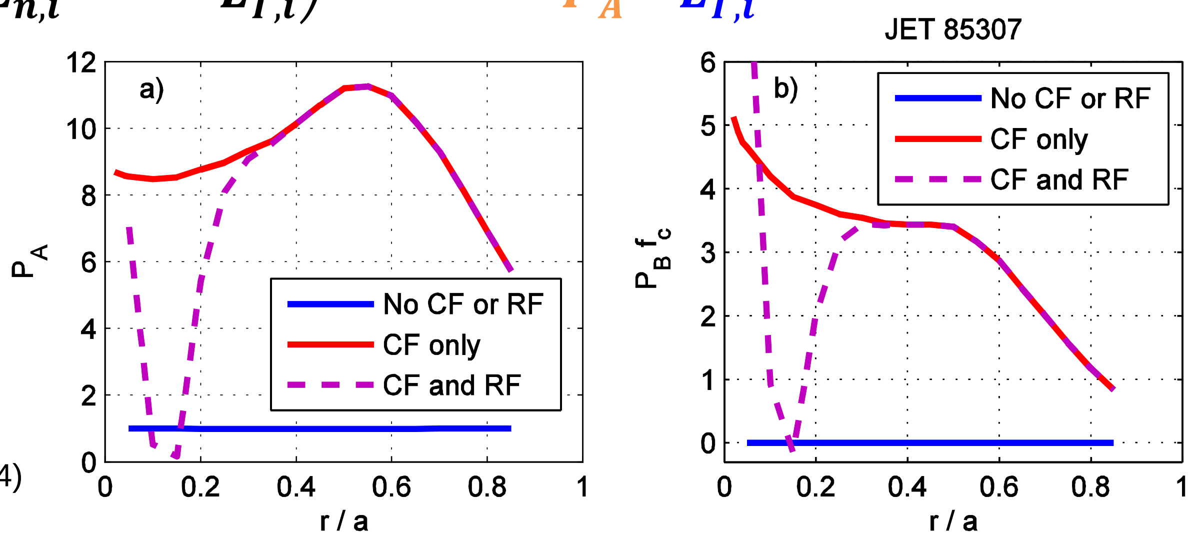

[1]C. Angioni & P. Helander PPCF **56** 124001 (2014)
[2]F. Casson, *et al*. PPCF **57** 014031 (2015)

Impurity Density Asymmetries Can Weaken or Enhance Effect of Temperature Screening

- poloidal n_z variation interacts with poloidal variation in magnetic field[1]
  - have **change the magnitude (P_A)** and **additional term (P_B)** and add back in the **diffusive term[2]** ordered out as 1/Z

$$\langle \Gamma_z \cdot \nabla\psi \rangle \sim \left[\left(\frac{1}{n_i}\frac{dn_i}{d\psi} - 0.5\frac{1}{T_i}\frac{dT_i}{d\psi} - \frac{1}{Z}\frac{1}{n_z}\frac{dn_z}{d\psi} \right) P_A + 0.33 f_c \frac{1}{T_i}\frac{dT_i}{d\psi} P_B \right]$$

  - Compute the zero-flux impurity density scale length: a/L_{nZ}

$$\frac{a}{L_{n,Z}} = Z\left(\frac{a}{L_{n,i}} - 0.5\frac{a}{L_{T,i}}\right) + 0.33\frac{Z f_c P_B}{P_A}\frac{a}{L_{T,i}}$$

$\delta/\varepsilon = 0, P_A = 1 \;\&\; P_B = 0$

$|\delta|/\varepsilon \sim 1$ modifies effect of temperature screening, RF effects enhance it

CF effects weaken it

$|\delta|/\varepsilon \gg 1$ then $P_B/P_A \rightarrow 1$

then strong LFS or HFS impurity localization will both increase the magnitude of the neoclassical flux and alter the a/LnZ profile

impact at high ν_* can be larger[3]

[1]C. Angioni & P. Helander PPCF **56** 124001 (2014)

[2]F. Casson, *et al*. PPCF **57** 014031 (2015)

[3]E. Belli, *et al*. PPCF **56** 124002 (2014)

Turbulent Impurity Transport With Poloidal Density Asymmetries

- additional drift terms from mechanisms that cause asymmetries to be included in gyrokinetic formalism
  - Coriolis, centrifugal, E×B ($E_\theta \times B_\phi$ – w/ magnetic shear dependence)
- interaction of the poloidally varying density with the poloidally varying mode structure; *'in/out' asymmetries & ballooning modes*
- [Mollen – PoP **19** 052307 (2012)]: using GYRO to compute turbulence, analytical model to compute zero-flux a/LnZ
  - assumes poloidal n_z variation just due to $\Phi(\theta)$ – valid for ICRH asym.
- [Angioni – PoP **19**122311 (2012)]: using GKW to compute quasi-linear impurity fluxes, and impact of asymmetries
  - includes rotation and non-thermal $\Phi(\theta)$ – valid for ICRH & centrifugal

trace limit, $Z^2 n_Z / n_i << 1$ typically well satisfied for high-Z impurities, thus they don't contribute to turbulence, $\langle \Gamma_z \cdot \nabla\psi \rangle$ post-processed

Combination of Turbulent and Neoclassical Flux

$$\frac{\Gamma_z}{n_z} = D_Z^{TURB} \left.\frac{R}{L_{nZ}}\right|_{\theta=0} + D_Z^{NEO} \left.\frac{R}{L_{nZ}}\right|_{\theta=0} + RV_Z^{TURB} + RV_Z^{NEO}$$

$$\frac{R}{L_{nZ}} = \frac{\frac{\chi_{i,AN}}{\chi_{i,NEO}} \frac{RV_Z^{TURB}}{\chi_{i,TURB}} + \frac{RV_Z^{NEO}}{\chi_{i,NEO}}}{\frac{\chi_{i,AN}}{\chi_{i,NEO}} \frac{RD_Z^{TURB}}{\chi_{i,TURB}} + \frac{RD_Z^{NEO}}{\chi_{i,NEO}}}$$

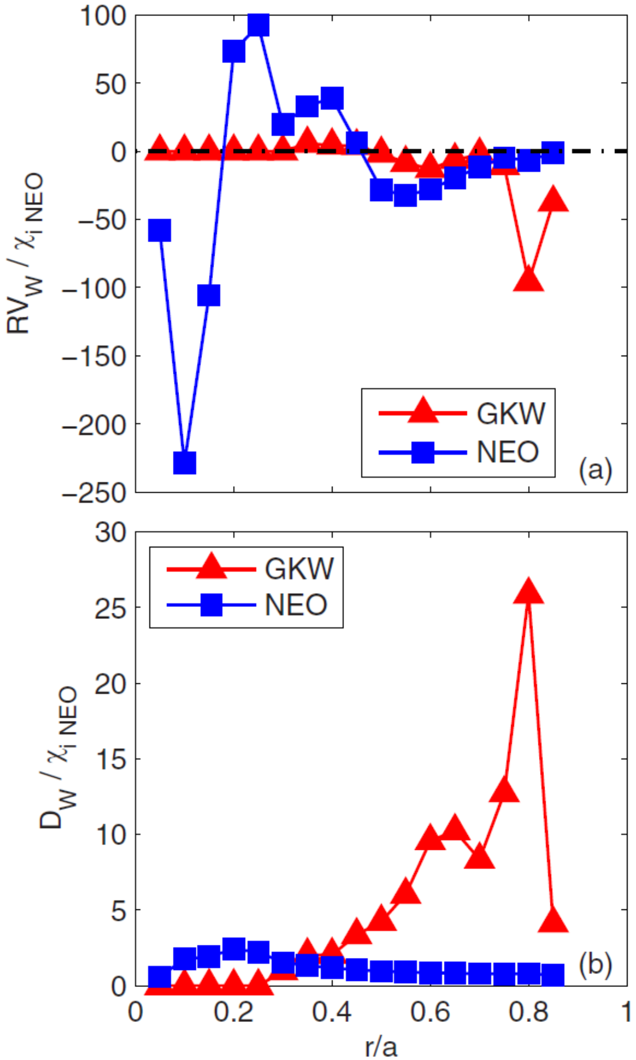

C. Angioni, *et al*. NF **54** 083028 (2014)

- assume $\chi_{i,AN} = \chi_{i,PB} - \chi_{i,NEO}$ and scale the computed turbulent contributions to experiment
- an important factor will be where be where the turbulent diffusion is too weak to balance the (likely) dominant neoclassical convection
  - transition from a ‘flat’ high-Z profile to one shaped by neoclassical transport

Effect of Auxiliary Heating on Core Transport

- many prior demonstrations of ICH & ECH being used to mitigate/avoid core neoclassical peaking, but mechanism(s) still under investigation
  [R. Dux, PPCF 45 1815 (2003)], [D. Ernst, PoP 11 2637 (2004)], [H. Takenaga NF **43** 235 (2003)]
  - stimulating turbulence to increase anomalous impurity diffusivity?
  - change main-ion profiles to modify standard neoclassical flux?
  - change impurity asymmetry to modify neoclassical flux terms?
  - other effects: MHD, fast-ion impurity friction?
  - (lots of recent work on JET and AUG see: EPS 2013, 2014)
- impact for NSTX-U plans to move to a high-Z wall
  - want to understand the role large asymmetries play in neoclassical transport as centrifugal force will be present and likely dominate
  - what/where is the balance of neoclassical and anomalous impurity transport in an ST which has reduced ITG turbulence?
  - how can the (limited/different) set of wave-heating tools be used to mitigate effects possible on-axis accumulation

What Level of Understanding is Required?

- atomic physics uncertainty limits accuracy of a/LnZ ~ 2, making quantitative validation efforts difficult (for foreseeable future)
- a primary concern is conditions which lead to strong impurity peaking, **a/LnZ > 10**, which reduces the acceptable 0-D high-Z fraction (f_W)
  - **'profile stability' limit when high-Z peaking leads to local radiation exceeding local heating**

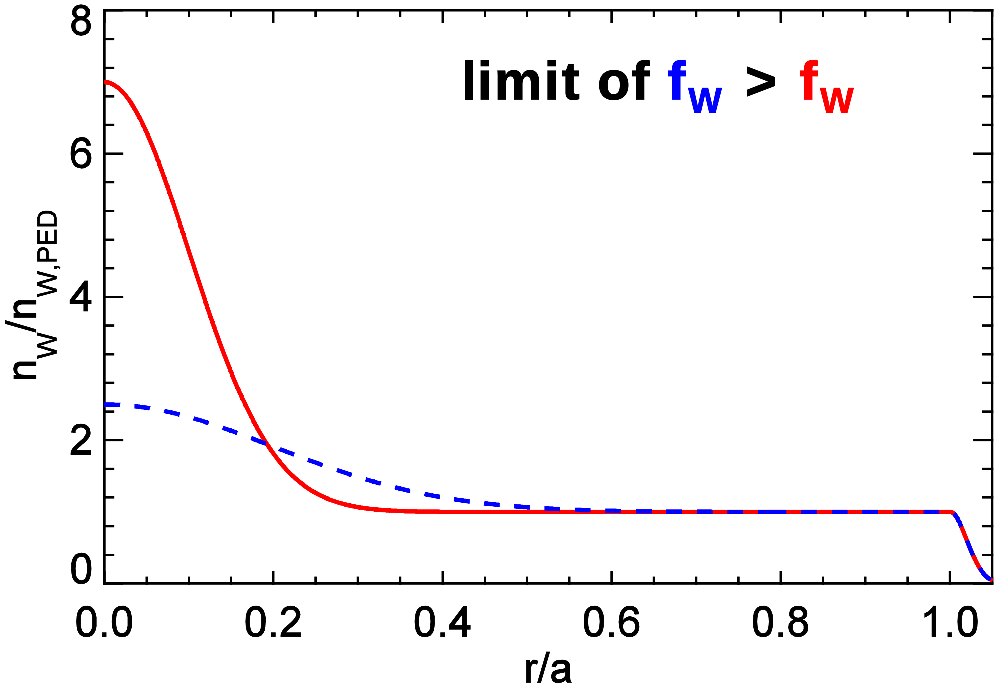

What Level of Understanding is Required?

- atomic physics uncertainty limits accuracy of a/LnZ ~ 2, making quantitative validation efforts difficult (for foreseeable future)
- a primary concern is conditions which lead to strong impurity peaking, **a/LnZ > 10**, which reduces the acceptable 0-D high-Z fraction (f_W)
  - **'profile stability' limit when high-Z peaking leads to local radiation exceeding local heating**

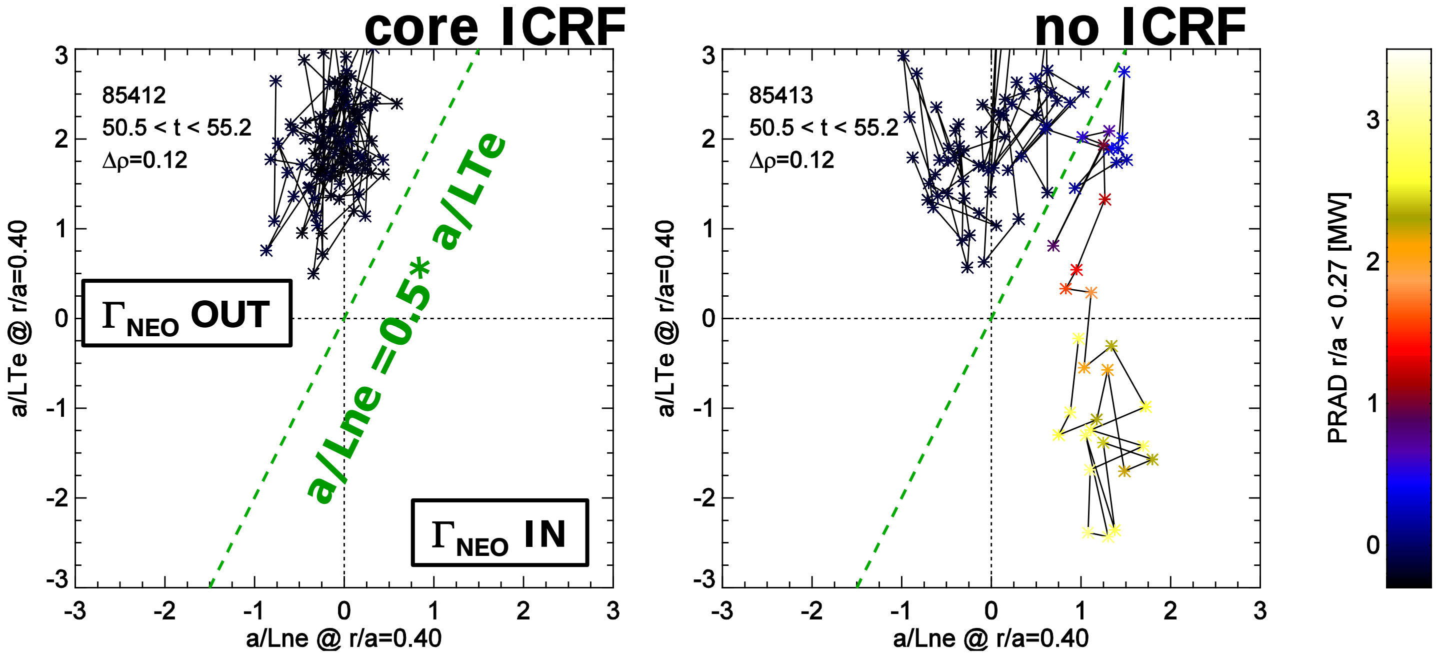

$$\frac{a}{L_X} = -\frac{a}{X}\frac{dX}{dr}$$

more details: see C. Giroud EPS 2014
(submitted to PPCF)

What Level of Understanding is Required?

- atomic physics uncertainty limits accuracy of a/LnZ ~ 2, making quantitative validation efforts difficult (for foreseeable future)
- a primary concern is conditions which lead to strong impurity peaking, **a/LnZ > 10**, which reduces the acceptable 0-D high-Z fraction (f_W)
  - **'profile stability' limit when high-Z peaking leads to local radiation exceeding local heating**
- desire to understand **how/why** core auxiliary heating avoids peaking through changes in: neo & turbulent transport, changes in MHD, etc.
- we also want to be able to tailor the confined plasma radiation profile
- high-Z impurities can help solve the divertor exhaust problem in systems where P_{SEP}/R is large (i.e. DEMO)
  - can radiate massive amounts of power without diluting fusion reactions

Diagnosis and Interpretation of High-Z Impurity Emission

Example: Diagnosing Tungsten on JET

- rotation drives LFS localization, leads to a problem of *diagnosing* the 0-D tungsten concentration

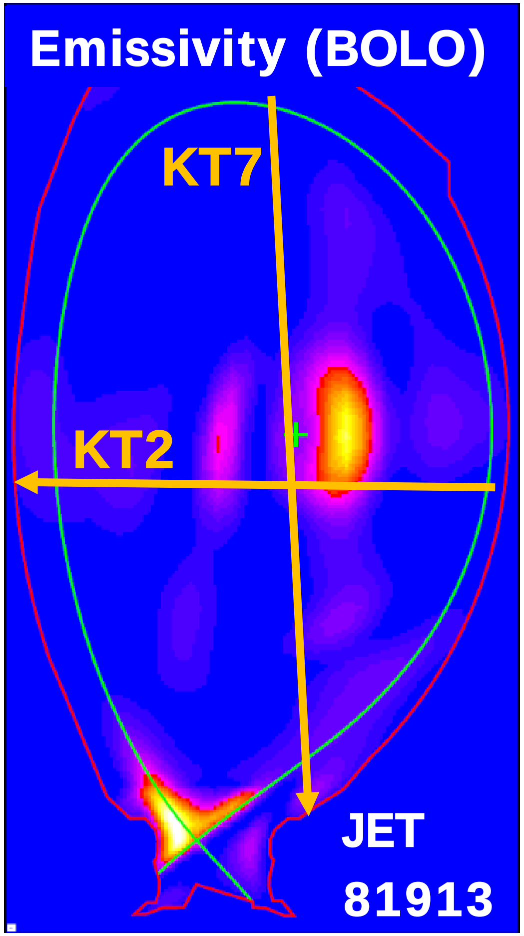

E. Joffrin, *et al*. Nucl. Fusion **54** (2014) 013011

Example: Diagnosing Tungsten on JET

- rotation drives LFS localization, leads to a problem of *diagnosing* the 0-D tungsten concentration
- motivated the development of a multi-diagnostic ‘W-analyzer’
  - VUV spec. vertical and horizontal SXR cameras
  - remove bremsstrahlung & metal contribution [Ni, Cu] (symmetric)
  - fit remainder to centrifugal ‘form’ of emissivity [R. Dux NF 1999]

$$\varepsilon(\rho, R) = \varepsilon(\rho, R_o)\, exp\left[\lambda(\rho)\left(R^2 - R_o^2\right)\right]$$

  - $\lambda(\rho)$ function of ω_ϕ and can be checked against CXRS data

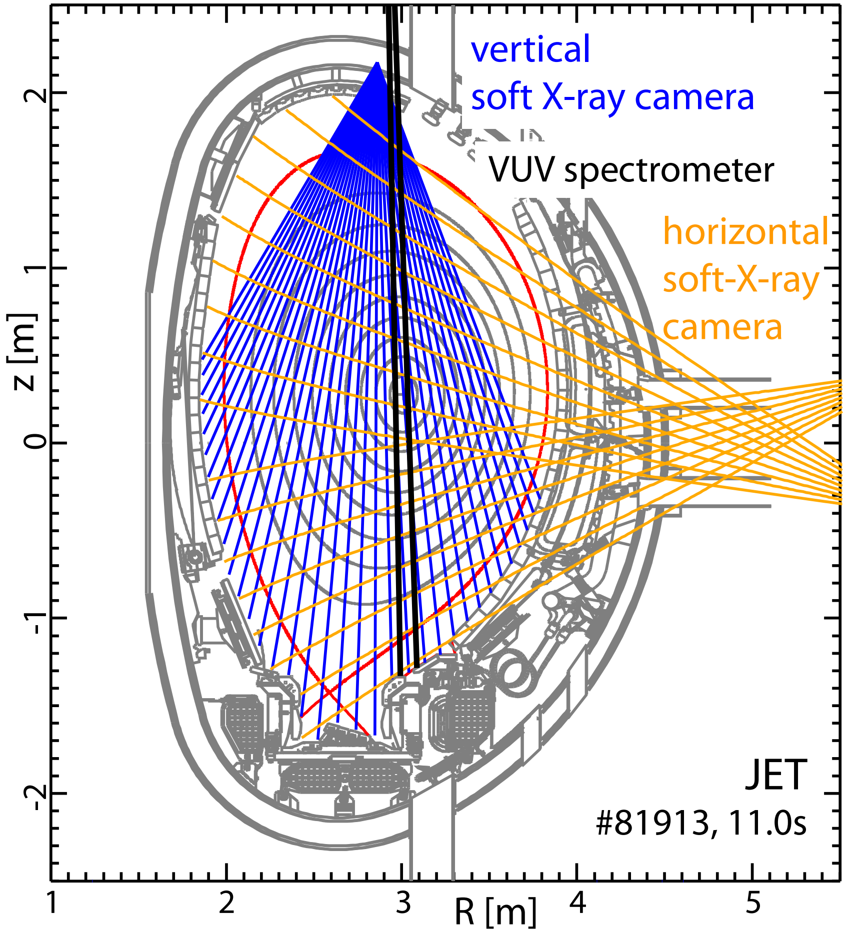

T. Püetterich – IAEA 2012, E1/E2 TF meeting 2013

Challenges in Interpreting High-Z Emissivity

EXAMPLE: Tungsten for JET Soft X-Ray

$$n_W = \frac{\varepsilon_{SXR}(r)}{n_e L_W(T_e)}$$

$$\frac{\nabla n_W}{n_W} = \frac{\nabla \varepsilon_{SXR}}{\varepsilon_{SXR}} - \frac{T_e}{L_W}\left({}^{\partial L_w}/_{\partial T_e}\right)\frac{\nabla T_e}{T_e} - \frac{\nabla n_e}{n_e}$$

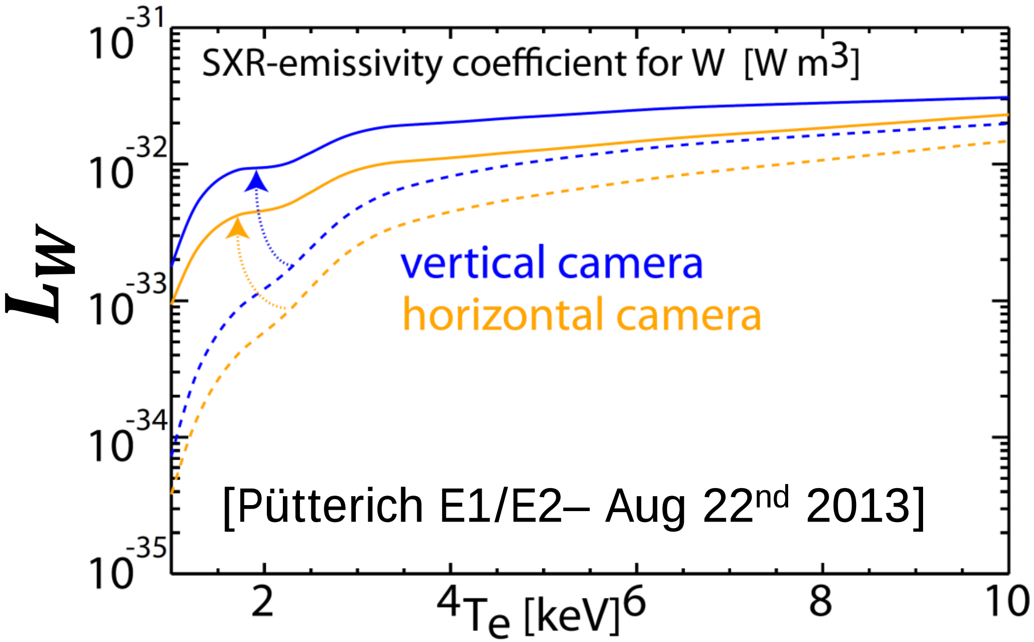

- high ion/rec rates lead to coronal W charge state distribution
- use SXR emissivity to compute density profile
- originally calculated rates (----) inconsistent with VUV emission & total radiation
  - atomic physics?
  - SXR diode/filter damage?
- proposed change has implication on $\nabla n_W/n_W$

Utilize Resistive Bolometers to *In-Situ* Calibrate the SXR System for Tungsten Density Profiles

Empirically Determine $L_{W,SXR}(T_e)$ from $L_{W,BOLO}(T_e)$

$$L_{W,SXR}(T_e) = L_{W,BOLO}(T_e)\left(\frac{\varepsilon_{SXR} - n_e^2 Z_{eff} L_{Brem,SXR}(T_e)}{\varepsilon_{BOLO} - n_e^2 Z_{eff} L_{Brem,BOLO}(T_e)}\right)$$

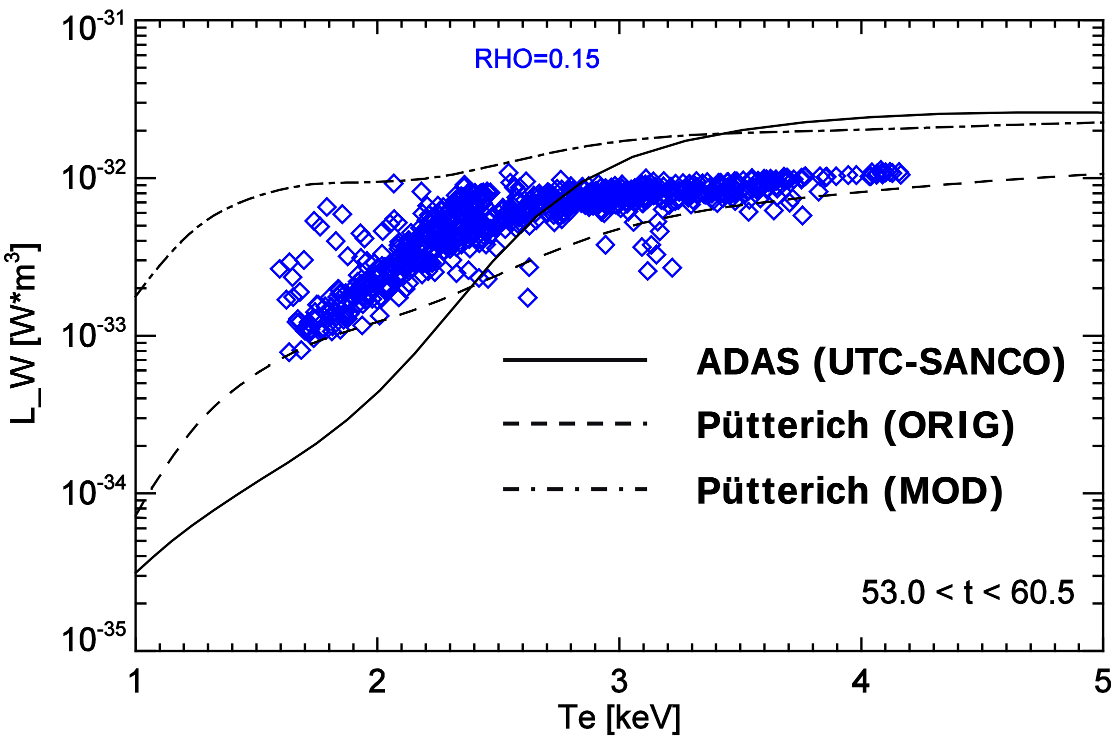

- on-axis ICRF power scan in a simple L-mode plasma
  - 'standard candle'
- estimate local n_W from **bolometry** and compare to **SXR emission**
- as plasma T_e increases (ICRF, sawteeth) **a smooth L_W curve** is drawn at each radius

$L_{W,BOLO}$ from T. Pütterich, *et. al.* Nucl. Fusion **50** 025012 (2010)

Example: Diagnosing Tungsten on Alcator C-Mod

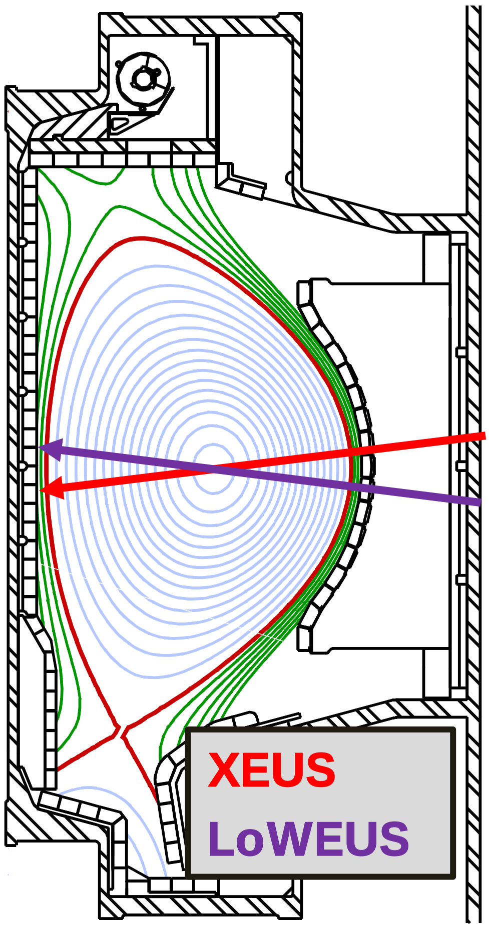

- use XEUS and LoWEUS through LLNL collaboration
  - ‘classic’ SPRED does not resolve tungsten
- nearly radial view through core makes brightness measurements ~insensitive to poloidal asymmetries
- XEUS: measure quasi-continuum W^{27+}-W^{35+}

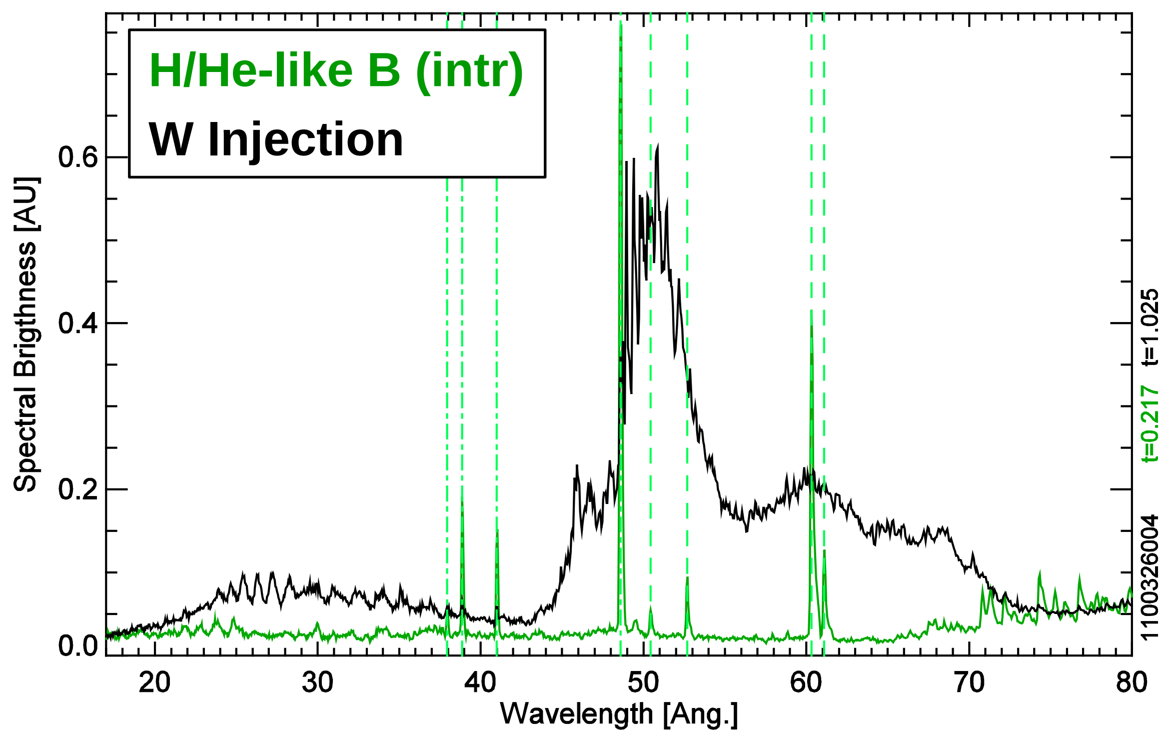

Example: Diagnosing Tungsten on Alcator C-Mod

- use XEUS and LoWEUS through LLNL collaboration
- nearly radial view through core makes brightness measurements ~insensitive to poloidal asymmetries
- XEUS: measure quasi-continuum W^{27+}-W^{35+}
- LoWEUS: measure discrete lines W^{40+}-W^{45+}

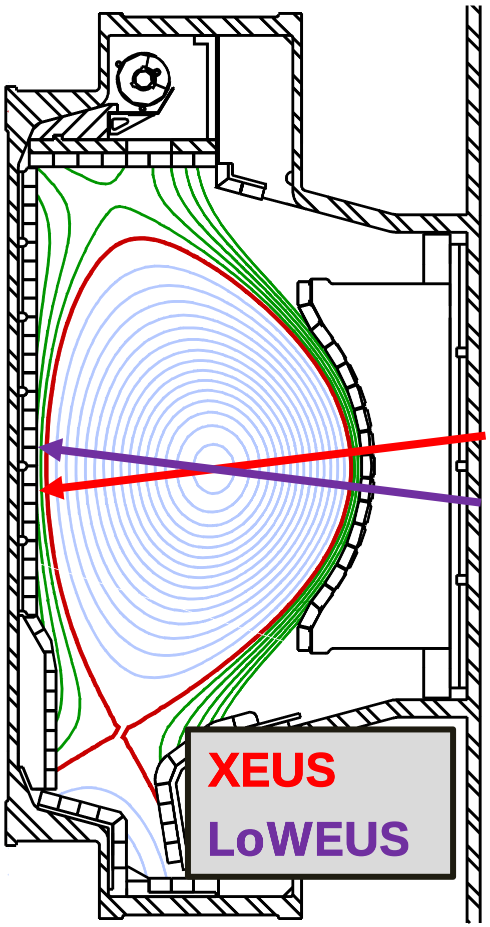

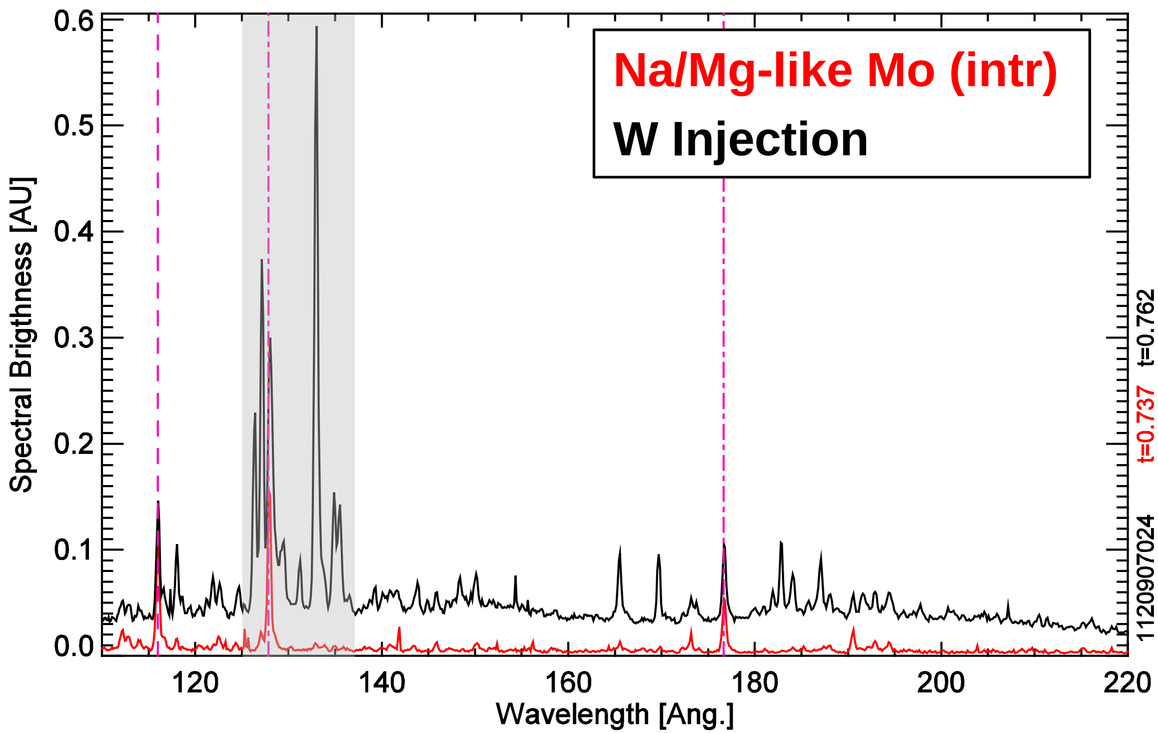

Higher T_e (> 3 keV) Forces X-Ray Measurements

- use XEUS and LoWEUS through LLNL collaboration
- nearly radial view through core makes brightness measurements ~insensitive to poloidal asymmetries
- XEUS: measure quasi-continuum W^{27+}-W^{35+}
- LoWEUS: measure discrete lines W^{40+}-W^{45+}

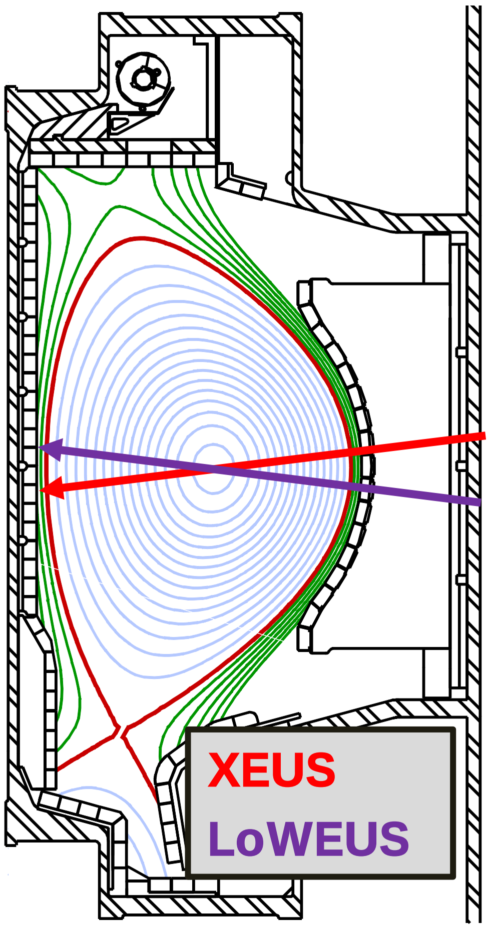

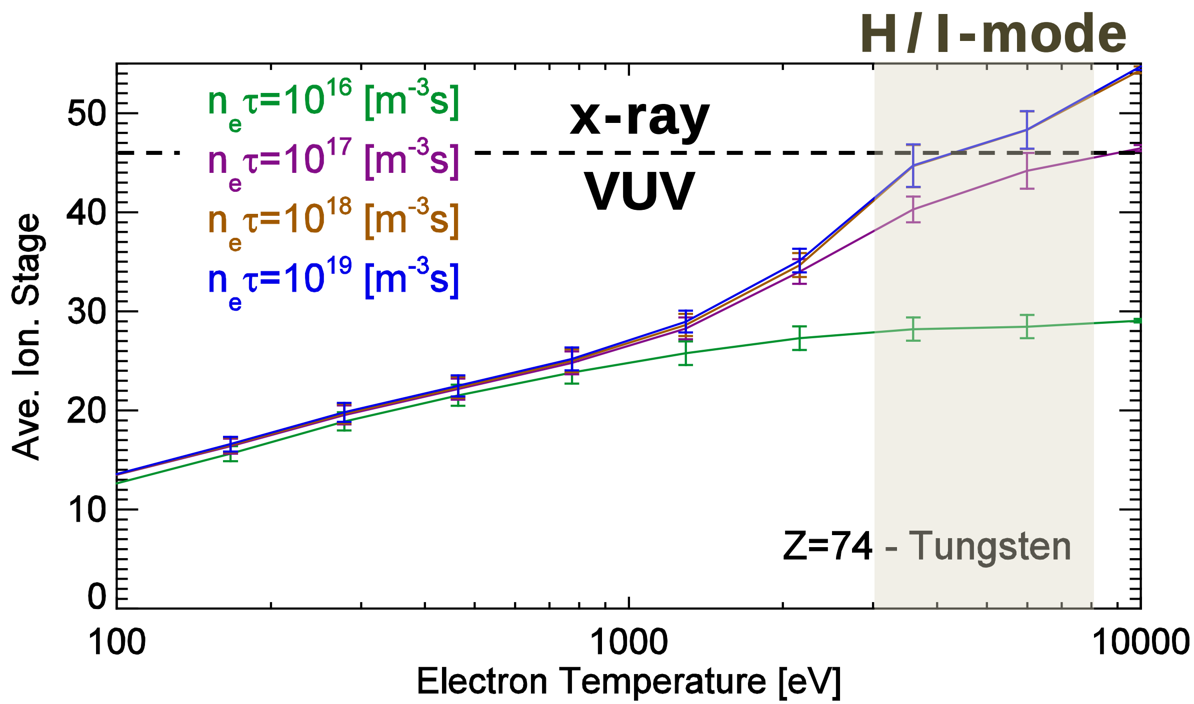

X-Ray Imaging Crystal Spectroscopy for Radial Profiles from Partially-Ionized Impurities

spherically-bent crystals and advanced x-ray imaging detectors have enabled spatially resolved measurements

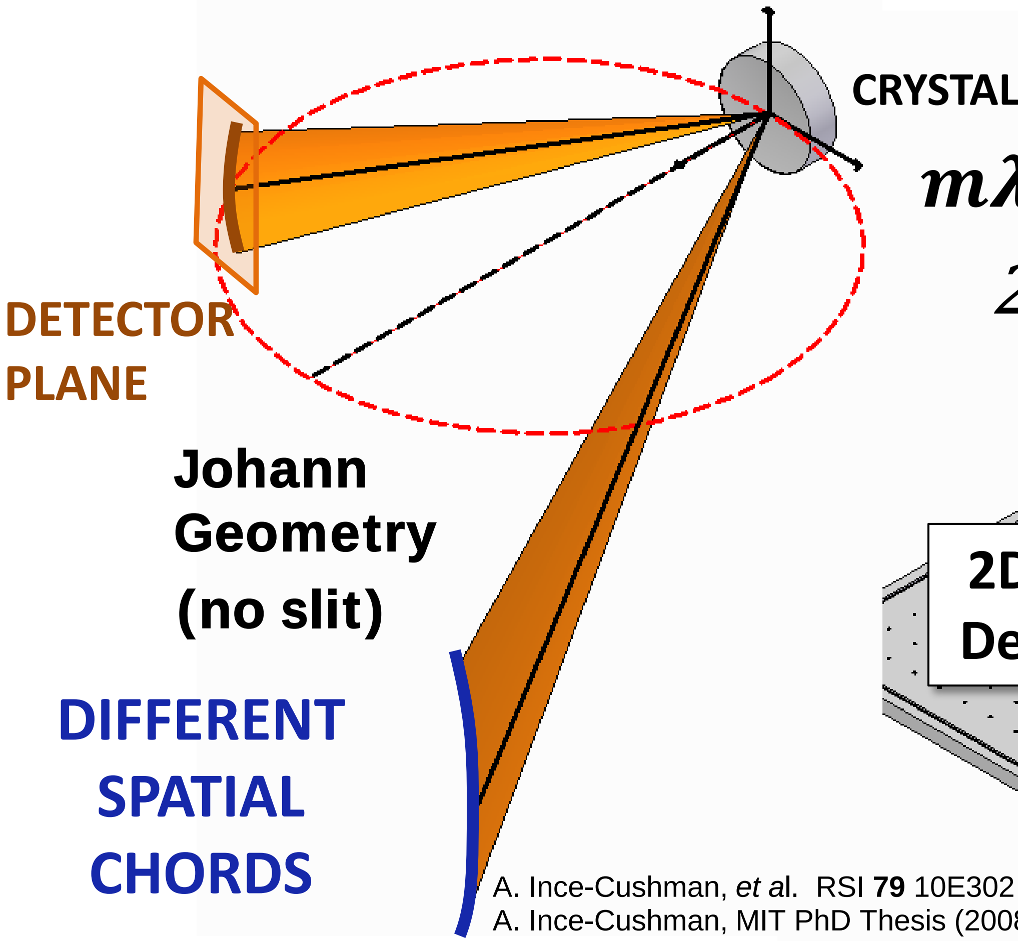

$$m\lambda = 2d \sin\theta$$

$$2d = 4.56\ \text{Å}$$

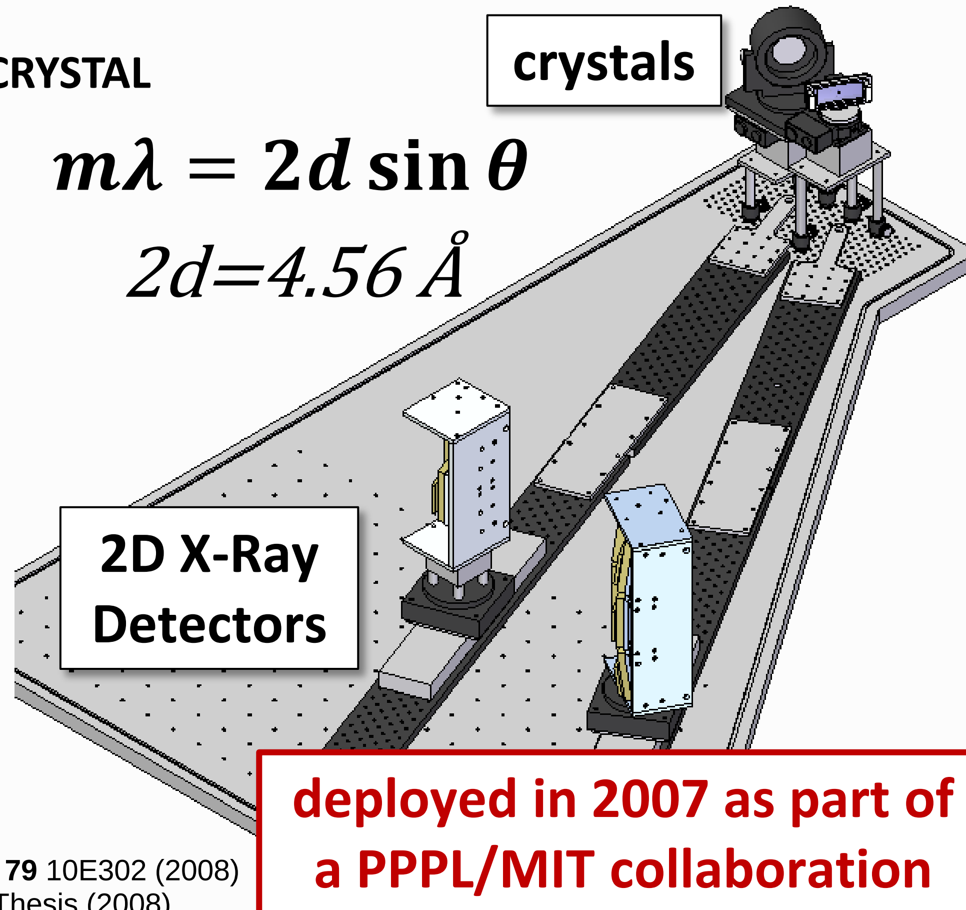

A. Ince-Cushman, *et al*. RSI **79** 10E302 (2008)
A. Ince-Cushman, MIT PhD Thesis (2008)

deployed in 2007 as part of a PPPL/MIT collaboration

Technology Advance Allows High Resolution Imaging of Full C-Mod Plasma Cross-Section

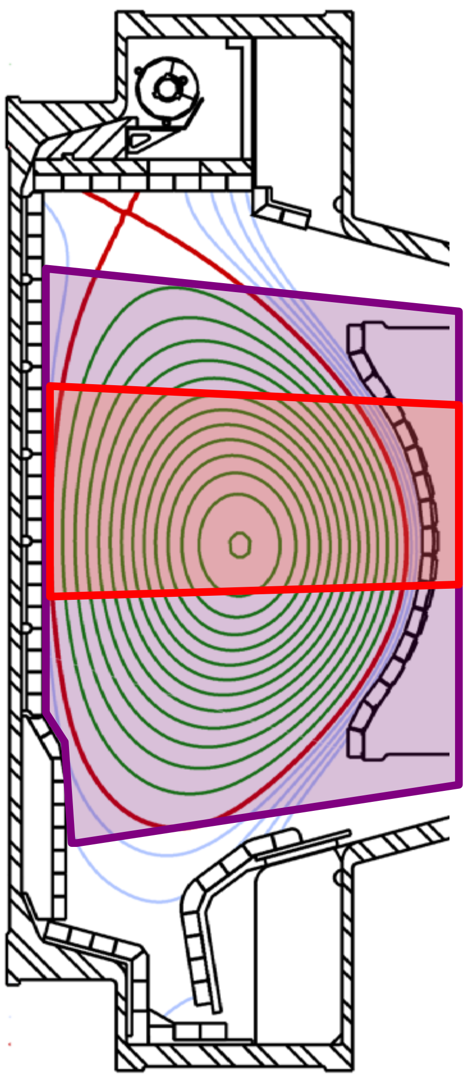

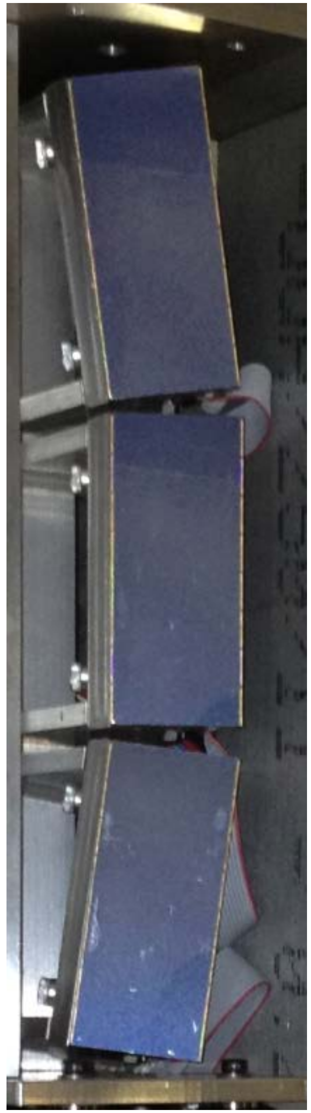

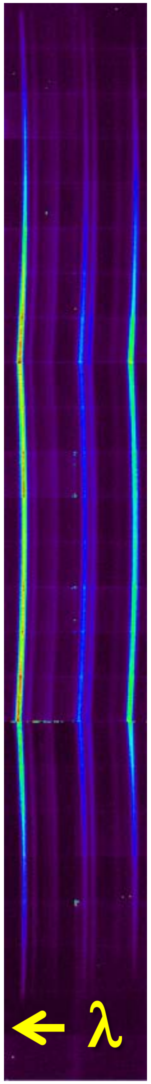

uses the Pilatus [DECTRIS]

- 195 x 487 pixels (0.172 mm)
- each pixel is an individual photon counter ($d\gamma/dt < 10^6$ /s)
- 200 Hz frame rate
- E_γ > 3 keV (newer > 1.75 keV)

full poloidal cross-section measured using x3 detectors viewing Ar^{16+}

core measured using with single detector, Ar^{17+}

used for LBO impurity transport experiments (Ca^{18+})

N.T. Howard *et al Nucl. Fusion* **52** 063002 (2012)

XICS Enables Radial Profiles of Impurity Flow and Temperature in Plasmas w/o Neutral Beams

- Doppler tomography used to invert line-integrated measurements to find local plasma data [M.L. Reinke, *et al*. RSI **83**, 113504 (2012) & PSFC/RR-11-9 (2013)]
- demonstration of technique by comparing ion temperature reconstruction from **peaked H-like argon** and **hollow He-like argon**

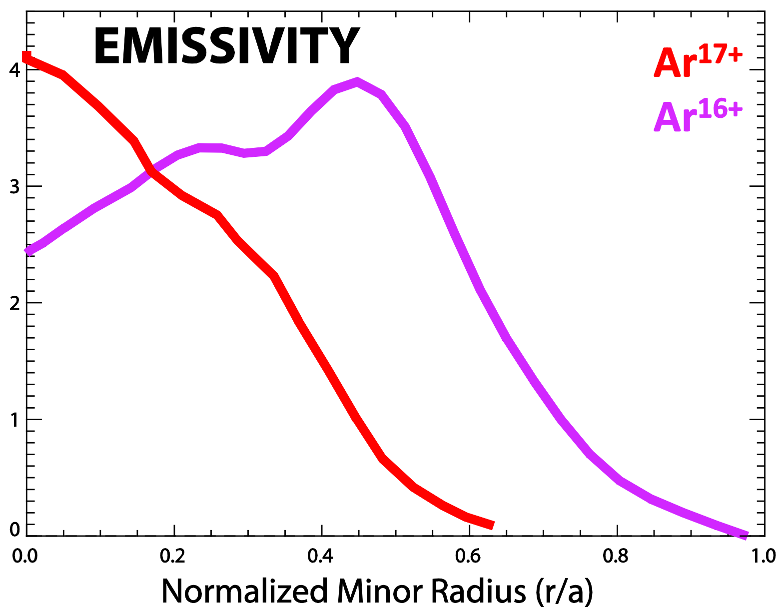

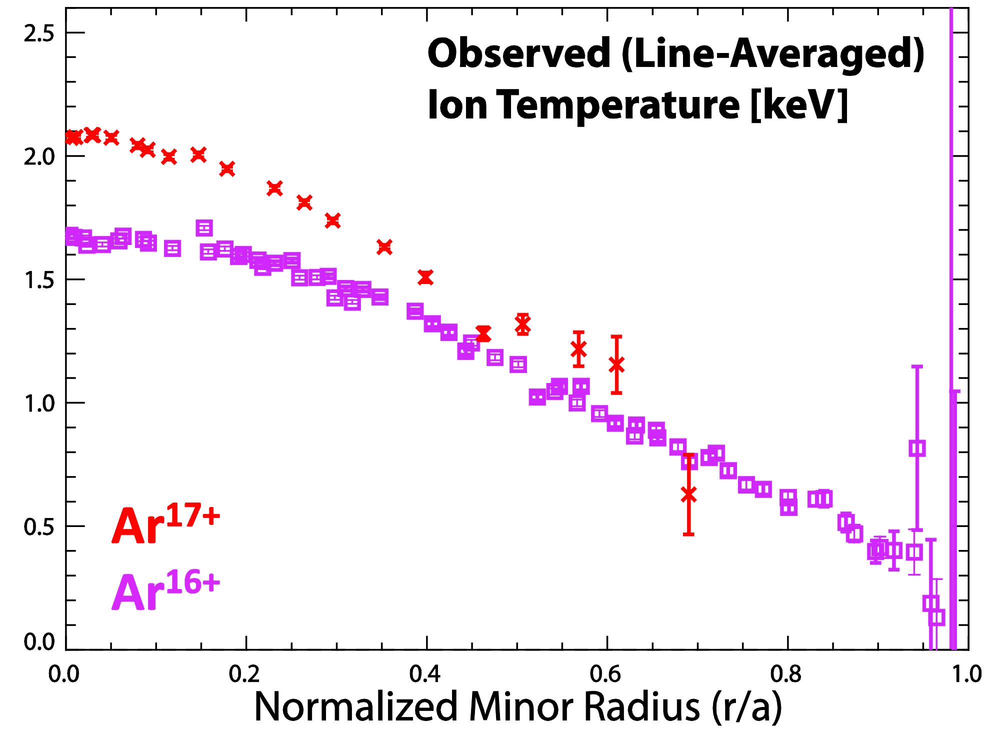

XICS Enables Radial Profiles of Impurity Flow and Temperature in Plasmas w/o Neutral Beams

- Doppler tomography used to invert line-integrated measurements to find local plasma data [M.L. Reinke, *et al*. RSI **83**, 113504 (2012) & PSFC/RR-11-9 (2013)]
- demonstration of technique by comparing ion temperature reconstruction from **peaked H-like argon** and **hollow He-like argon**
- difference in observed ion temperature vanishes after inversion

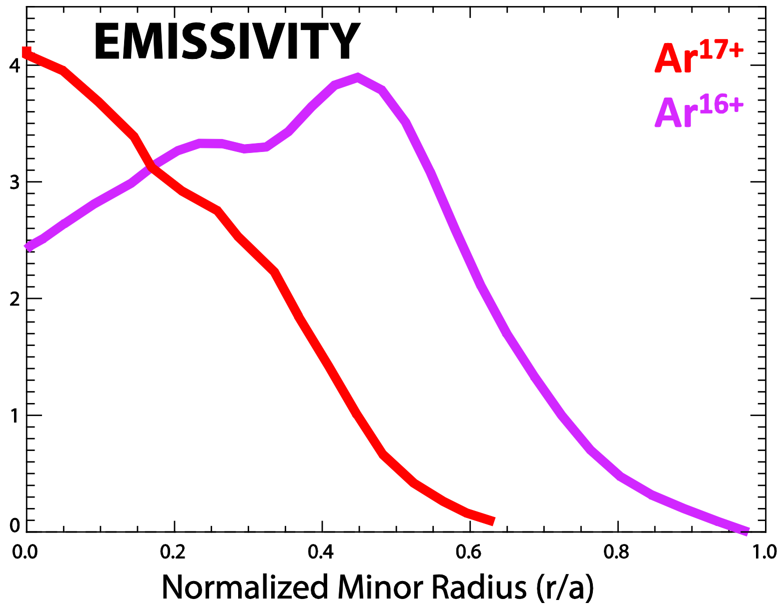

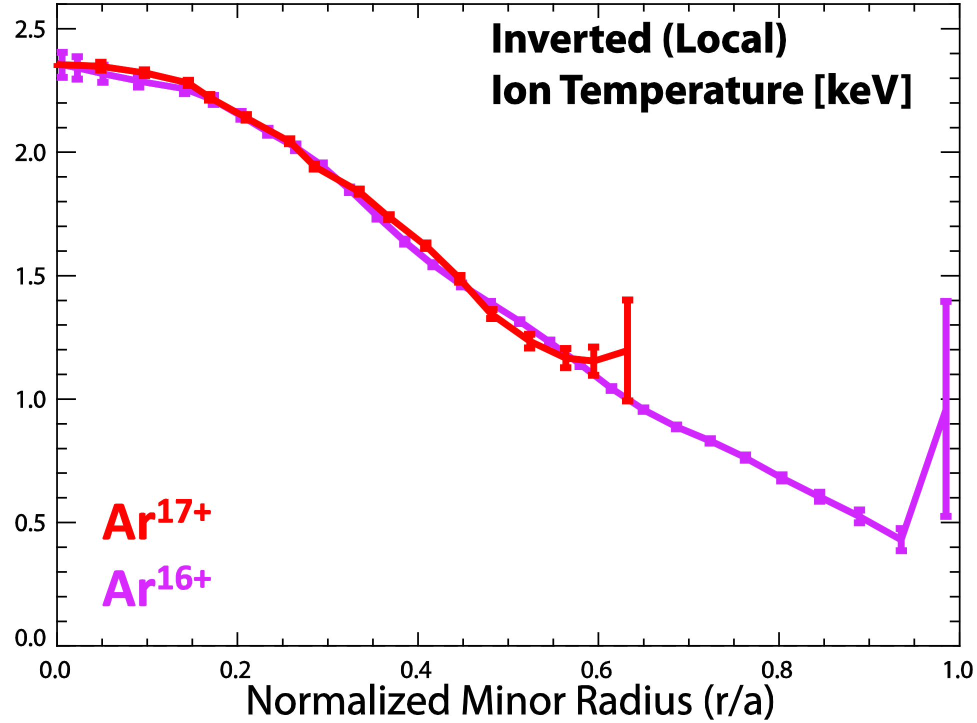

C-Mod XICS Used to Validate Atomic Physics Models Used for Line-Ratio T_e Profiles

- He-like argon spectrum contains lines populated by a variety of mechanisms leading to a sensitivity to electron temperature

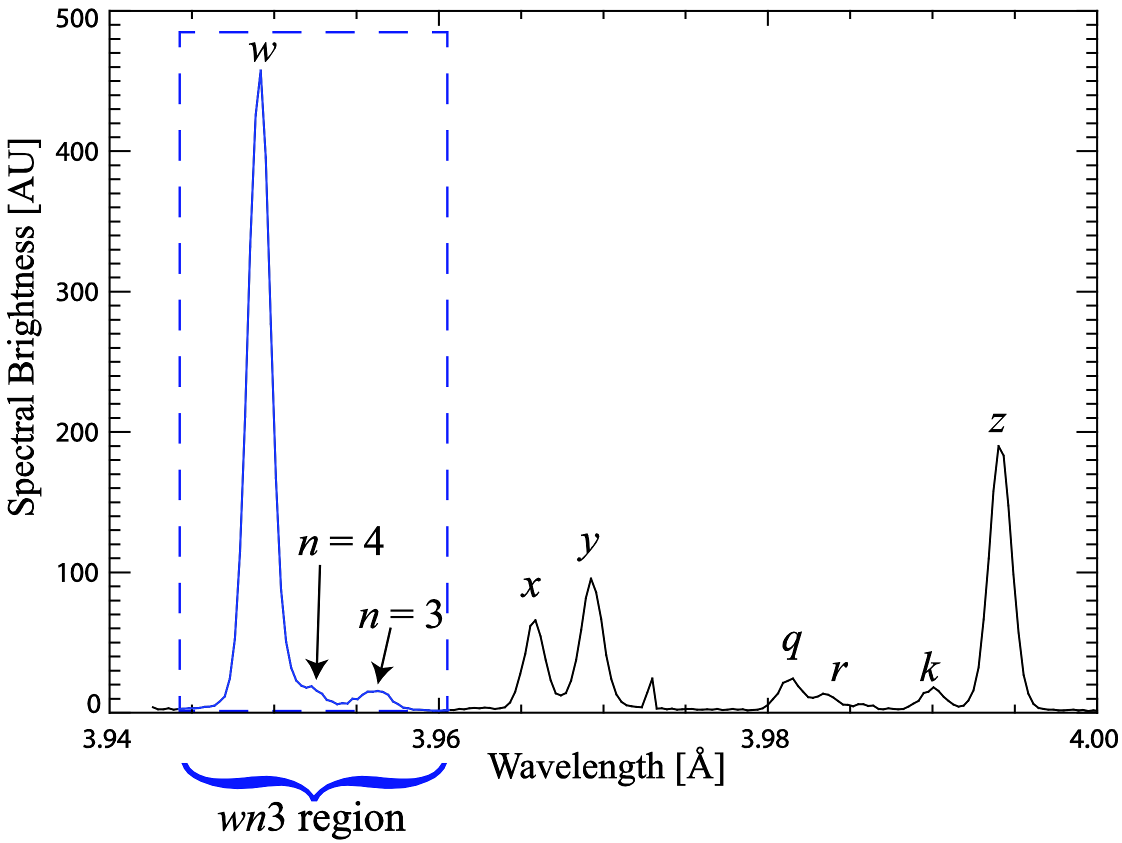

intense $1s^2$-1s2p line (w) populated by excitation (threshold reaction)

weaker n ≥ 3 satellite lines populated by dielectronic recombination (resonance reaction)

A. Rosen, *et al.* J.Phys. B. **47** 105701 (2014)

C-Mod XICS Used to Validate Atomic Physics Models Used for Line-Ratio T_e Profiles

- He-like argon spectrum contains lines populated by a variety of mechanisms leading to a sensitivity to electron temperature

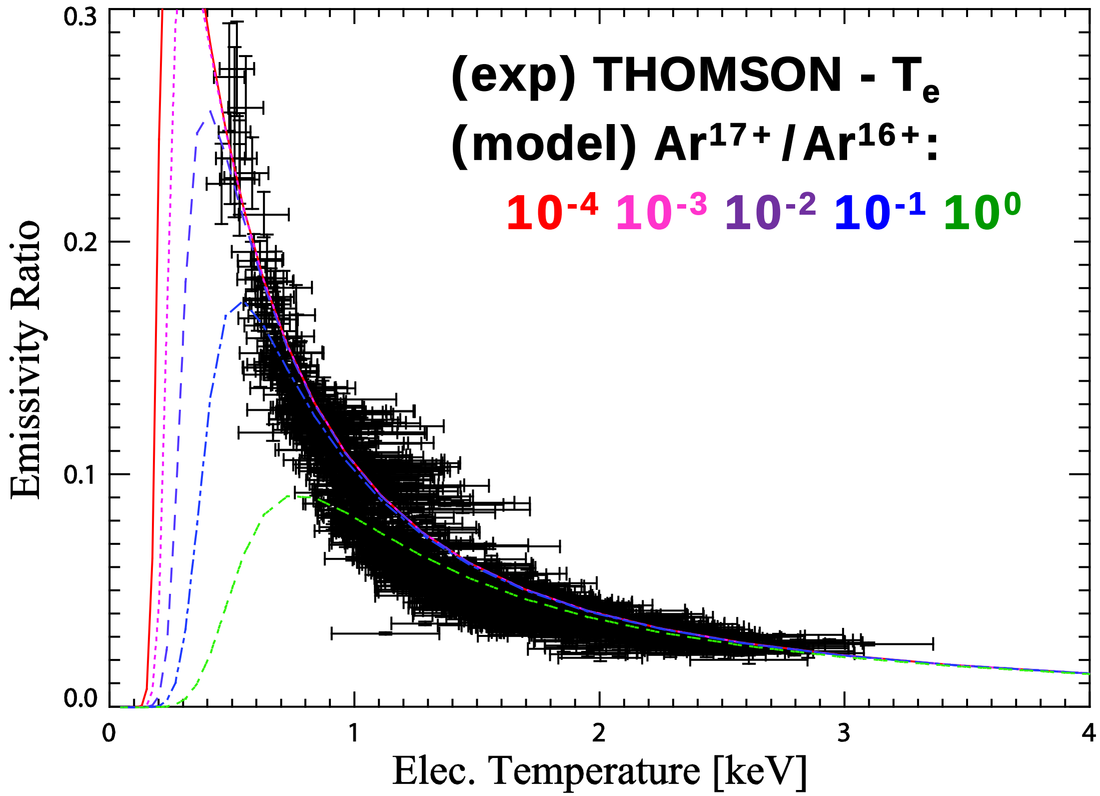

- compared to ECE/TS independent measures of T_e in Ohmic plasmas
- inverted data compares ***emissivity*** ratio to T_e

A. Rosen, *et al.* J.Phys. B. **47** 105701 (2014)

C-Mod XICS Used to Validate Atomic Physics Models Used for Line-Ratio T_e Profiles

- He-like argon spectrum contains lines populated by a variety of mechanisms leading to a sensitivity to electron temperature

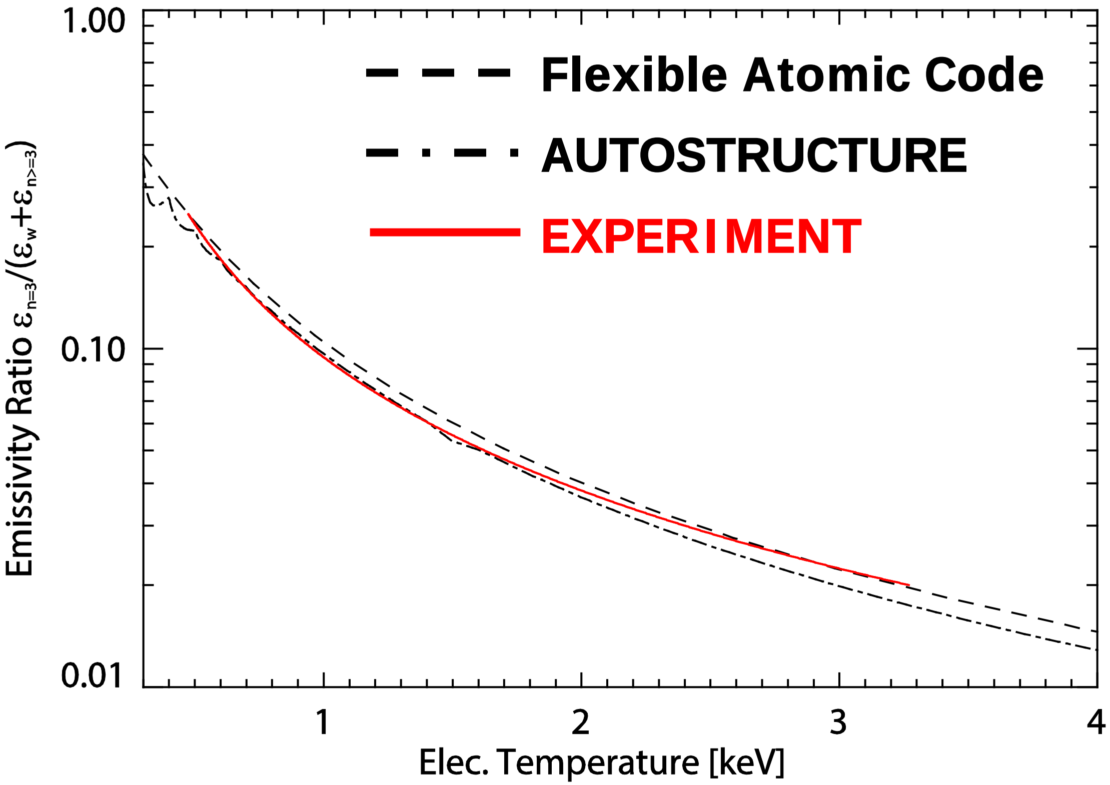

A. Rosen, *et al.* J.Phys. B. **47** 105701 (2014)

- compared to ECE/TS independent measures of T_e in Ohmic plasmas
- inverted data compares *emissivity* ratio to T_e
- results compare well to multiple codes
  - not too surprising
- question of systematic error in using technique for $\nabla T_e/T_e$

Imaging X-Ray Spectroscopy During Laser Ablation of Molybdenum

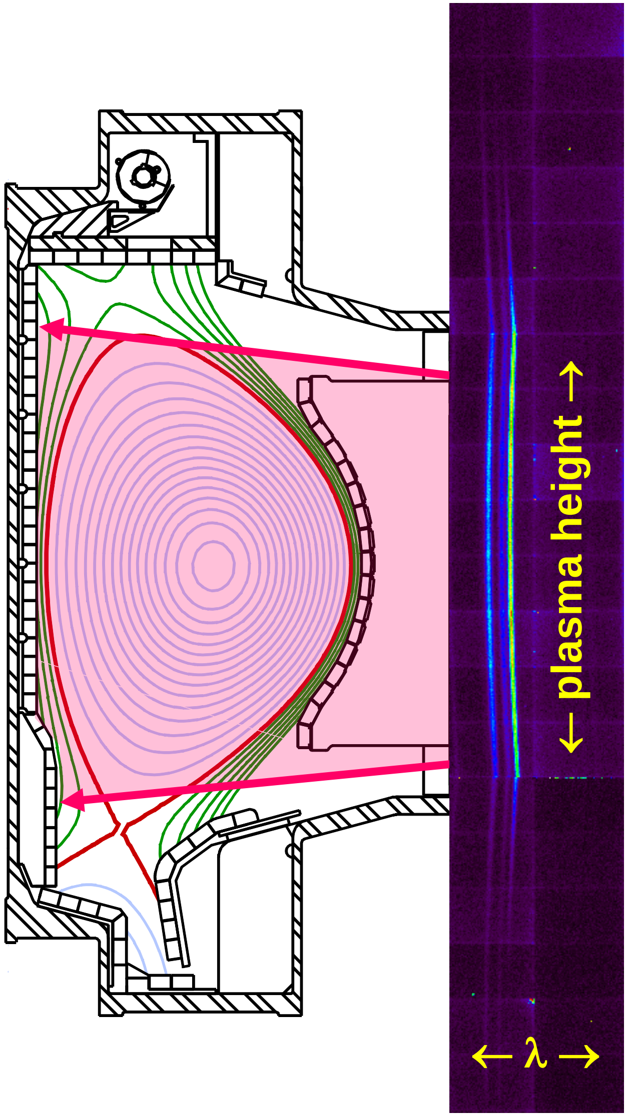

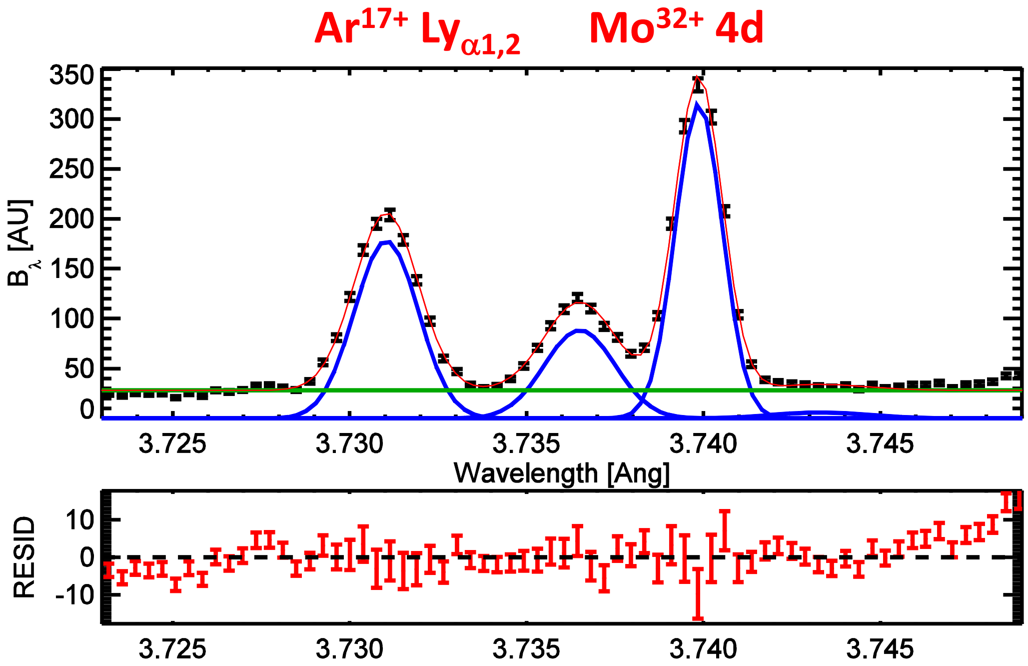

- observe H-like Ar and Ne-like Mo
  - full cross-section for ‘high-Te’ configuration for I-mode studies
  - r/a < 0.5 for ‘low-Te’ studies
- examining configurations for W emission

Invert Brightness Profiles for Time-Evolving Emissivity from Mo^{32+}

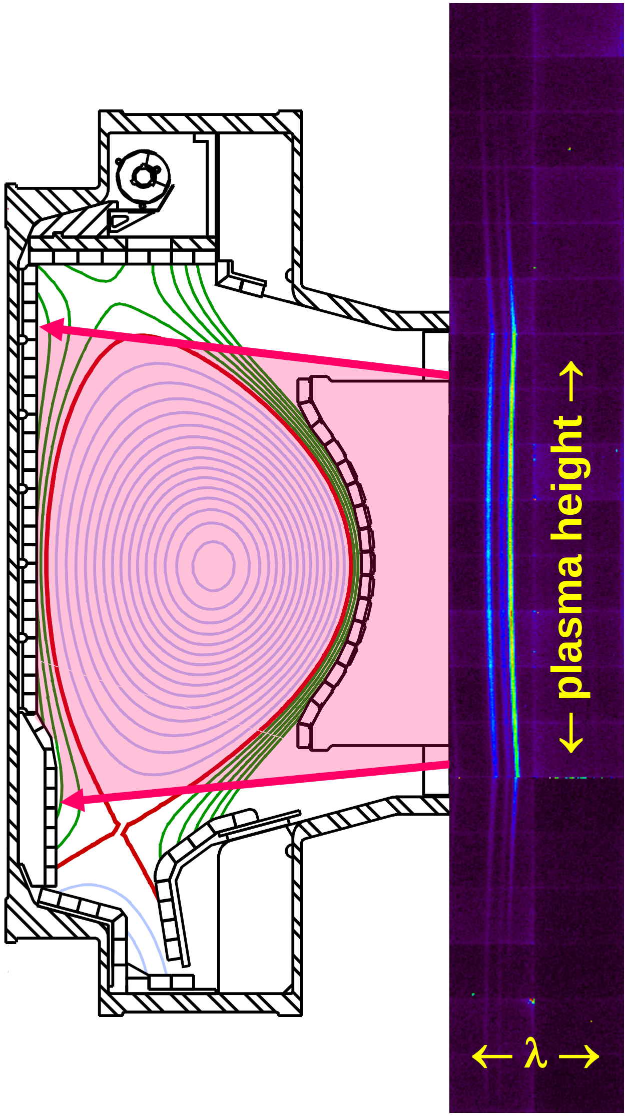

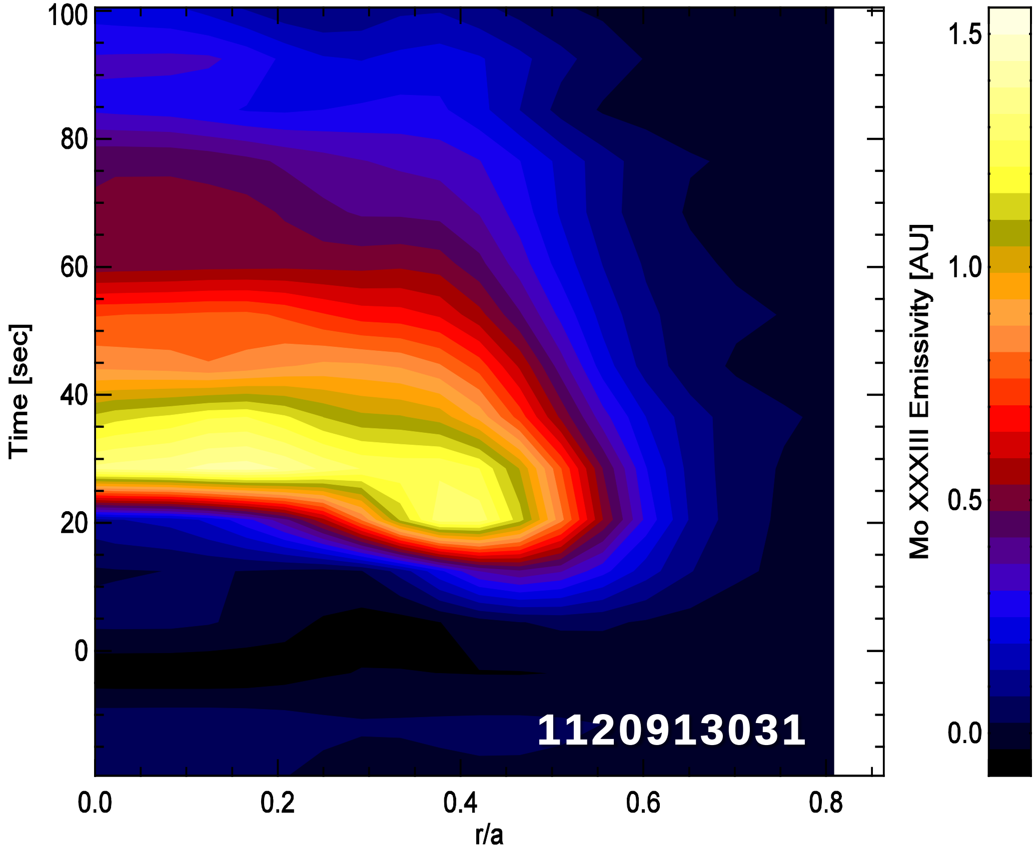

- spatio-temporal evolution of Mo XXXIII emissivity can be used to constrain impurity transport simulations

Difficulties Reconstructing XICS Emission Highlight Challenge of Interpreting Data

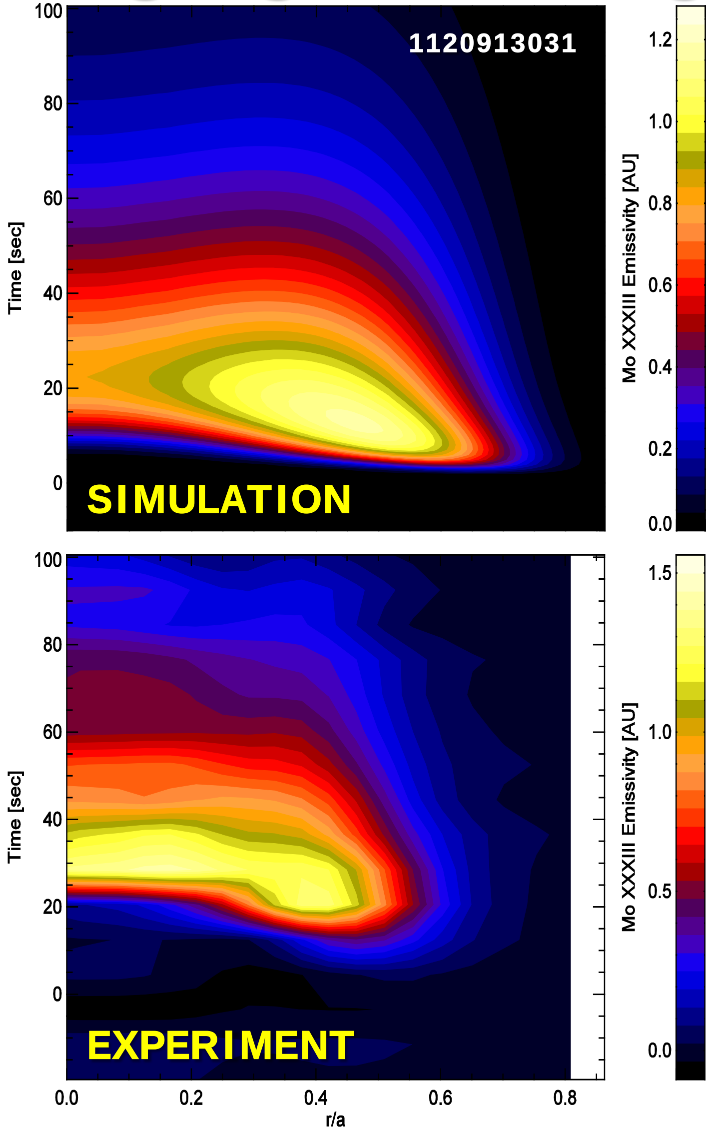

- solving coupled continuity equation for many charge states, q

$$\frac{\partial n_q}{\partial t} + \nabla \cdot \Gamma_q = n_e\left[n_{q+1}R_{q+1} + n_{q-1}\, I_{q-1} - n_q\left(I_q + R_q\right)\right]$$

$$\Gamma_q = -D\nabla n_q + v n_q$$

- errors in recombination, $R(T_e)$ or ionization, $I(T_e)$, rates are 'absorbed' into transport coefficients, D & v
- **example**: diffusive STRAHL simulation of C-Mod Mo LBO into L-mode plasma
- manual or automated codes suggest very strong inward convection, but this depletes lower charge states not seen by XICS
  - qualitative disagreement with bolometry

Background Charge Exchange Identified as an Important Mechanism for High-Z Ion. Balance

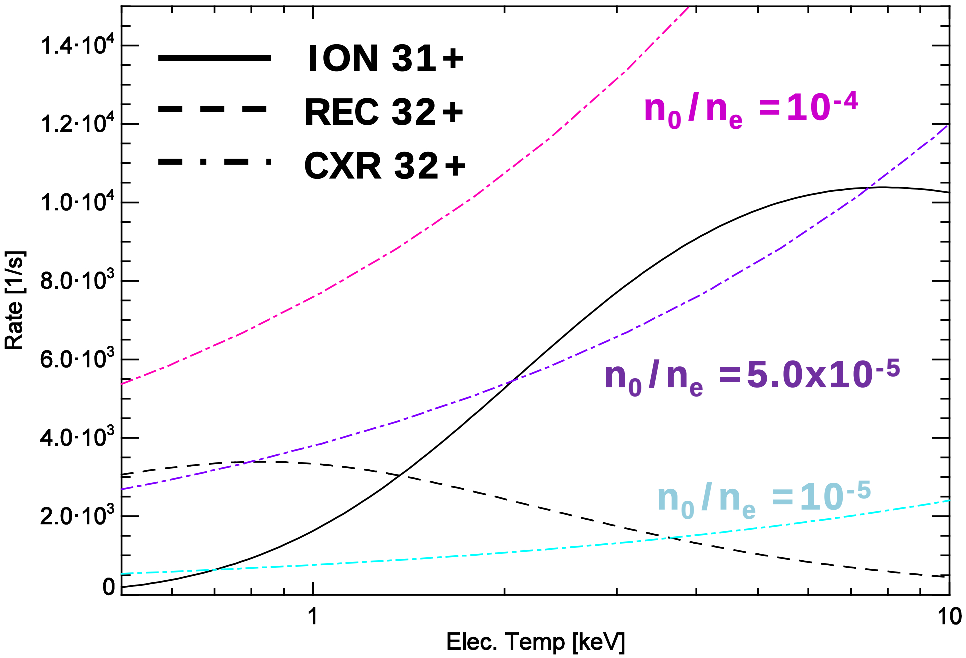

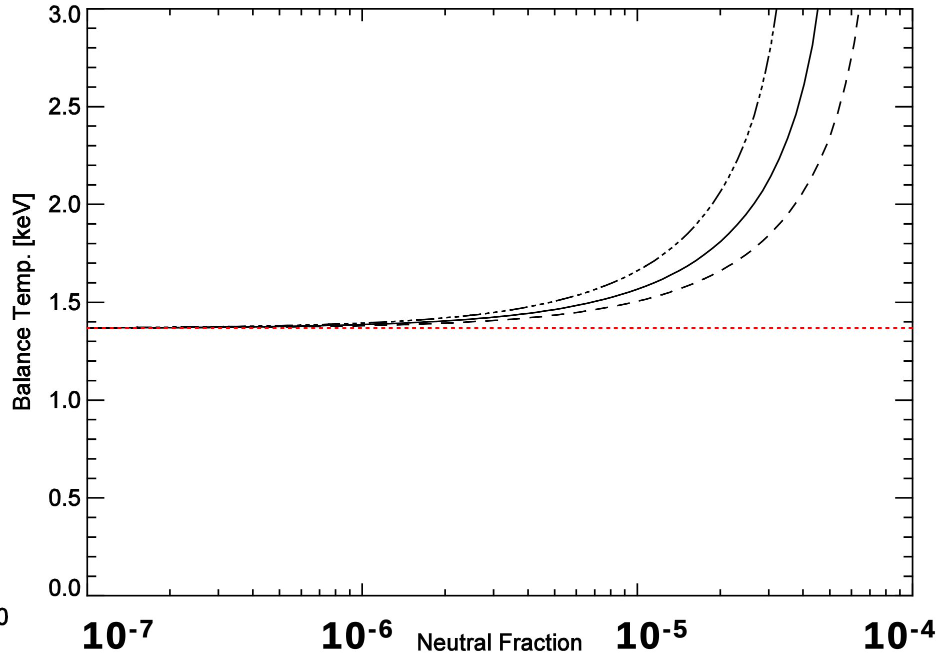

- solve for the T_e at which ION=REC+CXR for various n_0/n_e
- total recombination rate of Mo^{32+} will be strongly perturbed by even small neutral fractions, $n_0/n_e > 10^{-6}$
- neutral density rises, shifts Mo^{32+} production to higher T_e which ***acts like an inward convection***

Confirmed with Steady-State Impurity Simulation

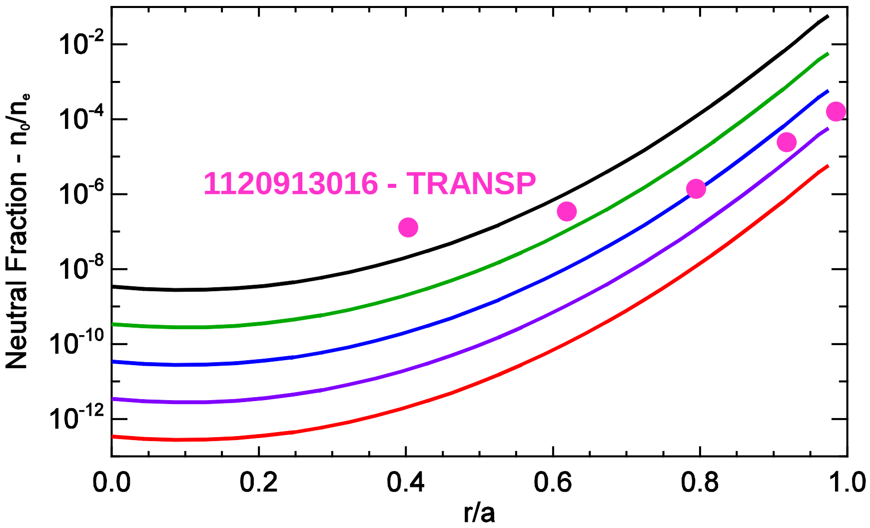

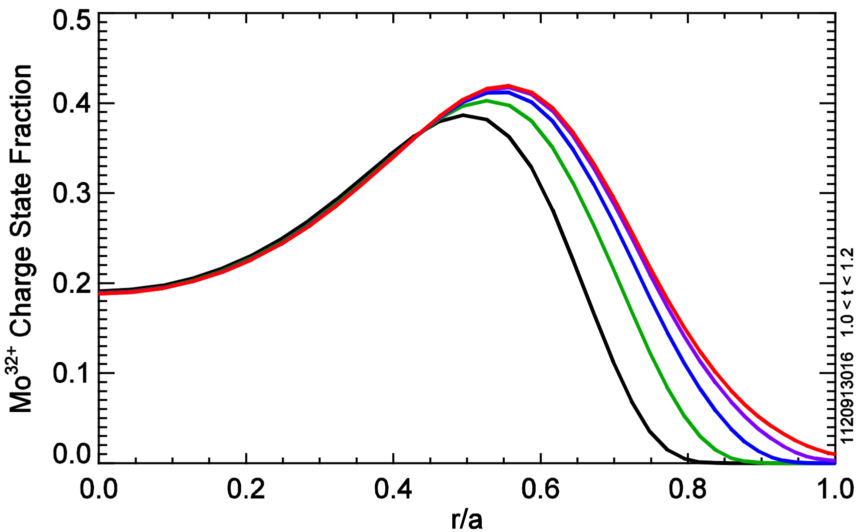

- solve for charge state density profiles under various assumed neutral density profiles
- covers range of experiment where strongly hollow profile decays to ionization balance
- comparing simulated n_0/n_e leads to shift of Mo^{32+} ~Δr/a seen in STRAHL reconstruction

Examining Better Means to Constrain Internal Neutral Density Profile

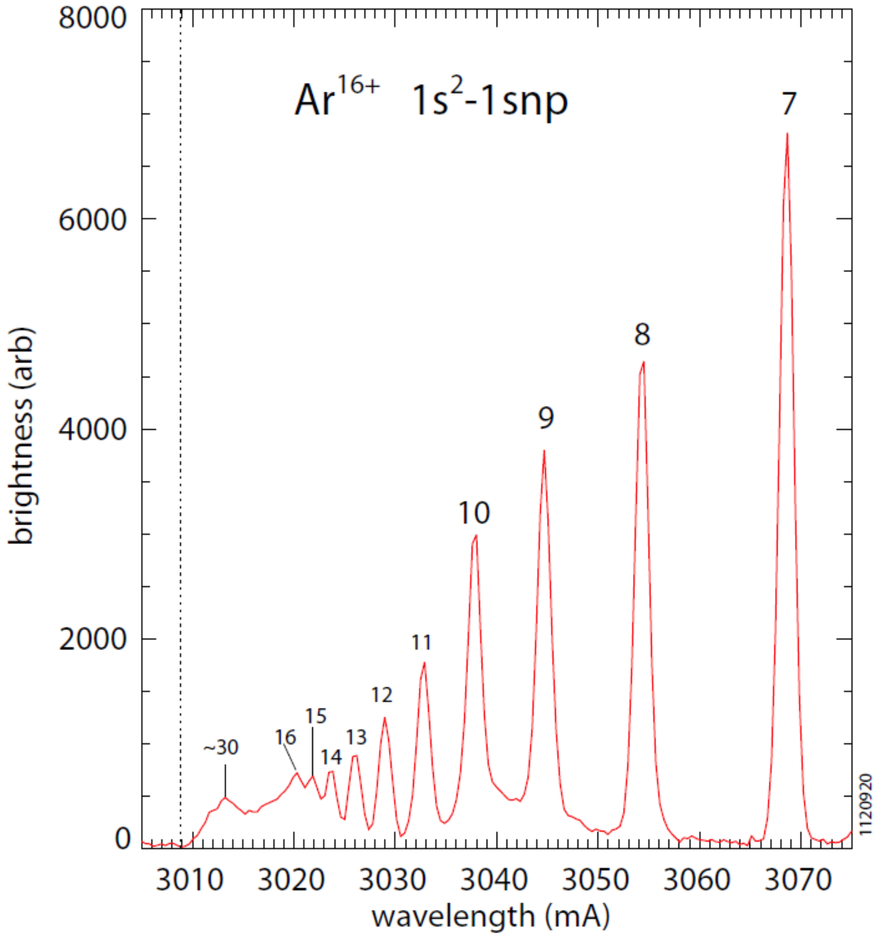

from: J.E. Rice, *et al.* J. Phys. B **47** 075701 (2014)

- solve for charge state density profiles under various assumed neutral density profiles
- covers range of experiment where strongly hollow profile decays to ionization balance
- comparing simulated n_0/n_e leads to shift of Mo^{32+} ~Δr/a seen in STRAHL reconstruction

can we estimate CXR contribution from high-n recombination from XICS?

Recent Experiments to Examine High-Z Impurity Transport

Validation of GKW+NEO Model for W on JET

impurity transport investigate quasi-steady tungsten in early (5.9 s) and late (7.5) phase of hybrid H-mode plasma

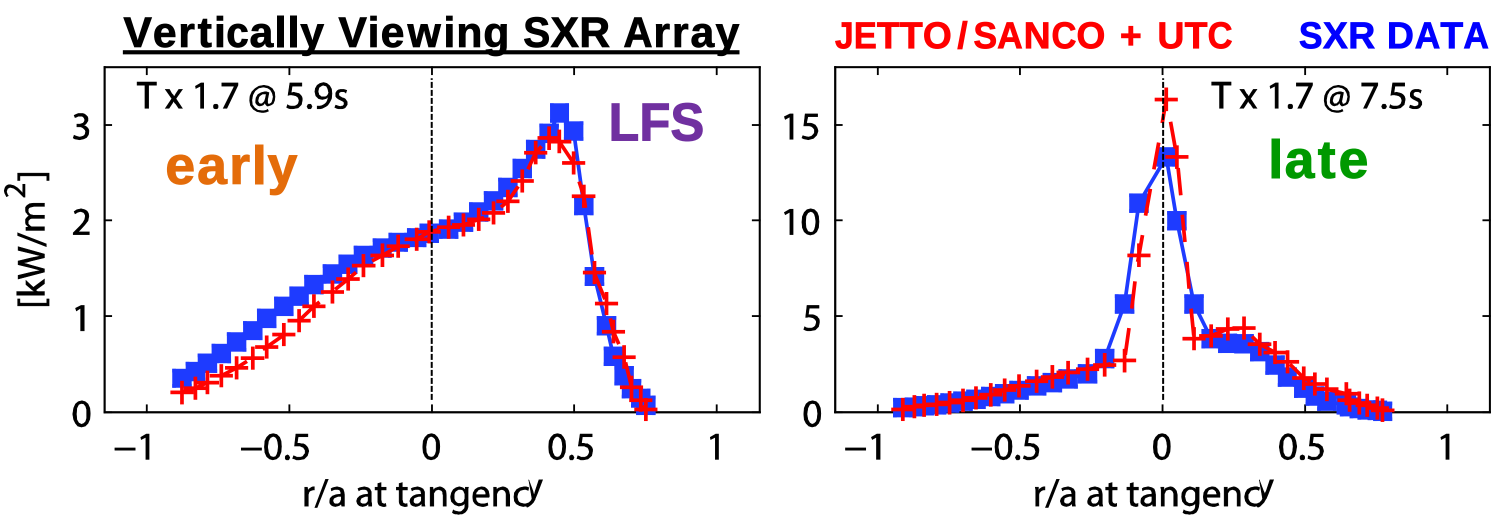

- **t=5.9 data** shows strong 2D variation with **LFS** localization
- **t=7.5 data** shows peaking on-axis, with off-axis in/out asymmetry
- **interpretive modelling** makes small modifications from theory D & v and uses measured ω_ϕ to estimate asymmetry

C. Angioni, *et al.* Nucl. Fusion **54** (2014) 083028

GKW+NEO Shows Good Agreement w/ Exp. Predicts Observed Peaked and Hollow Profiles

- **early** times had *hollow n_e profile leading to hollow n_W profile*, **late** profiles had *peaked n_e and peaked n_W profiles*
- **measurements** from two different techniques used to analyze SXR data agree well with **GKW+NEO modelling**
  - profile determined by neoclassical convection with both neoclassical and turbulent diffusivity participating
- centrifugal effects increase D_{neo} & v_{neo} to compete, with impact on $(v/D)_{neo}$ increasing with ν_*

C. Giroud, *et al.* accepted in PPCF (2014)
E. Belli, *et. al.* PPCF **56** 124002 (2014)

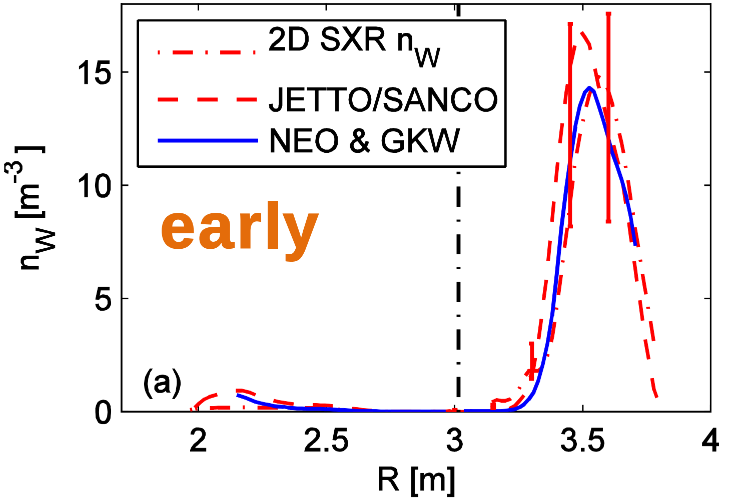

C. Angioni, *et al.* Nucl. Fusion **54** (2014) 083028

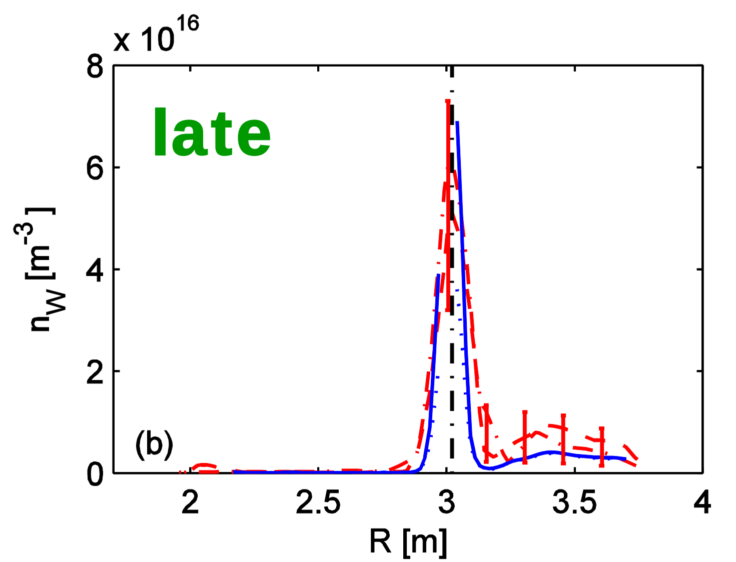

C-Mod Experiments Used to Examine Effect of HFS Impurity Localization on Impurity Transport

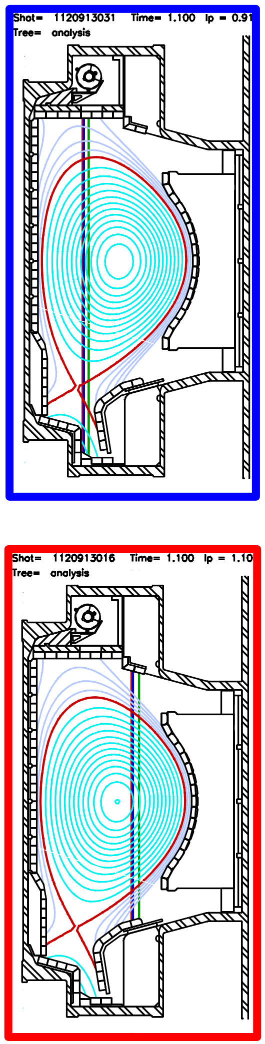

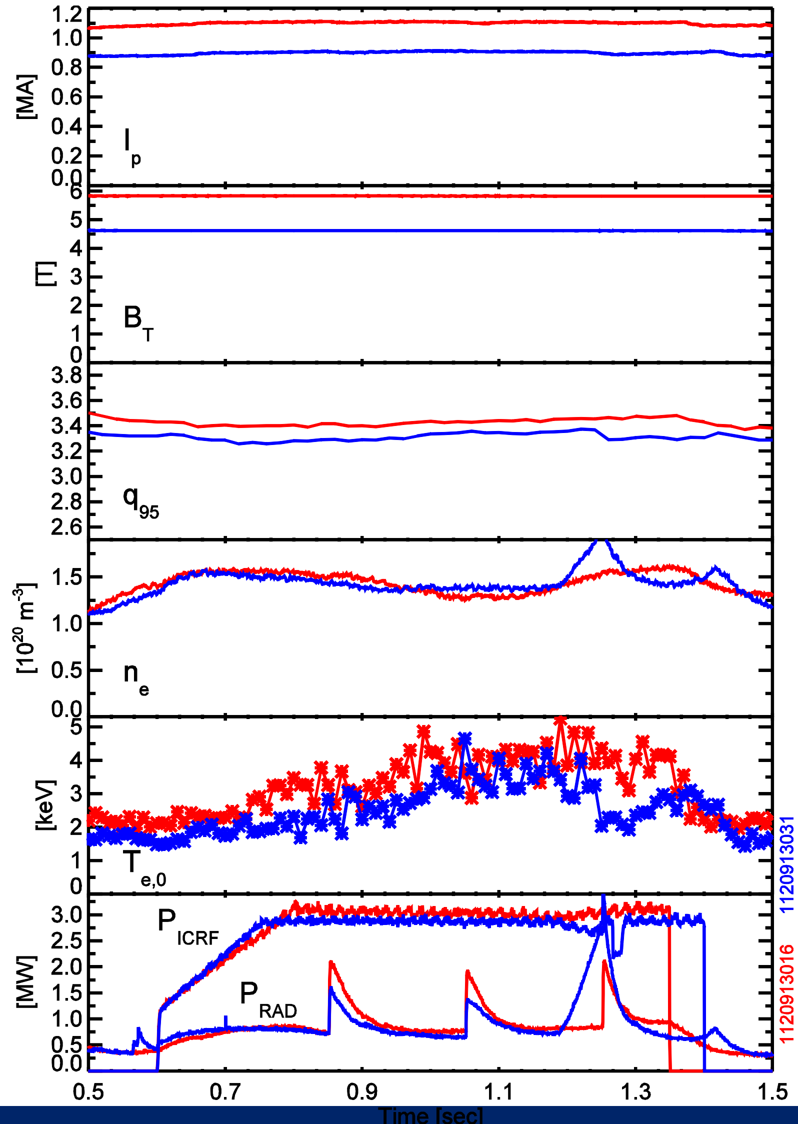

- molybdenum LBO into L-mode plasmas
- vary minority resonance layer via B_T, varying $T_{\perp}/T_{\parallel}$

HFS Heated → LFS n_z localization (centrifugal force)

LFS Heated → HFS n_z localization (poloidal electric fields)

- examine asymmetry using AXUV diodes and radial transport using imaging crystal spectrometer

Challenges to Designing Experiments to Test Asymmetry-Induced Transport Theories

- no direct external control of asymmetry – modification is through heating/flow/current-drive systems which also modify standard neoclassical/turbulent/MHD or confinement regime
- changes observed in confinement times, but large co-variances exist

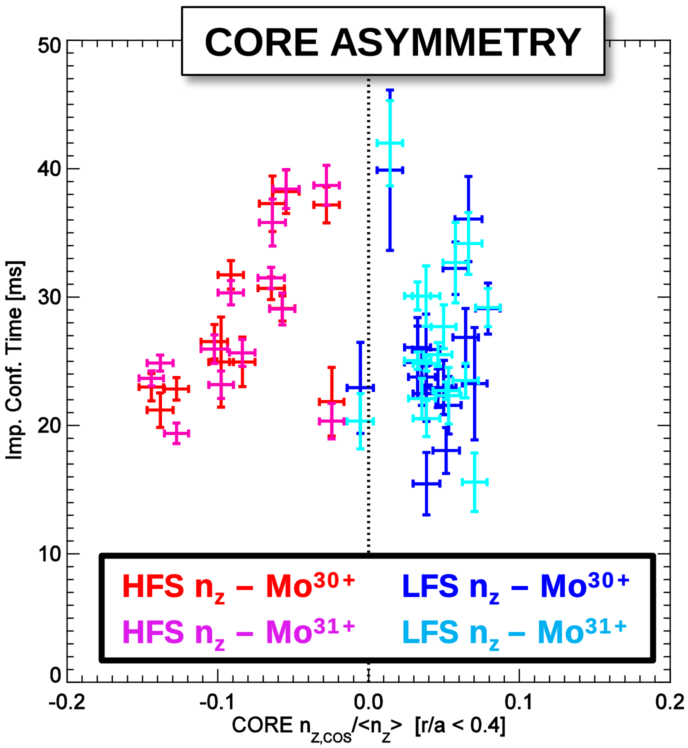

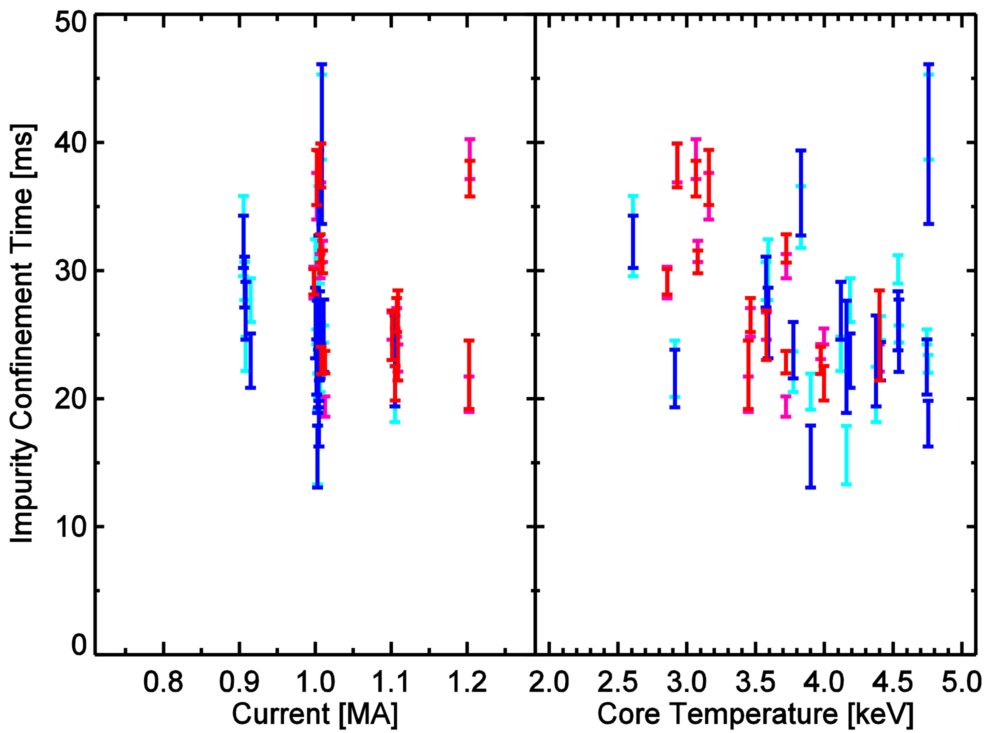

C-Mod Results Compared to Chalmers Model for Asymmetry Turbulent Impurity Transport

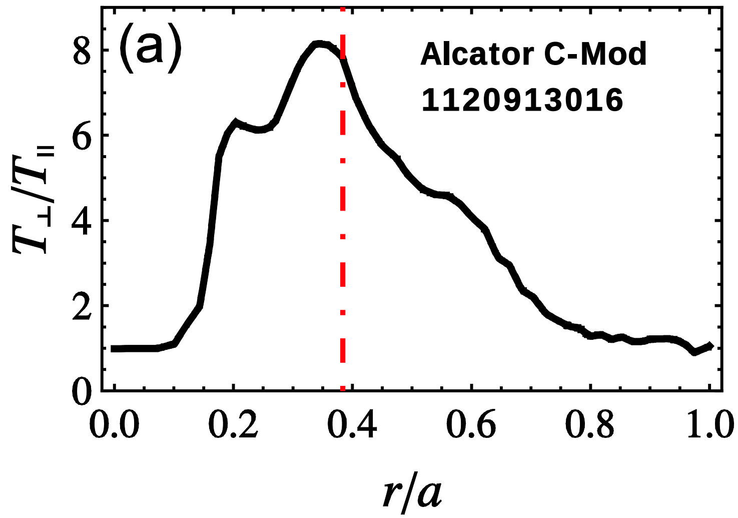

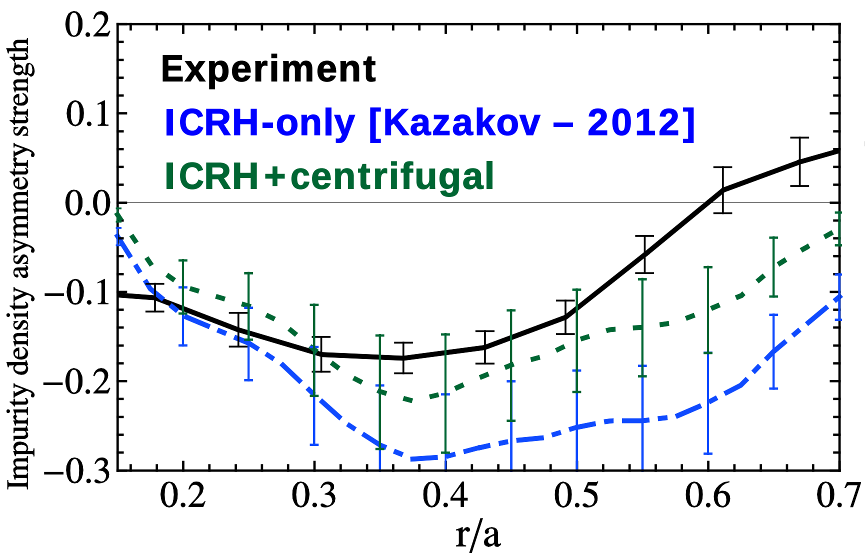

- off-axis LFS heating [3 MW D(H)] results in high minority anisotropy at mid-radius (from TRANSP)
- HFS impurity localization observed by AXUV diodes, matching theory

A. Mollen, *et al*. PPCF **56** 124005 (2014)

Weak Changes in Asymmetry-Driven Turbulence Predicted, Disagreements Remain

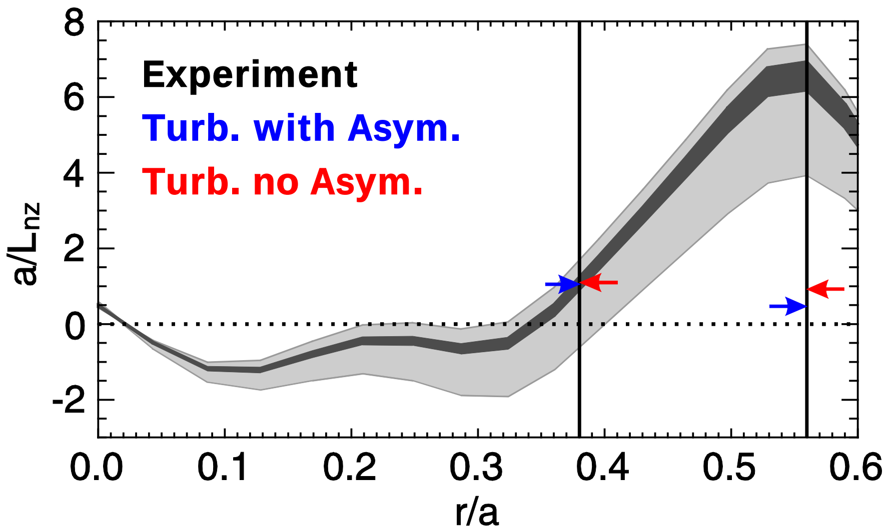

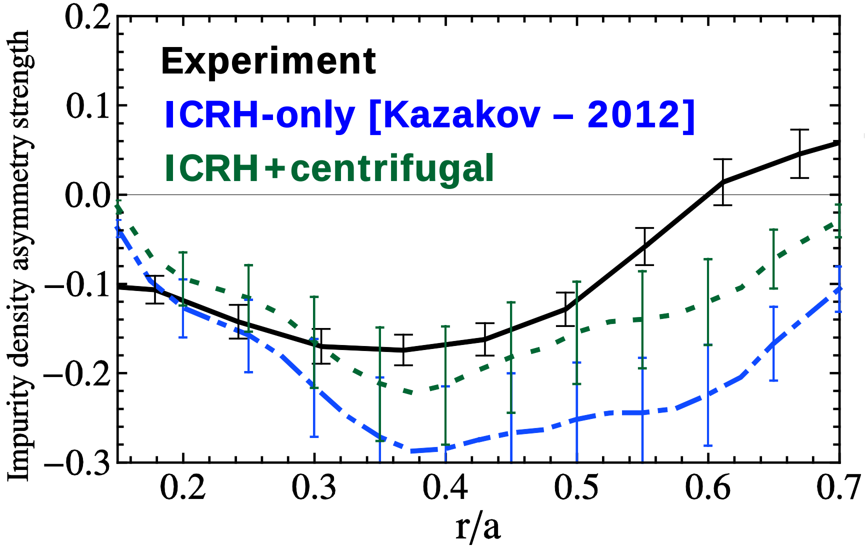

- off-axis LFS heating [3 MW D(H)] results in high minority anisotropy at mid-radius (from TRANSP)
- HFS impurity localization observed by AXUV diodes, matching theory
- gradient scale length computed from Ne-like Mo profiles from XICS
- compared to linear turbulent (ITG) transport modelling using GYRO with varying agreement
  - at large r/a, questions on atomic physics used in experimental data
- asymmetry shows little difference relative to discrepancy, analysis through GKW+NEO is on-going

A. Mollen, *et al*. PPCF **56** 124005 (2014)

W Transport Probed Alcator C-Mod EDA H-modes to Study Transport with Weak Asymmetries

- low-Ip, high P_{RF} allows access to low $0.3 < \nu_{EFF}$ 1.0, peaked density regimes [Greenwald NF 2007]
- experiments scanned P_{RF} operating space with LBO
  - <u>LOW POWER</u>: LBO causing H/L back transition (W-persists!)
  - <u>HIGH POWER</u>: operational limit due to fast-ion orbit loss
- most of the dataset shows poloidally symmetric impurities
  - $|n_{z,cos}| < 0.05$ for $r/a < 0.4$
  - weak centrifugal effect (hollow rotation profiles) balanced by minority anisotropy

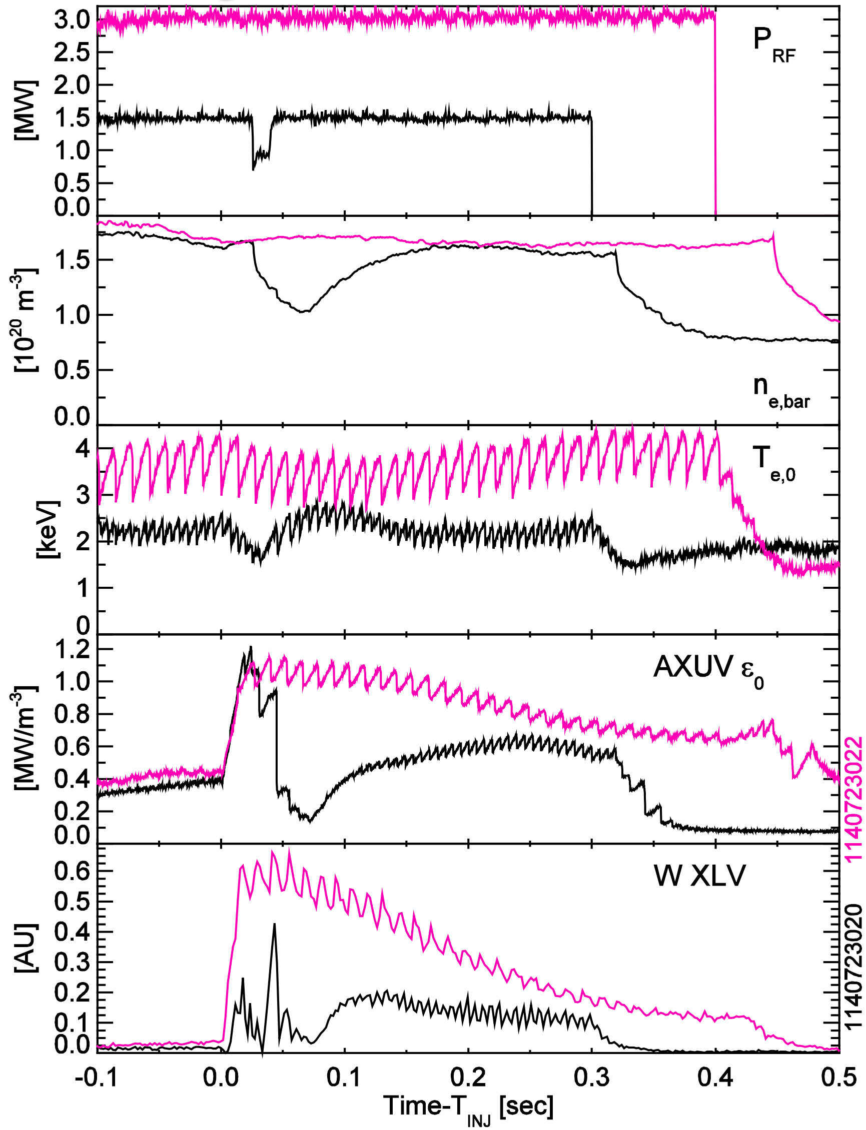

A. Loarte, *et al*. submitted to PoP (2014)

RF Power Modifies a/Lne, a/LTi and Changes Direction of Neoclassical Impurity Flux

- pre-LBO profiles in each plasma (x16) examined, looking at cases modifying direction of neo. imp. transport (a/Lni – 0.5a/LTi > 0)

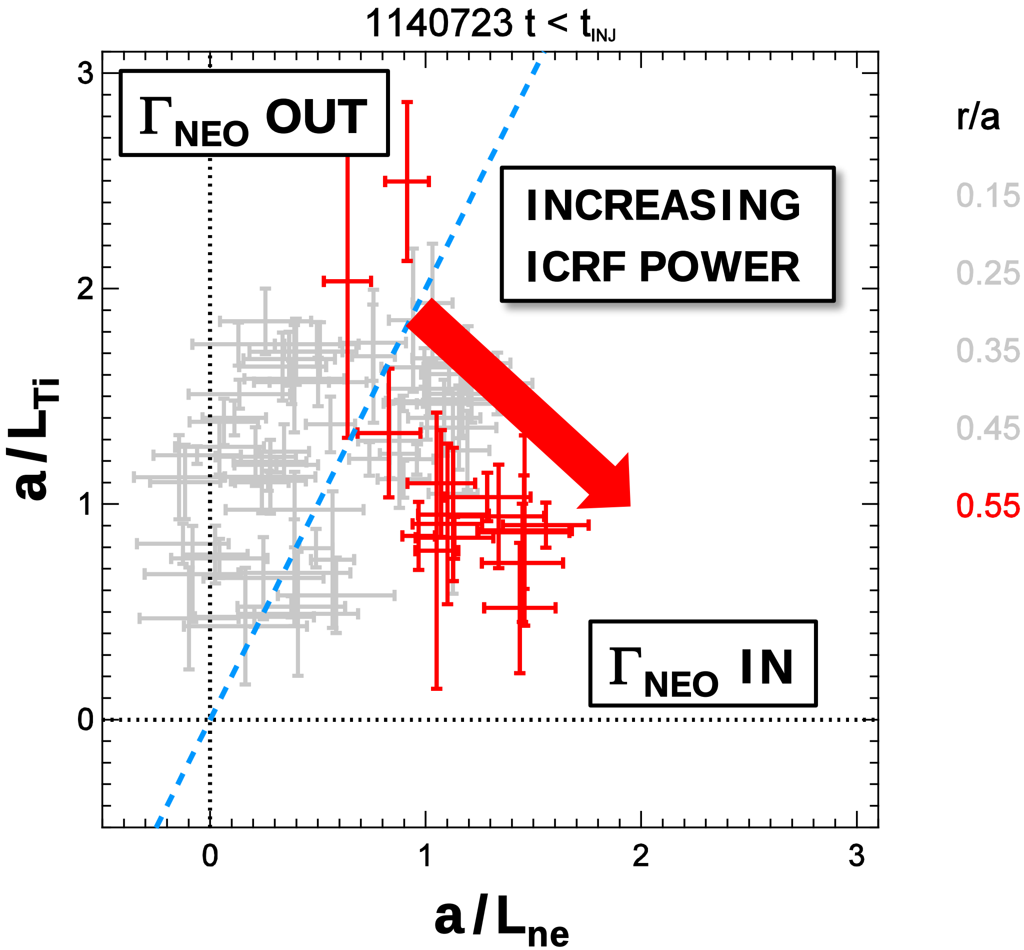

$$\frac{a}{L_X} \equiv -\frac{1}{X}\frac{\partial X}{\partial \rho} \qquad \rho = \frac{R_{LFS} - Ro}{a_{LFS}}$$

- **r/a=0.55**: increased P_{RF} modifies profiles from outward to inward neo. imp. transport

RF Power Modifies a/Lne, a/LTi and Changes Direction of Neoclassical Impurity Flux

- pre-LBO profiles in each plasma (x16) examined, looking at cases modifying direction of neo. imp. transport (a/Lni – 0.5a/LTi > 0)

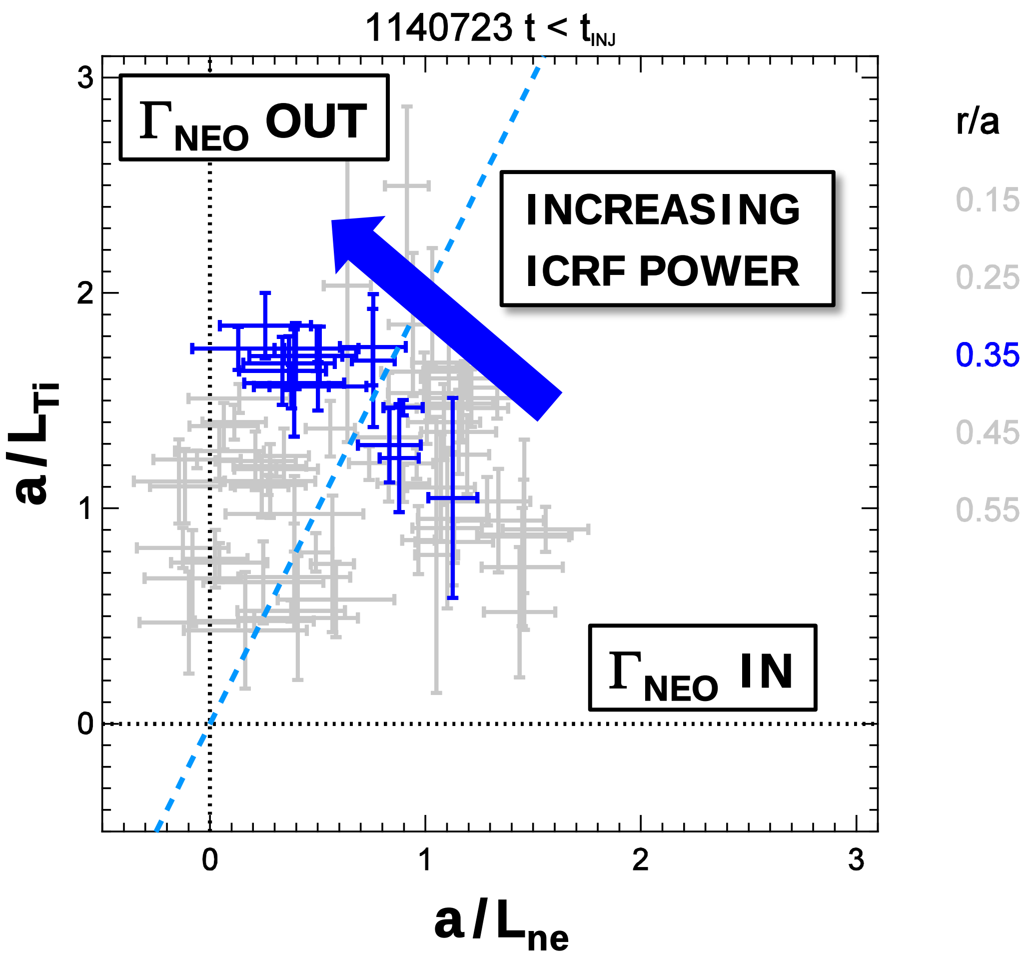

$$\frac{a}{L_X} \equiv -\frac{1}{X}\frac{\partial X}{\partial \rho} \qquad \rho = \frac{R_{LFS} - Ro}{a_{LFS}}$$

- **r/a=0.55**: increased P_{RF} modifies profiles from outward to inward neo. imp. transport
- **r/a=0.35**: increased P_{RF} modifies profiles from inward to outward neo. imp. transport
- evidence of neoclassical transport would show impurity build-up $0.35 < \rho < 0.55$

Mid-Radius Transport Appears Anomalous Despite Profile Changes

- AXUV diode arrays show prompt inward radiation front
  - no change between **r/a=0.55** and **r/a=0.35** where neo. impurity flux changes sign
- spectroscopy **(W UTA)** shows fast (< 10 ms) rise time

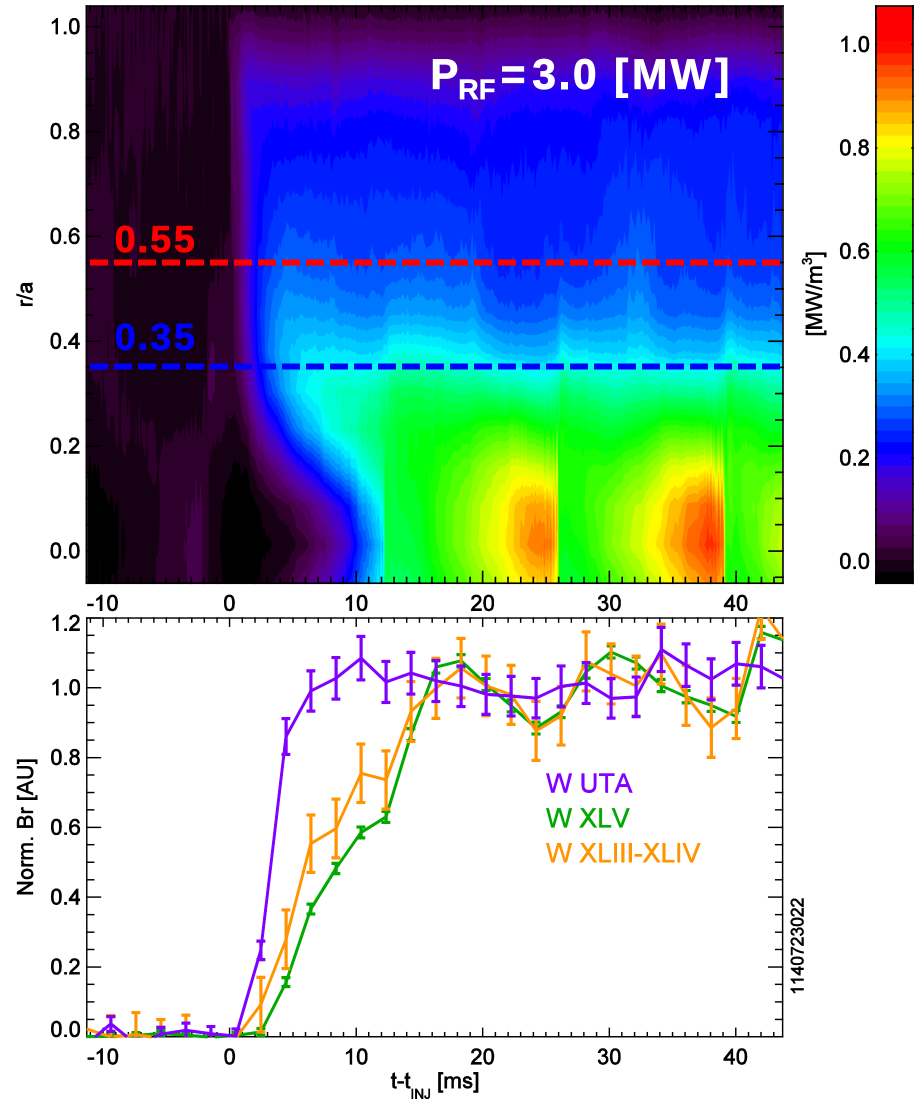

GOOD NEWS: n_i peaking in regions with anomalous impurity transport avoid W accumulation and improve ITER fusion performance

(not too surprising if density peaking is turbulent driven)

Approaching Core Transport Slows, Sawteeth Impact Observed

- AXUV show for r/a < 0.3, front slows, becomes modulated by sawtooth instability
- core localized spectroscopy (**W XLIII/XLIV** and **XLV**) show slower (~20 ms) rise time and sawtooth perturbations

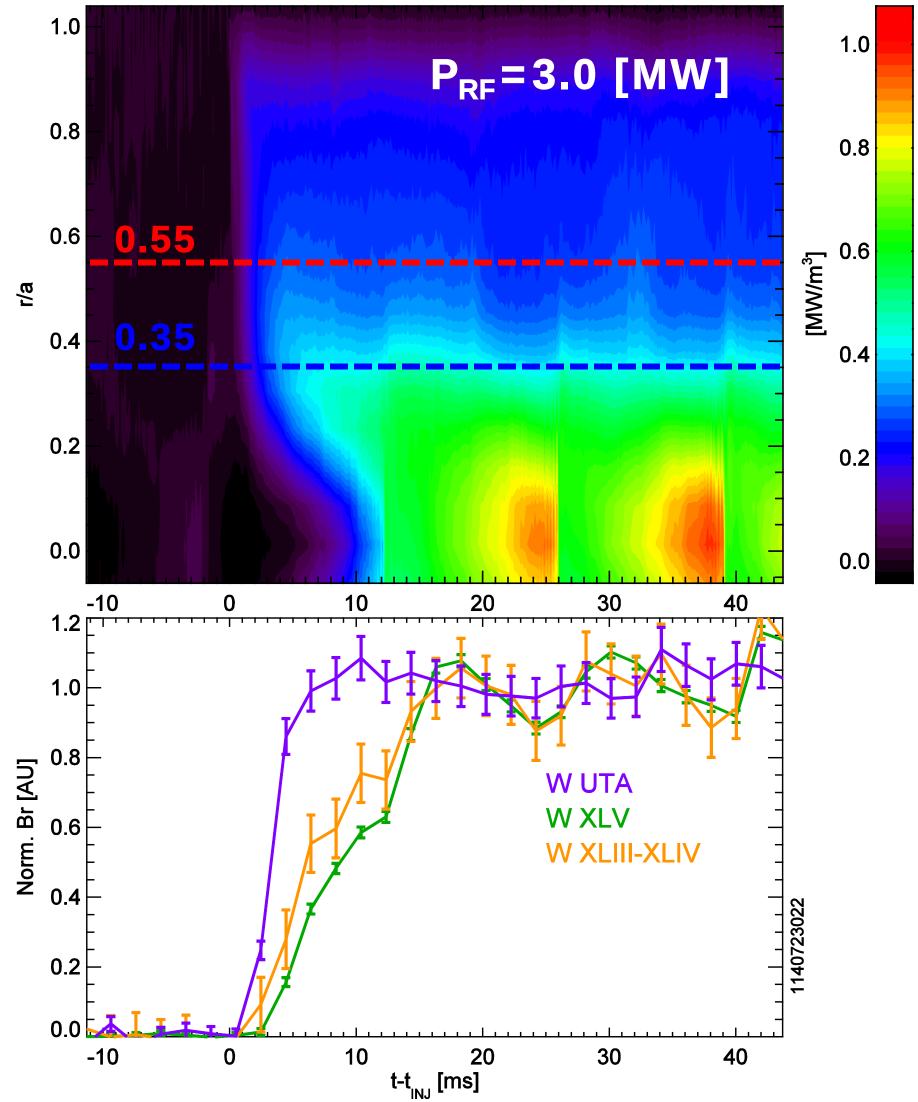

<u>CHALLENGE:</u> investigate if core, intra-sawtooth changes represent tungsten peaking and if ICRF power is having an impact on imp. transport

Summary - So Where Does This Leave Us?

- core transport of high-Z impurities in tokamaks can be explained in many cases by a balance of neoclassical and turbulent transport
- both neoclassical and turbulent transport are modified by the poloidal variation of the impurity density observed in many present scenarios
  - centrifugal effects (LFS localization) and poloidal electric fields (HFS localization for ICRH) from non-thermal particles drive the important 'in/out' asymmetries
  - this theory has been developed and has/is working its way into our codes
  - there is still a VERY open topic of pedestal high-Z impurity transport where these concepts will likely play an important role (see M. Churchill's work)
- we have advanced spectroscopic tools to resolve charge state-specific high-Z impurity emission
  - the poloidal density asymmetries are a big diagnostic nuisance
  - the uncertainties in atomic physics data mean we must be cautious
- we should have what is needed to demonstrate an understanding of the mechanism(s) by which RF heating mitigates of core impurity peaking
  - including initial validation of high-Z transport in low-aspect ratio devices!

EXTRA SLIDES

AXUV DIODES ARE NOT BOLOMETERS!!!!!

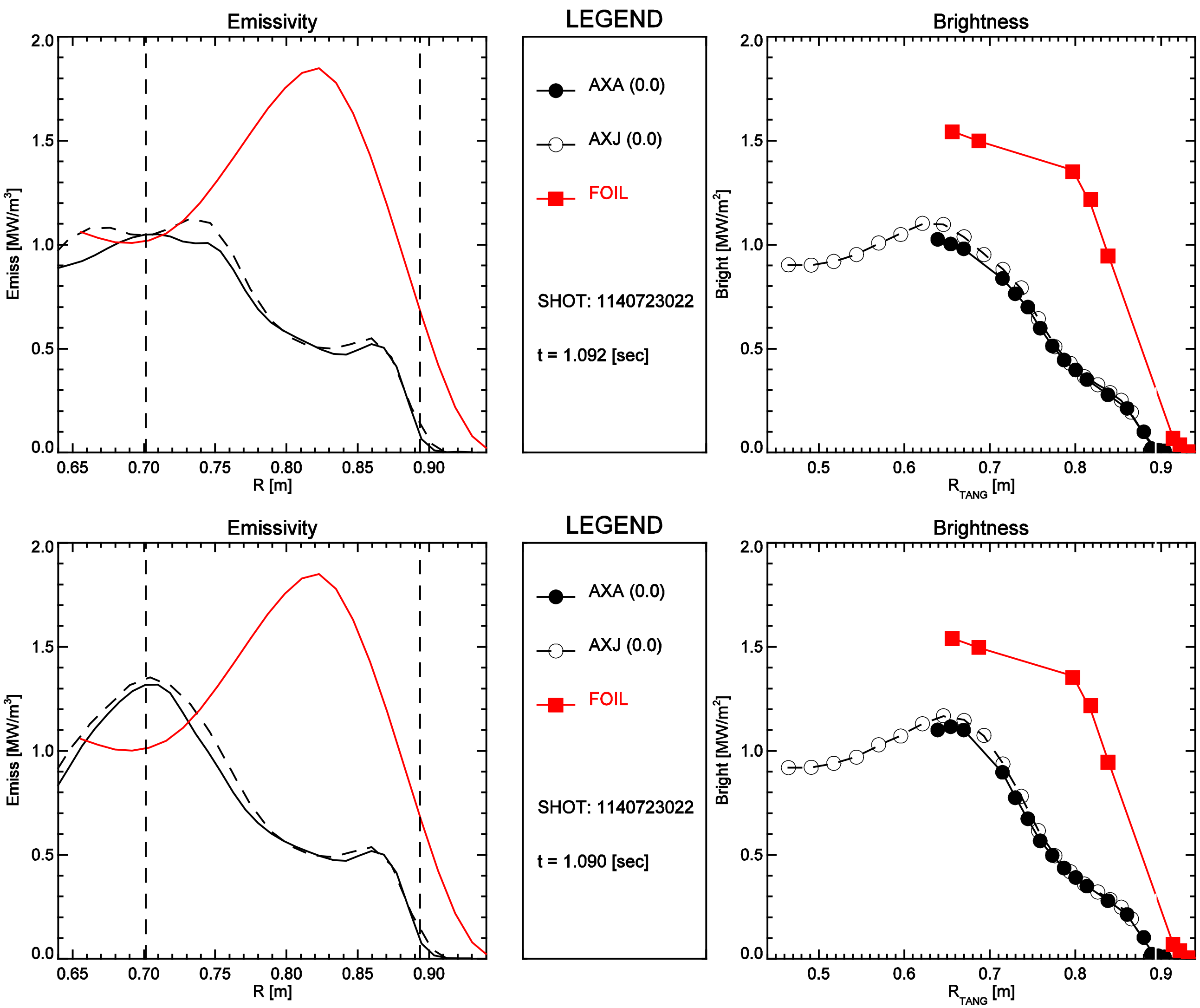

- showing post and pre-sawtooth
- comparing resistive bolometers and AXUV diode profiles shows large differences off-axis
- **qualitatively different profile shape (peaked vs. hollow)**
- on-axis AXUV and bolometry ~ match
  - higher-Te, emission in AXUV bandpass
- 1140821 data w/ more complete brightness profiles support results

XICS Temperature Profiles Impacted by Unresolved Asym.

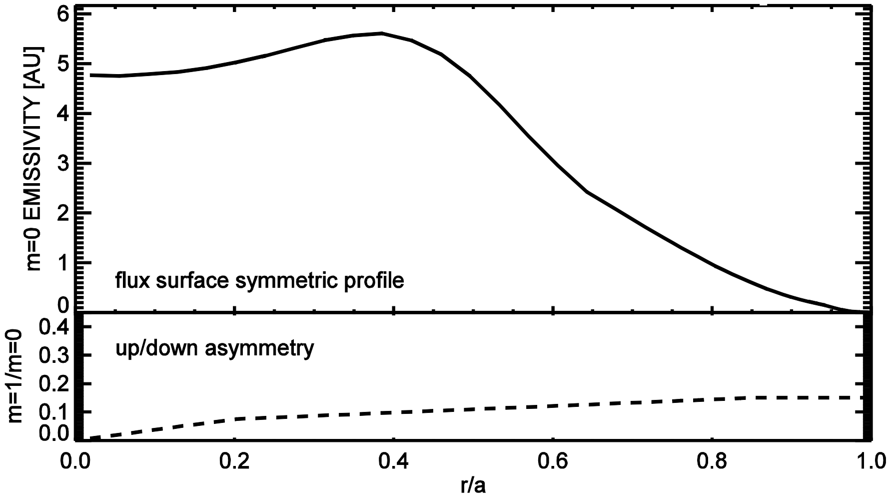

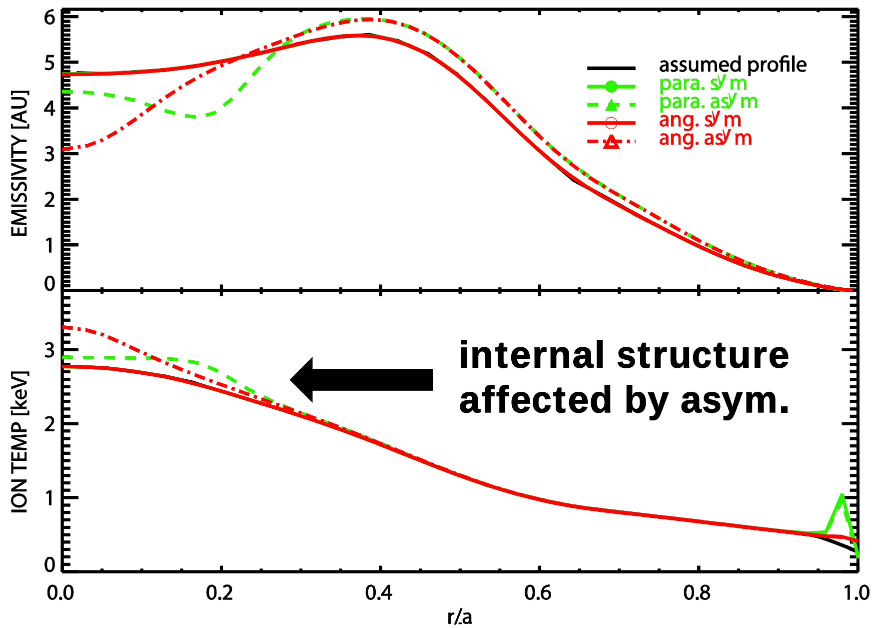

- two limiting cases of viewing geometries (**PARALLEL**) (**ANGLED**)
- specify (m=0) radial profile and asymmetry (m=1/m=0) $n_{z,sin}/\langle n_z \rangle$
  - at level currently observed but not understood
- find ε, T_i with and w/o asymmetry

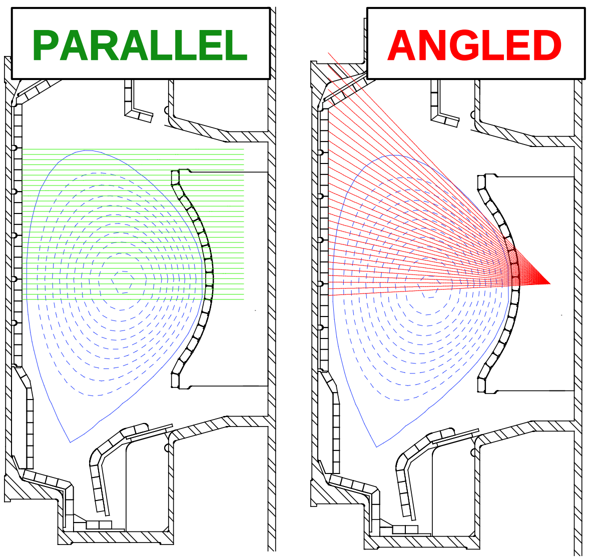

XICS Temperature Profiles Impacted by Unresolved Asym.

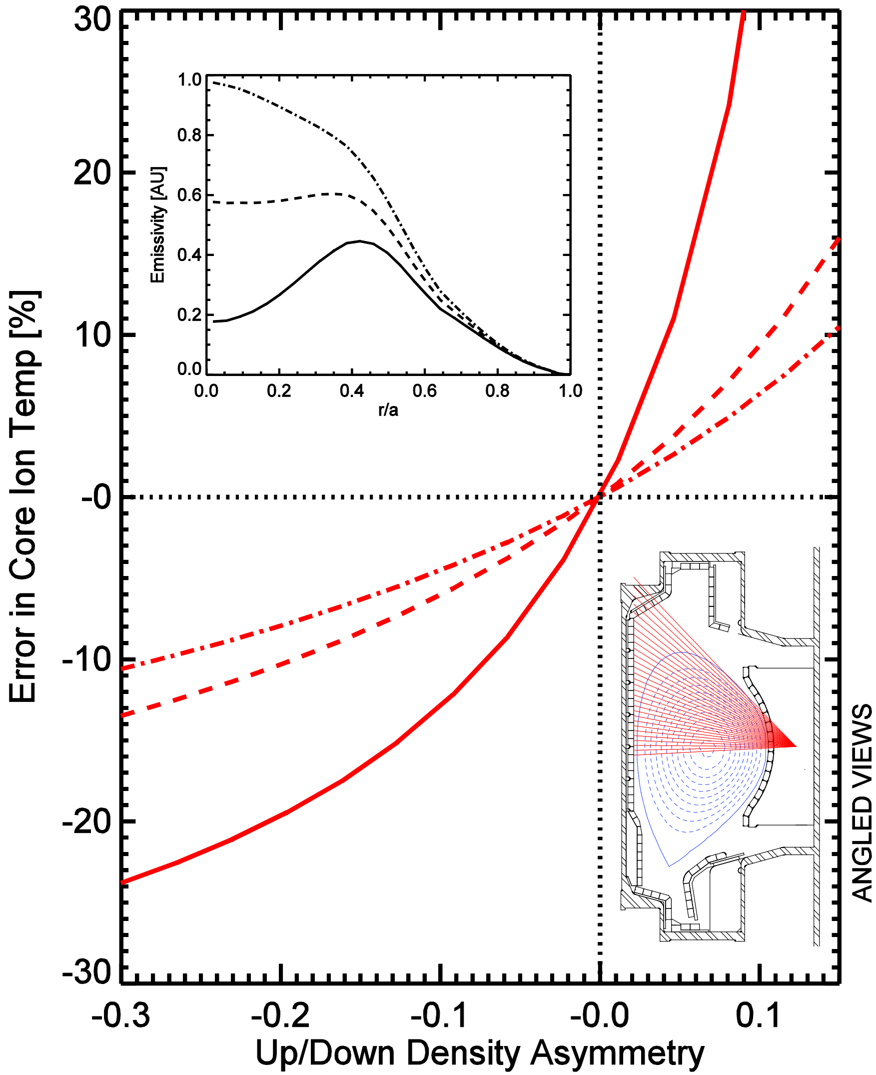

- find maximum error in the ion temperature inside of r/a < 0.4 for different up/down asymmetry levels and radial profile shapes
- solution: fully resolve the top & bottom of the plasma and account for asymmetry in the inversion
- solution: understand asymmetry physics well enough to predict and include as *a-priori* in inversion
- motivates the implementation and testing of high-Z based imaging crystal spectroscopy on present devices
  - ITPA DIAG-6

EXAMPLE: Intra-Sawtooth SXR Analysis

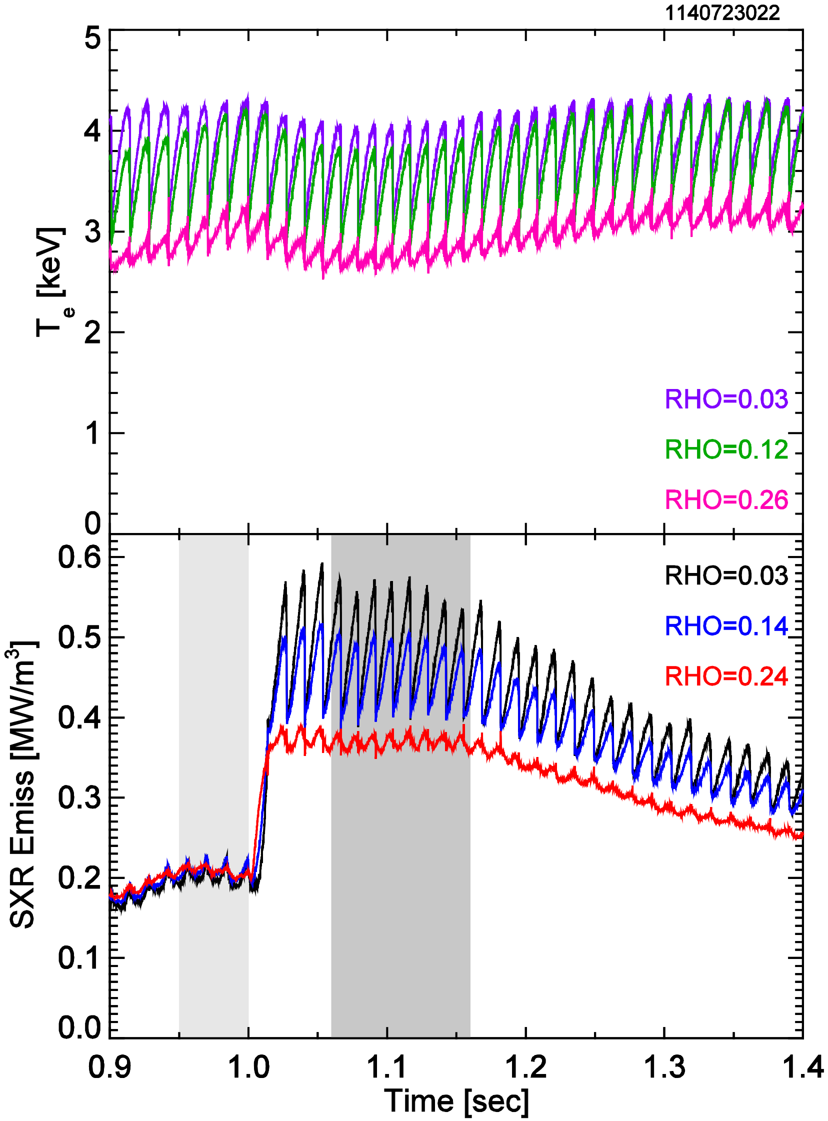

- LBO increases SXR emission well above background
- results in varying impact on $T_{e,0}$

EXAMPLE: Intra-Sawtooth SXR Analysis

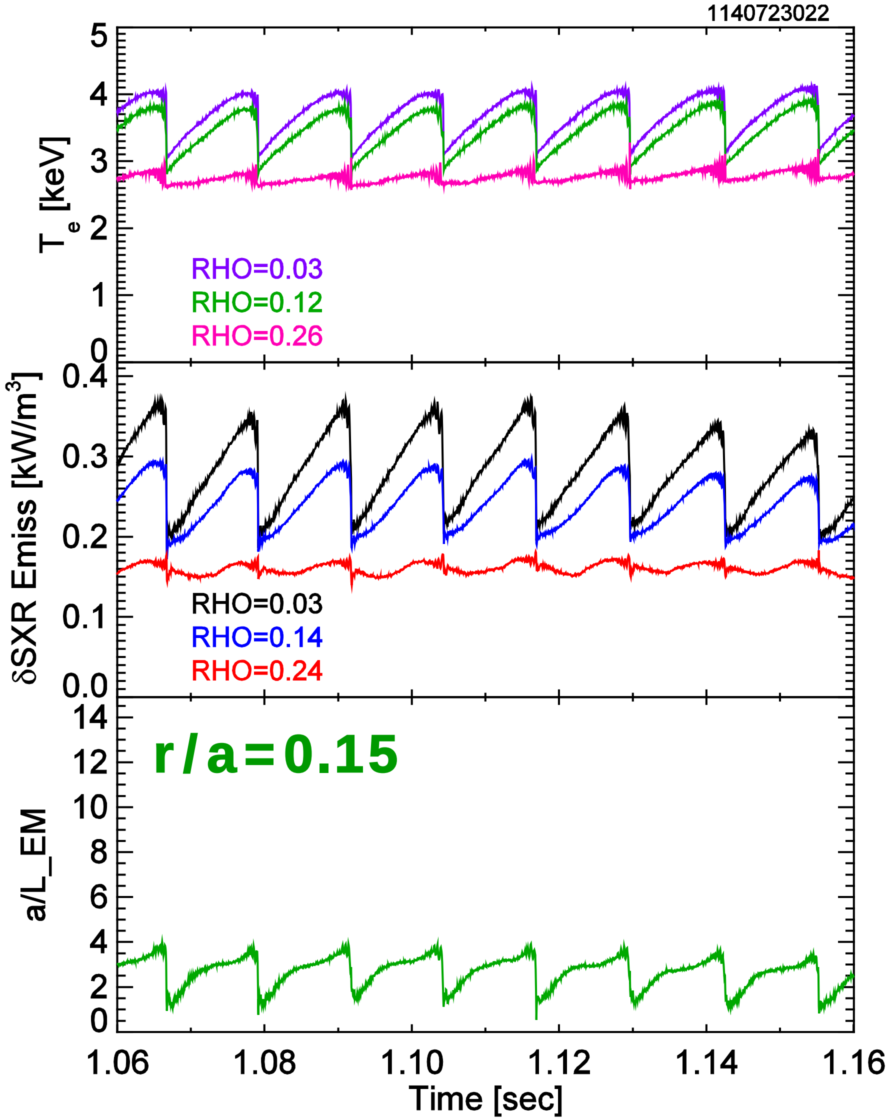

- LBO increases SXR emission well above background
- results in varying impact on $T_{e,0}$
- background subtracted emissivity used to compute emission gradient scale length a/Lem
- intra-sawtooth behavior shows repeatable cycle, reaching stationary scale length at r/a=0.15

ICRF Power Scan Shows Weak Change in Impurity Peaking at r/a ~ 0.15

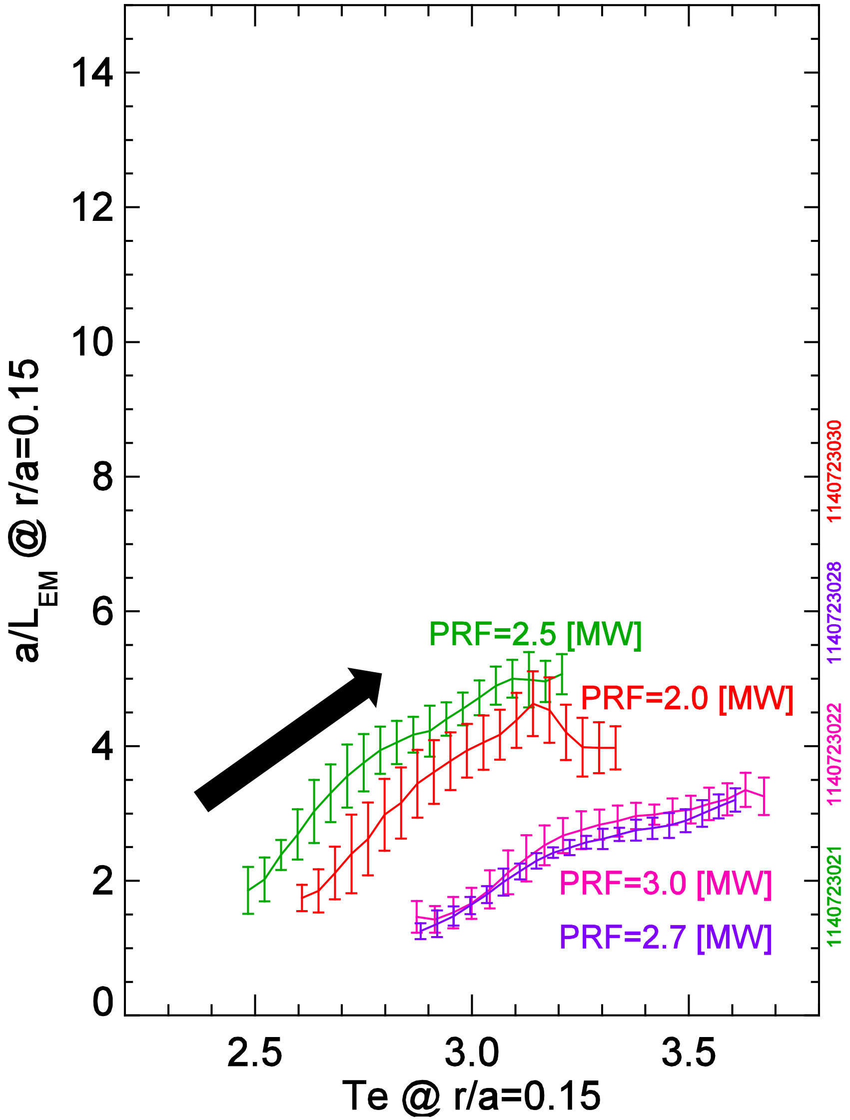

- intra-sawtooth trajectories of a/Lem show slight drop in peak as ICRF power is increased
  - a/Lem ~ 5 → 3
  - could simply be atomic physics
- absolute level consistent with flat to weakly peaked (a/LnW ~ 2) profiles

Increasing Minority Concentration Increases Core Impurity Peaking

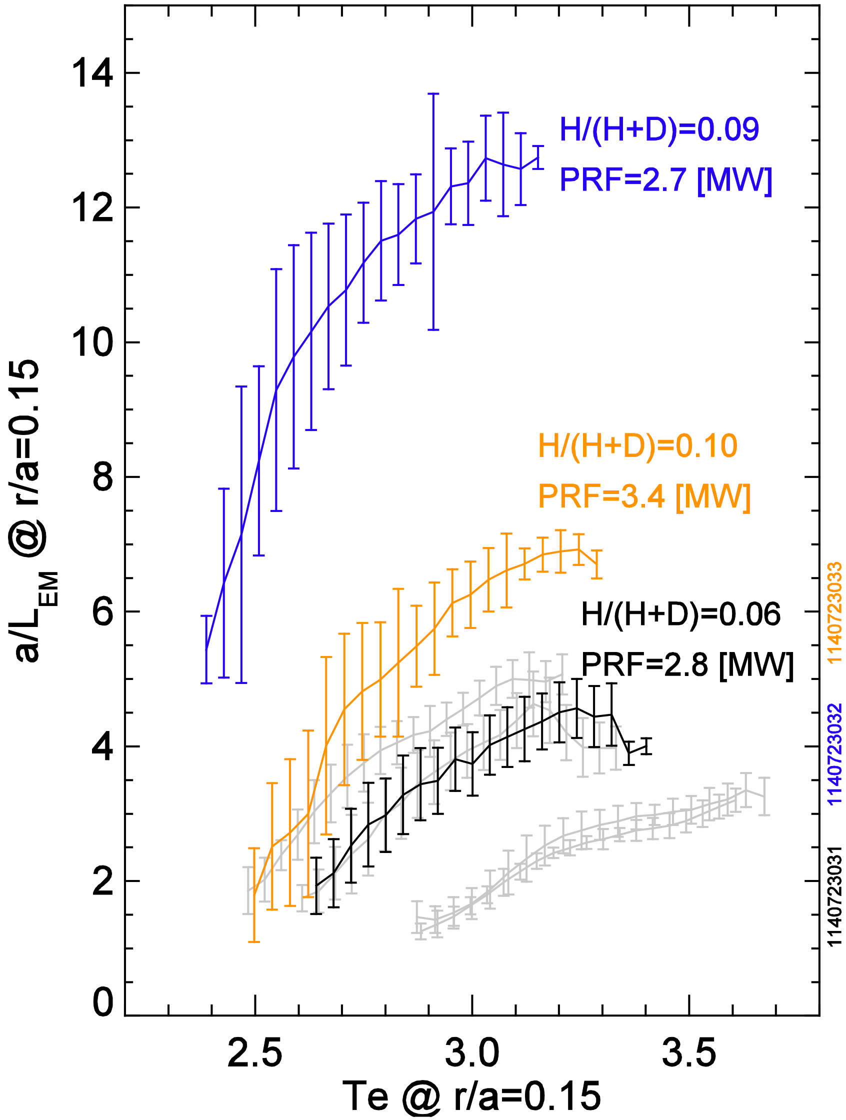

- limited scan of H_2 puff and ICRF power level shows strongest change in a/Lem within dataset
- increasing minority fraction at fixed ICRF power leads to x3 increase of a/Lem at nominally fixed T_e
- increasing ICRF power at fixed minority fraction drops a/Lem
- *trend shows peaking decreases as power/minority density increases*
  - i.e. high energy tail decouples minority and impurity ions

Increasing Minority Concentration Increases Core Impurity Peaking

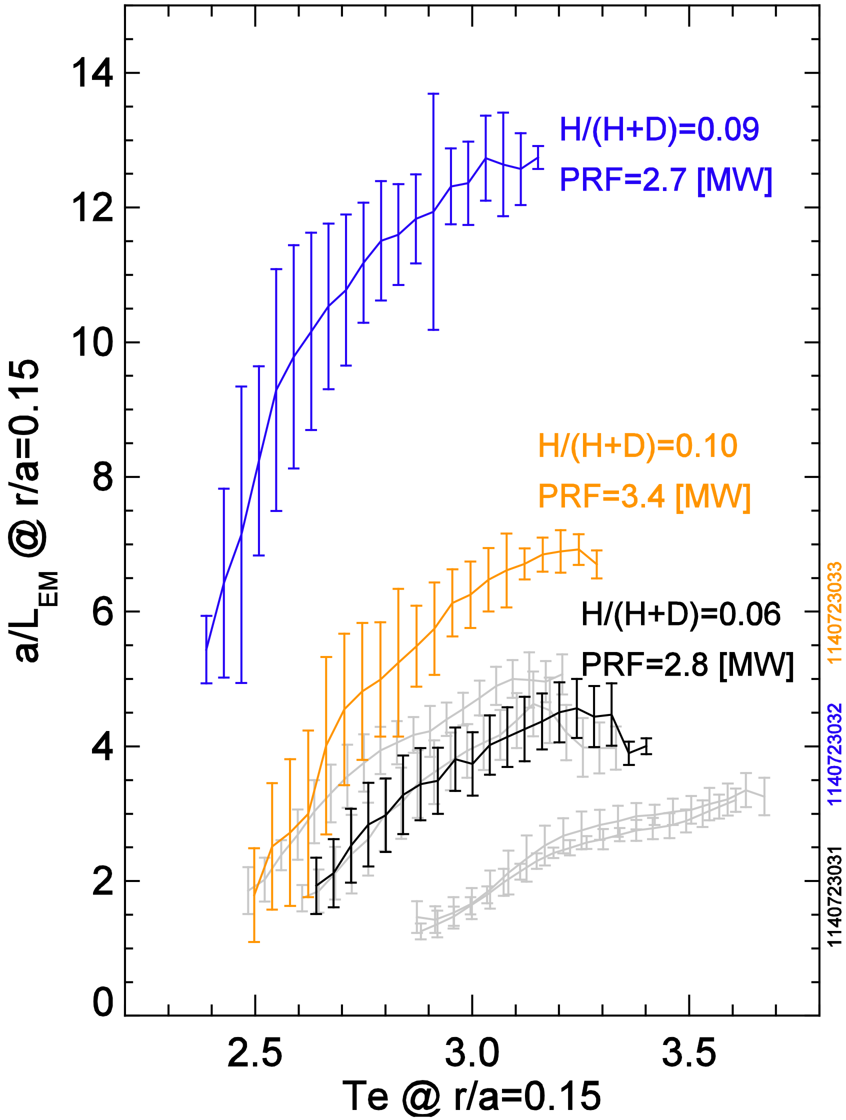

consistent with JET findings [Casson PPCF 2014] that highlight minority-impurity friction as an important component of high-Z neoclassical transport

potential implications for ITER simulations which only account interactions between high-Z impurities and thermal ions

XICS Contributions & Advantages, Development Remains

- development of robust XICS has led to substantial contributions of core transport validation from C-Mod group (Howard, White, Rice, etc.)
  - momentum and heat transport in Ohmic/wave-heated plasmas
- key advantages over Charge Exchange Recombination Spectroscopy
  - no issue of wall reflections for metal devices
  - scalable to large devices where C-X energy beams do not penetrate well
- technique still requires development; calibration issues, ion-impurity coupling understanding
- XICS on NSTX-U will be particularly challenging
  - no C-Mod-like near poloidal view possible due to small wall radius
  - tangential view leads to significant smearing in cases of large Mach shear
  - tangential view will (likely) be effected by charge-exchange from NBI or plume
  - poloidal asymmetries will be strong, complicating analysis
  - RECOMMENDATION: full poloidal and tangential system ($$$)

title

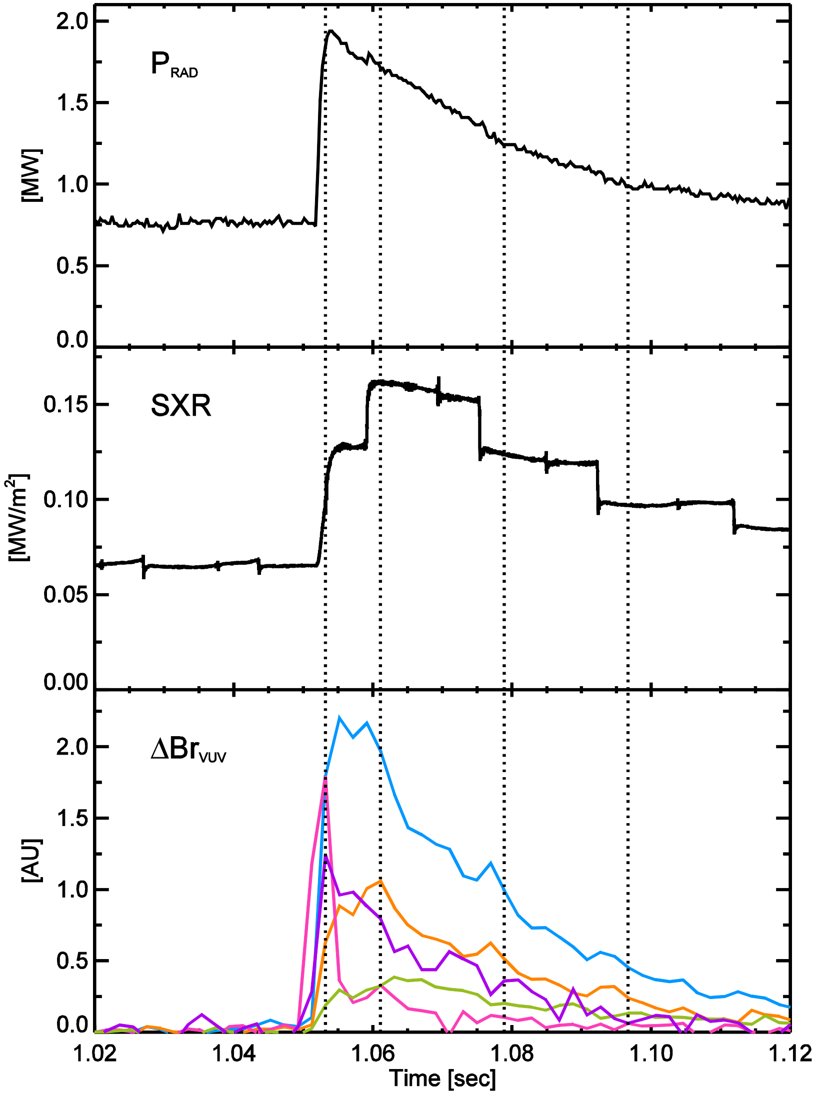

- see Mo^{8+} early, then Mo^{22+} rises, followed by more core localized Mo^{30+}, Mo^{31+} and Mo^{33+}
  - ion. states > 33+ seen transiently at peak in ST-cycle in hotter plasmas
- P_{RAD} follows charge states bellow 30+ while SXR follows those above 31+

how much of this can be used quantitatively?

title

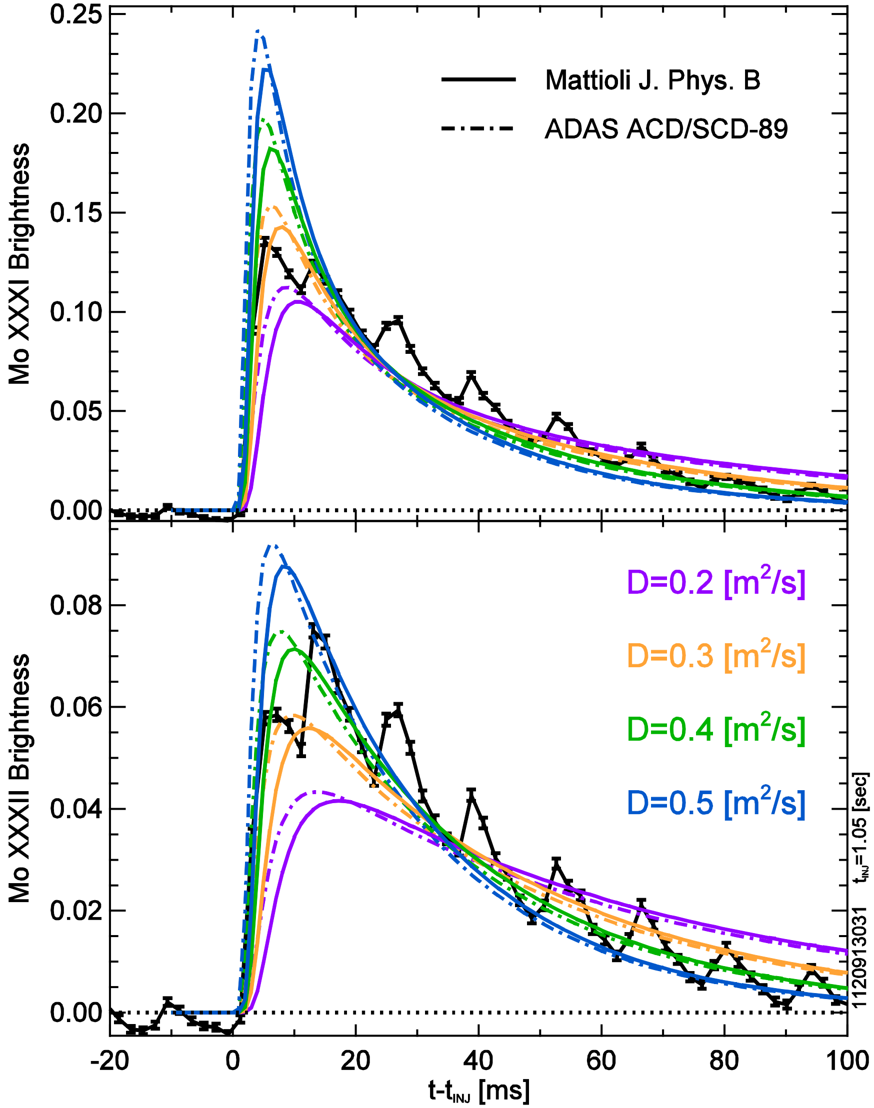

- assume flat diffusivity profiles
- use Na, Mg-like lines and rates from Rice, J.Phys. B
- individually normalize each signal by $\int Br\, dt$ over injection
- rise time slightly slower for Mattioli rate data – but cannot constrain with present data
  - improve ability to distinguish if spectra are relatively calibrated

qualitative changes in transport observable above the uncertainty

Centrifugal Force Driven Impurity Density Asymmetries

- for a tor. rotating plasma, centrifugal force pushes ions to the low-field side (LFS) effect scales as $m_z\omega^2R^2/T_z$ but since $T_z \sim T_i$, scales with **$M_i^2(m_z/m_i)$**
- in $v_i/v_{th,I} = M_i \sim 1$ plasmas, impacts main ions (MAST, NSTX)
- enhanced as aspect ratio drops, stronger variation in $R^2 - \langle R^2 \rangle$ over flux surface
- intrinsic flow sufficient for high-Z impurities on C-Mod
  - intrinsic + weak torque on ITER may be sufficient

OUTBOARD ACCUMULATION

centrifugal force from toroidal rotation moves impurities to LFS

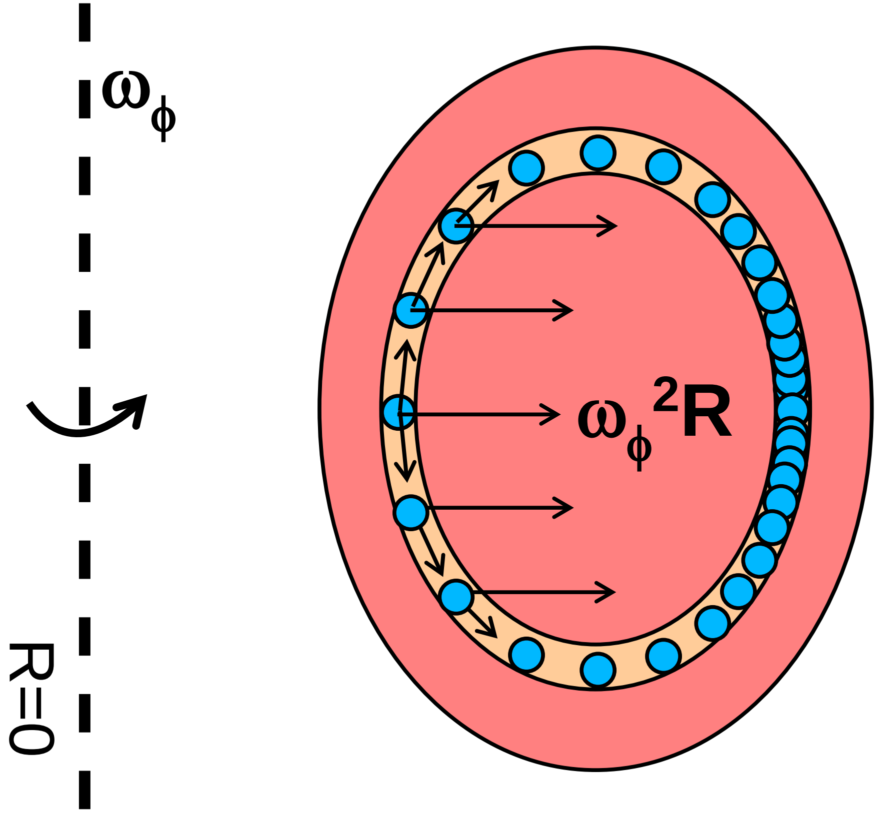

Poloidal Electric Field Driven Impurity Density Asymmetries

- the high charge of impurities causes sensitivity to poloidal variation of electrostatic potential

$$n_z/\langle n_z\rangle = \exp[-Ze\Phi(\theta)/T_z]$$

- first exp. observation in ICRF-heated Ni LBO shots on JET [Ingesson – 2000]
- may also be an effect from neutral beam ions* and non-thermal electrons
- weak in ITER at full-field

*DIII-D perfect place to test this

INBOARD ACCUMULATION

electric field from rf-heated minority ions moves impurities to HFS

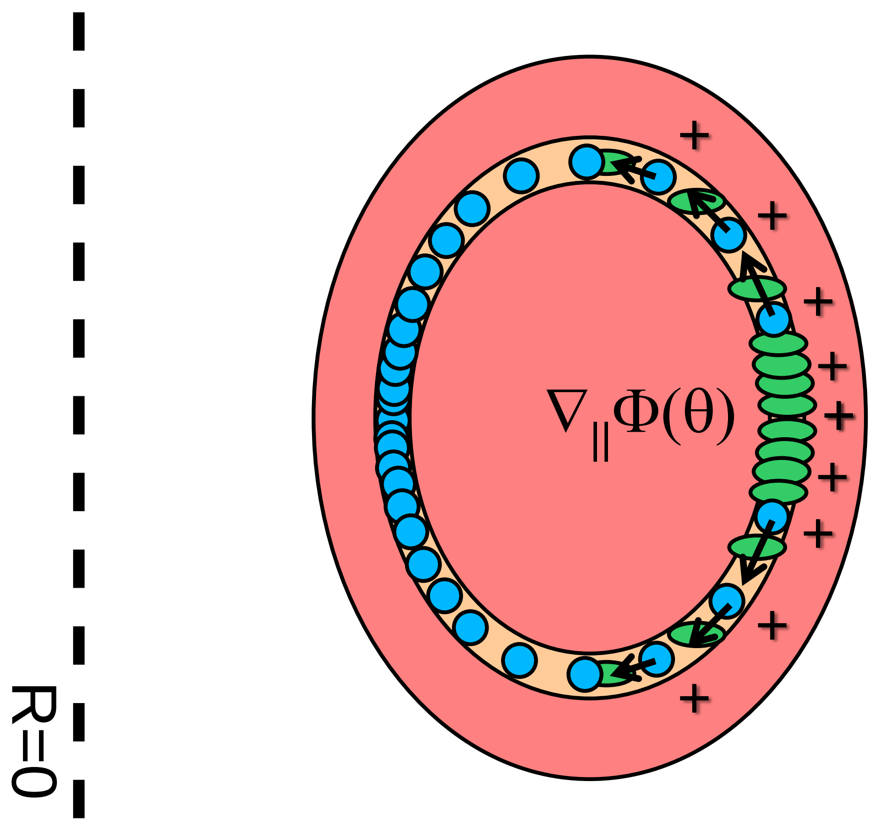

Other Asymmetries of Interest

- weaker (< 0.1) up/down asymmetries observed for Mo on Alcator C-Mod at mid-radius [Reinke – PoP 2013], poor agreement with theory
- substantial Ar up/down asymmetry ~ 1.0 near plasma edge in Ohmic plasmas, changes near LOC/SOC [Rice – NF 1997, Reinke – NF 2013]

Other Asymmetries of Interest

- weaker (< 0.1) up/down asymmetries observed for Mo on Alcator C-Mod at mid-radius [Reinke – PoP 2013], poor agreement with theory
- substantial Ar up/down asymmetry ~ 1.0 near plasma edge in Ohmic plasmas, changes near LOC/SOC [Rice – NF 1997, Reinke – NF 2013]

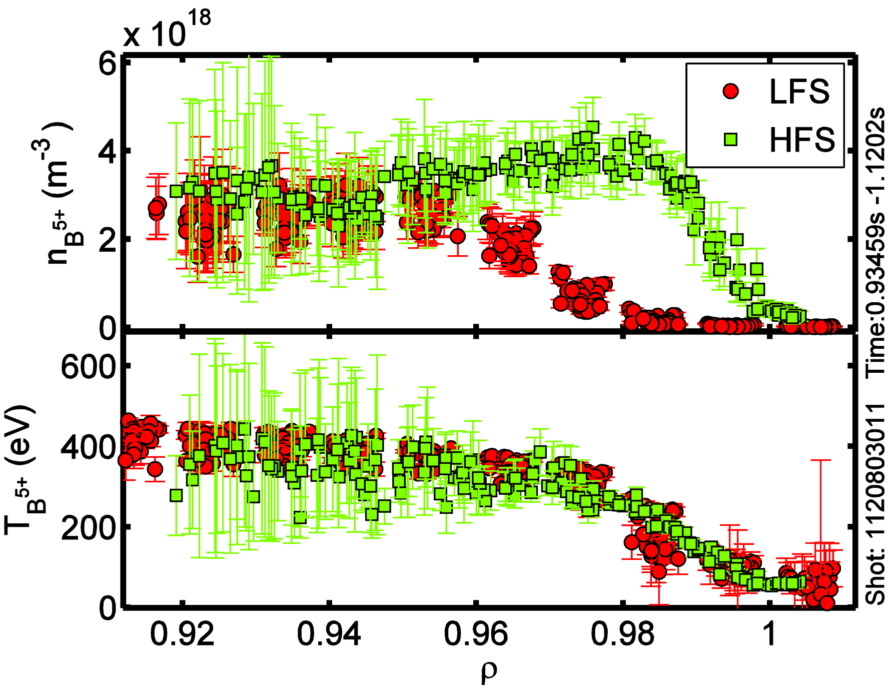

R.M. Churchill *et al* 2013 *Nucl. Fusion* **53** 122002

Strong In/Out Low-Z Impurity Asymmetries Obs. in Pedestal

- first seen on C-Mod [Pederson – 2002, Marr - 2010]
- detailed studies on C-Mod [Churchill – 2013] and AUG [Viezzer - 2013] for boron
- no work on high(er)-Z impurities
- recent work [Theiler – NF 2014] suggests small Er asymmetries possible → poloidal electric field

Combination of Turbulent and Neoclassical Flux

$$\frac{\Gamma_Z}{n_Z} = D_Z^{TURB}\frac{R}{L_{nZ}}\bigg|_{\theta=0} + D_Z^{NEO}\frac{R}{L_{nZ}}\bigg|_{\theta=0} + RV_Z^{TURB} + RV_Z^{NEO}$$

$$\frac{R}{L_{nZ}} = \frac{\frac{\chi_{i,AN}}{\chi_{i,NEO}}\frac{RV_Z^{TURB}}{\chi_{i,TURB}} + \frac{RV_Z^{NEO}}{\chi_{i,NEO}}}{\frac{\chi_{i,AN}}{\chi_{i,NEO}}\frac{RD_Z^{TURB}}{\chi_{i,TURB}} + \frac{RD_Z^{NEO}}{\chi_{i,NEO}}}$$

an important detail for comparing theory and experiment is comparing the same scale length: $a/L_{nZ}|_{\theta=0} \neq \langle a/L_{nZ}\rangle$ as spatially varying in/out asymmetry changes $a/L_{nZ}|_{\theta=0}$

$$\frac{n_Z}{\langle n_Z\rangle} = 1 + \delta(\rho)\cos\theta$$

$$\frac{a}{L_{nZ}}\bigg|_{\theta=0} - \left\langle\frac{a}{L_{nZ}}\right\rangle = -\frac{d\delta/d\rho}{(1+\delta)}$$

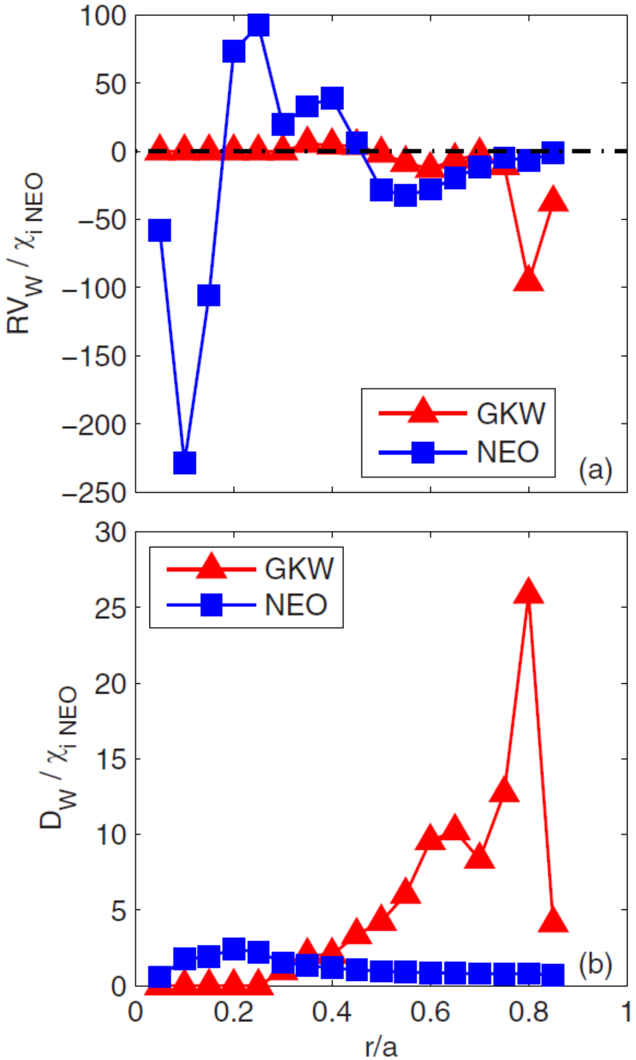

C. Angioni, *et al*. NF **54** 083028 (2014)

Utilize Resistive Bolometers to *In-Situ* Calibrate the SXR System for Tungsten Profiles

- use on-axis ICRF power scan in L-mode plasma to increase electron temperature in plasma with high tungsten content

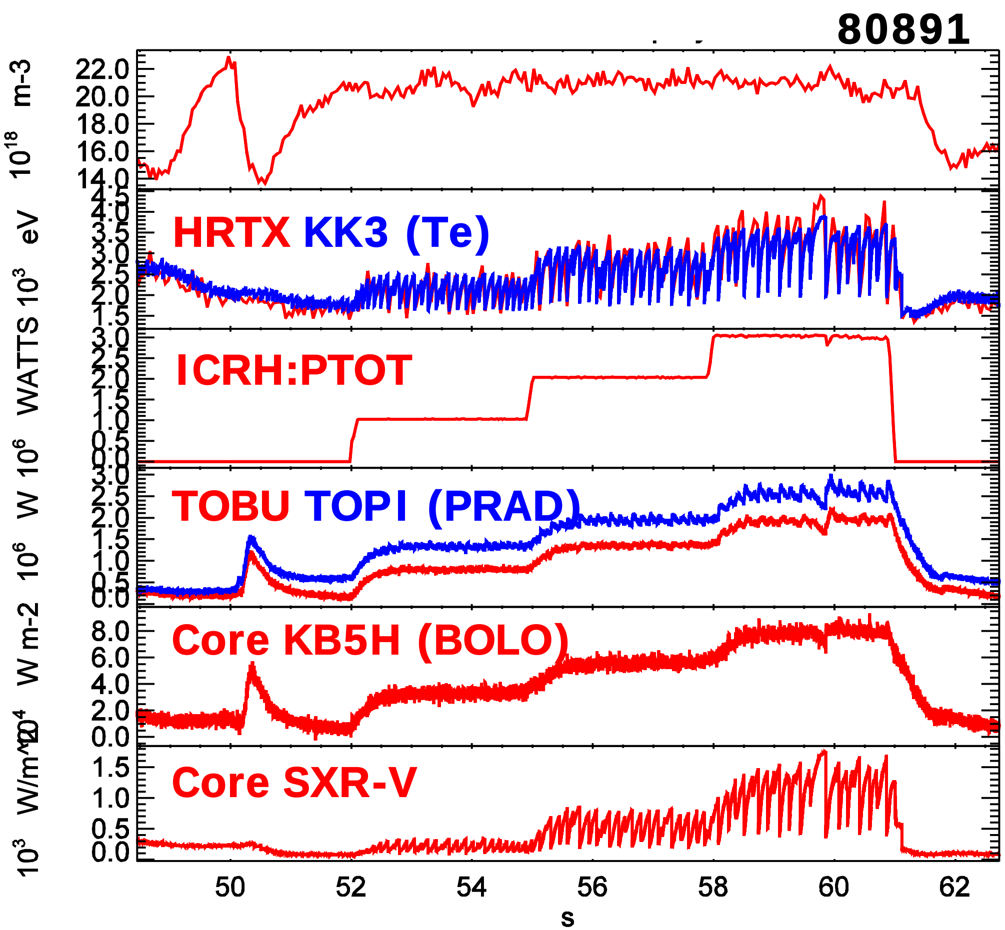

- steady density
- peak core T_e up to 4 keV with sawtooth variations resolvable
- see rise in radiated power and SXR emission with ICRH power

Use Non-Divertor Viewing KB5 Chords and Test Inversion Approach

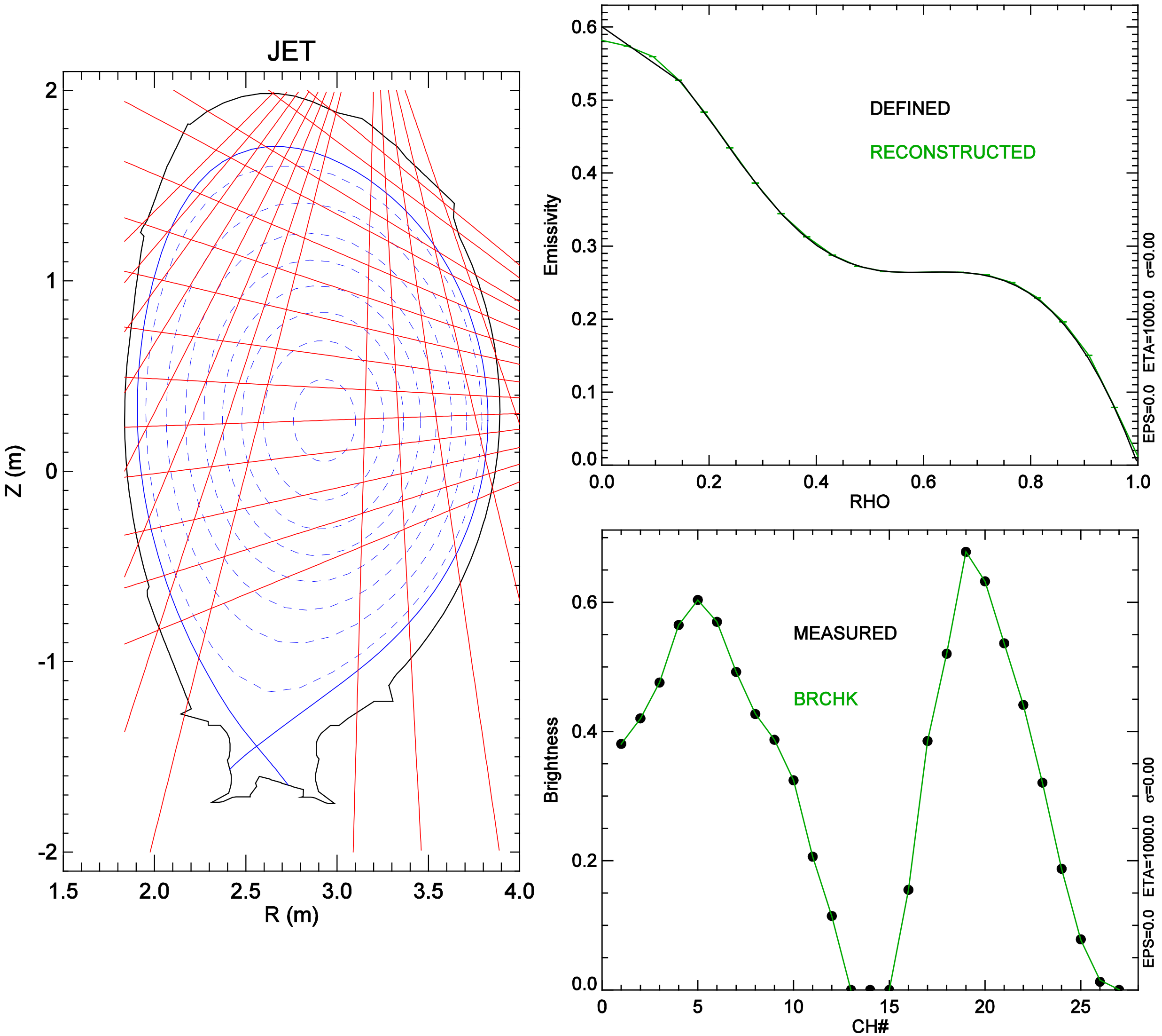

- **define** peaked emissivity profile
- line-integrate along chosen chords to get **measured** brightness
- invert using least squares with linear regularization
  - **reconstructed** emissivity matches w/o noise
  - **brchk** is brightness consistent with that emissivity

Utilize Resistive Bolometers to *In-Situ* Calibrate the SXR System for Tungsten Profiles

- use on-axis ICRF power scan in L-mode plasma to increase electron temperature in plasma with high tungsten content

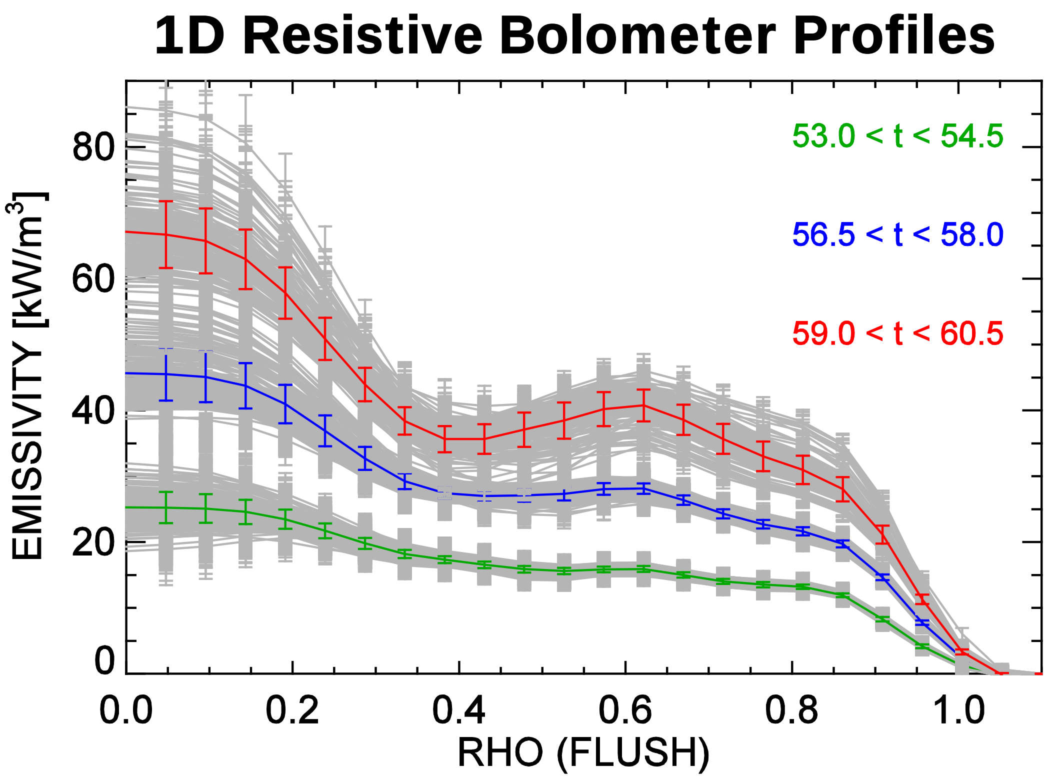

- steady density
- peak core T_e up to 4 keV with sawtooth variations resolvable
- see rise in radiated power and SXR emission with ICRH power
- utilize subset of poloidal tomography system to derive emissivity profile
- compare to existing SXR emissivity profile

- normalize all to experimental data at $3.7 < T_e < 4.3$ keV
- the modified Pütterich data agrees well for $T_e > 2.3$
- the ADAS (UTC-SANCO) data disagrees for $T_e < 3.0$

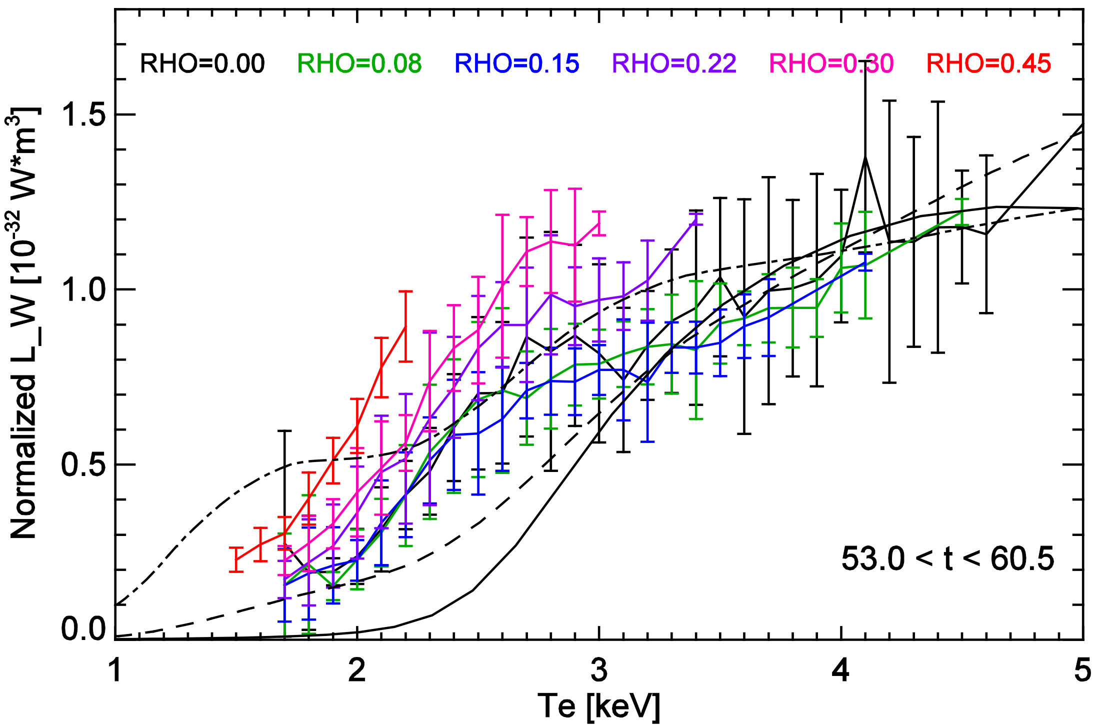

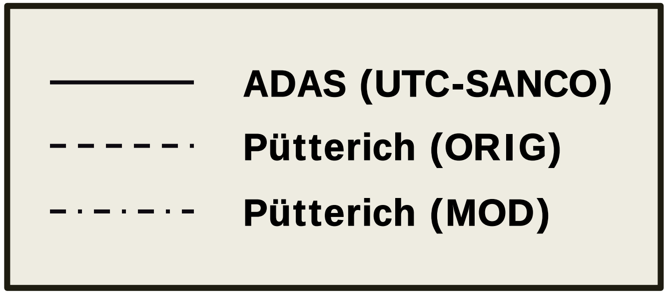

differences in the shape of L_W curves for $2 < T_e < 3$ keV will impact mid-radius shape of n_W profile

Mo32+ Emission Layer Predicted to Be Farther Out

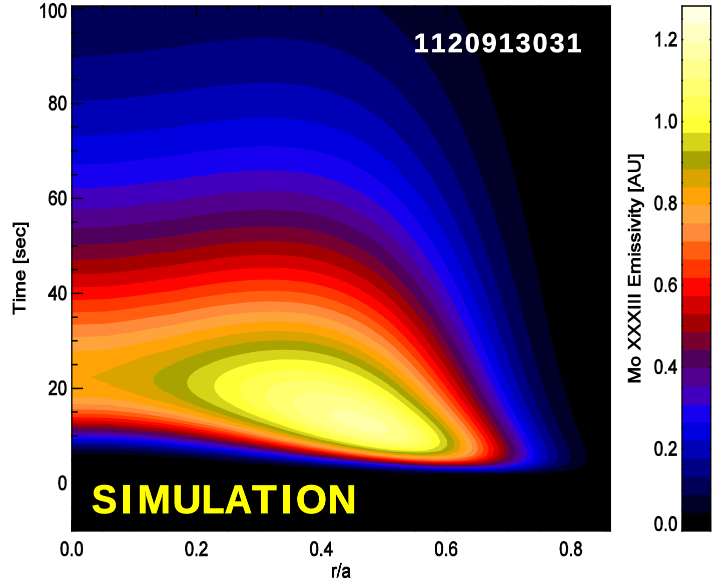

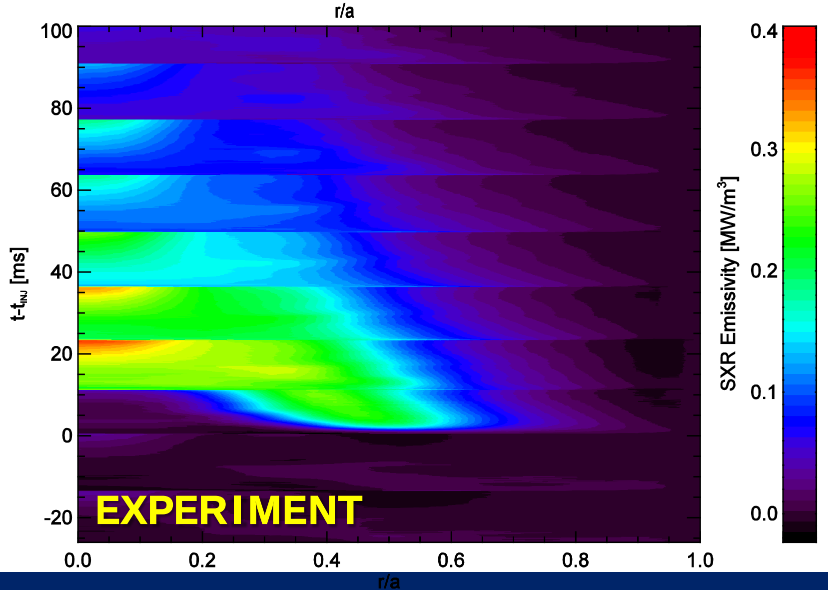

- pure diffusive simulation puts Mo^{32+} layer $\Delta r/a > 0.1$ outward
- adding inward convection in this region increases τ_{IMP} beyond exp.
- adding an inward and outward component $\int v(r)\, dr \sim 0$ depletes total Mo density in this region in disagreement with AXUV diodes
  - SXR emissivity, looking mainly at Ne-like and above, see similar inward shift as Mo^{32+}

Something is Missing from Simulation